

GEMS & GEMOLOGY

FALL 2018
VOLUME LIV

THE QUARTERLY JOURNAL OF THE GEMOLOGICAL INSTITUTE OF AMERICA



Proceedings of the
2018 GIA International Gemological Symposium



2018 GIA International Gemological Symposium

STEERING COMMITTEE

Kathryn Kimmel (Chair)

Senior Vice President and Chief Marketing Officer

Robert Claborn

Manager, Security

Clare Conway

Senior Coordinator, Corporate Events and Meetings

Craig Danforth

Director, Business Development

Vivianne Del Signore

Director, Digital Communications

Dona M. Dirlam

Librarian Emerita

Kate Donovan

Manager, Global Alumni Relations

Susan Elliott

Director, Education Resources

Emily Flener

Project Administrator, Marketing Communications

Dianne Gotla

Controller, United States

Sarah Hatfield

Senior Manager, Global Trade Shows

Vicki Gee Horiye

Director, Marketing Communications

Susan M. Jacques

President and Chief Executive Officer

Elizabeth Keating

Vice President and Chief Ethics and Compliance Officer

Craig LaBahn

Director, Facilities and Logistics

Anna Martin

Senior Vice President, Global Development

Michael McNally

Director, Global Physical Security

Carol Moffatt

Manager, Corporate Events and Meetings

Stephen Morisseau

Director, Corporate Communications

Thomas M. Moses

Executive Vice President and Chief Laboratory and Research Officer

Caroline Nelms

Library Research Analyst and Coordinator

Terri Ottaway

Curator, Museum Collections

Kimberly Overlin

Dean of Students

Stuart Overlin

Managing Editor, *Gems & Gemology*

Pritesh Patel

Senior Vice President and Chief Operating Officer

Duncan Pay

Vice President and Chief Academic Officer

Cathryn Ramirez

Director, Business Development

Susan Schindelar

Vice President, Global Marketing

Dr. James E. Shigley

Distinguished Research Fellow

Judith Shechter

Director, Business Development

David J. Tearle

Senior Vice President and Chief Financial Officer

Dr. Wuyi Wang

Vice President, Research and Development

Robert Weldon

Director, Richard T. Liddicoat Library and Information Center

Jennifer Wilson

Senior Vice President and General Counsel



October 7–9, 2018 | Carlsbad, CA
VOLUME 54, No. 3

2018 GIA International Gemological Symposium

Editorial	255
Speaker Presentations	
Colored Stones and Pearls	256
Diamond Identification	262
Diamond Geology	270
Gem Characterization	274
Gem Localities	277
General Gemology and Jewelry	281
New Technologies and Techniques	285
Photo Montage	289
Poster Presentations	
Colored Stones and Pearls	294
Diamond Identification	303
Diamond Geology	306
Gem Characterization	308
Gem Localities	321
General Gemology and Jewelry	325
New Technologies and Techniques	340
Futurescape Forum	348
Index of Presenters	350



Editorial Staff

Editor-in-Chief

Duncan Pay
dpay@gia.edu

Managing Editor

Stuart D. Overlin
soverlin@gia.edu

Editor

Jennifer-Lynn Archuleta
jennifer.archuleta@gia.edu

Technical Editors

Tao Z. Hsu
tao.hsu@gia.edu
Jennifer Stone-Sundberg
jstone@gia.edu

Editors, Lab Notes

Thomas M. Moses
Shane F. McClure

Editors, Micro-World

Nathan Renfro
Elise A. Skaltwold
John I. Koivula

Editors, Gem News

Emmanuel Fritsch
Gagan Choudhary
Christopher M. Breeding

Editorial Assistants

Brooke Goedert
Erin Hogarth

Contributing Editors

James E. Shigley
Raquel Alonso-Perez
Donna Beaton

Editor-in-Chief Emeritus

Alice S. Keller

Customer Service

Martha Erickson
(760) 603-4502
gandg@gia.edu

Production Staff

Creative Director

Faizah Bhatti

Production and Multimedia Specialist

Juan Zanahuria

Photographer

Robert Weldon

Photo/Video Producer

Kevin Schumacher

Video Production

Larry Lavitt
Pedro Padua
Nancy Powers
Albert Salvato
Betsy Winans

Editorial Review Board

Ahmadjan Abduriyim
Tokyo, Japan

Timothy Adams
San Diego, California

Edward W. Boehm
Chattanooga, Tennessee

James E. Butler
Washington, DC

Alan T. Collins
London, UK

John L. Emmett
Brush Prairie, Washington

Emmanuel Fritsch
Nantes, France

Eloïse Gaillou
Paris, France

Gaston Giuliani
Nancy, France

Jaroslav Hyršl
Prague, Czech Republic

Dorrit Jacob
Sydney, Australia

A.J.A. (Bram) Janse
Perth, Australia

E. Alan Jobbins
Caterham, UK

Mary L. Johnson
San Diego, California

Anthony R. Kampf
Los Angeles, California

Robert E. Kane
Helena, Montana

Stefanos Karamelas
Manama, Bahrain

Lore Kiefert
Lucerne, Switzerland

Ren Lu
Wuhan, China

Thomas M. Moses
New York, New York

Aaron Palke
Carlsbad, California

Nathan Renfro
Carlsbad, California

Benjamin Rondeau
Nantes, France

George R. Rossman
Pasadena, California

Andy Shen
Wuhan, China

Guanghai Shi
Beijing, China

James E. Shigley
Carlsbad, California

Elisabeth Strack
Hamburg, Germany

Nicholas Sturman
Bangkok, Thailand

Fanus Viljoen
Johannesburg, South Africa

Wuyi Wang
New York, New York

Christopher M. Welbourn
Reading, UK

J.C. (Hanco) Zwaan
Leiden, The Netherlands

Subscriptions

Copies of the current issue may be purchased for \$29.95 plus shipping. Subscriptions are \$79.99 for one year (4 issues) in the U.S. and \$99.99 elsewhere. Canadian subscribers should add GST. Discounts are available for renewals, group subscriptions, GIA alumni, and current GIA students. To purchase print subscriptions, visit store.gia.edu or contact Customer Service. For institutional rates, contact Customer Service.

Database Coverage

Gems & Gemology's impact factor is 1.844, according to the 2017 Thomson Reuters Journal Citation Reports (issued July 2018). *G&G* is abstracted in Thomson Reuters products (Current Contents: Physical, Chemical & Earth Sciences and Science Citation Index—Expanded, including the Web of Knowledge) and other databases. For a complete list of sources abstracting *G&G*, go to gia.edu/gems-gemology, and click on "Publication Information."

Manuscript Submissions

Gems & Gemology, a peer-reviewed journal, welcomes the submission of articles on all aspects of the field. Please see the Author Guidelines at gia.edu/gems-gemology or contact the Managing Editor. Letters on articles published in *G&G* are also welcome. Please note that Field Reports, Lab Notes, Gem News International, Micro-World, and Charts are not peer-reviewed sections but do undergo technical and editorial review.

Copyright and Reprint Permission

Abstracting is permitted with credit to the source. Libraries are permitted to photocopy beyond the limits of U.S. copyright law for private use of patrons. Instructors are permitted to reproduce isolated articles and photographs/images owned by *G&G* for noncommercial classroom use without fee. Use of photographs/images under copyright by external parties is prohibited without the express permission of the photographer or owner of the image, as listed in the credits. For other copying, reprint, or republication permission, please contact the Managing Editor.

Gems & Gemology is published quarterly by the Gemological Institute of America, a nonprofit educational organization for the gem and jewelry industry.

Postmaster: Return undeliverable copies of *Gems & Gemology* to GIA, The Robert Mouawad Campus, 5345 Armada Drive, Carlsbad, CA 92008.

Our Canadian goods and service registration number is 126142892RT.

Any opinions expressed in signed articles are understood to be opinions of the authors and not of the publisher.

About the Cover

The 2018 GIA International Gemological Symposium, held October 7–9 in Carlsbad, California, was the sixth such event dedicated to groundbreaking research across the gem and jewelry industry. A number of presentations discussed inclusions in gem materials. The cover photo uses differential interference contrast to show the interior scene of a diamond, where localized areas of high solubility appear as dissolution trigons decorating twin planes in a linear, crystallographically aligned arrangement. Photomicrograph by Nathan Renfro; field of view 0.83 mm.

Printing is by L+L Printers, Carlsbad, CA.

GIA World Headquarters The Robert Mouawad Campus 5345 Armada Drive Carlsbad, CA 92008 USA

© 2018 Gemological Institute of America

All rights reserved.

ISSN 0016-626X



GIA's 2018 Symposium: Up and Away!

Since GIA's first International Gemological Symposium in 1982, this event has served as a platform for advancing knowledge in the research and business sides of gemology. For three days, October 7–9, we celebrated the centennial of the incomparable Richard T. Liddicoat by hosting GIA's sixth Symposium. Nearly 800 attendees from 36 countries gathered in Carlsbad, California, including more than 100 presenters and panelists.

We've prepared this special Symposium Proceedings volume of *G&G* to capture the insights and the spirit of this unforgettable event. Scenes from all three days and nights are shown in the photo montage on pages 289–293.



The Symposium experience began with a powerful opening session featuring *The Music Paradigm*. Audience members found themselves seated within a live symphony orchestra as maestro Roger Nierenberg offered dynamic lessons on leadership and teamwork. This performance was followed by an opening gala at GIA World Headquarters. On display at the campus were some extraordinary new exhibits assembled by the GIA Museum. This gala was the first of three evening social events for rekindling old friendships and creating new ones.

In the Symposium research track, 37 speaker presentations and 68 poster sessions covered seven important themes: colored stones and pearls, diamond geology, diamond identification, gem characterization, gem localities and formation, general gemology and jewelry, and new technologies and techniques. In the speaker abstracts on pages 256–288 and the poster abstracts on pages 294–347,

you'll find a wealth of informative research summarized. An index of all the presenters appears in the back of the issue.

"Technological breakthroughs, changing consumer tastes, and sustainability concerns continue to reshape the gem and jewelry landscape..."

In a parallel program, classes taught by three professors from the Harvard Business School explored real-life case studies on authentic leadership, customer centricity, and disruptive innovation. Participants gained a deep understanding of these strategic concepts through classroom sessions and discussion groups.

The Symposium's closing session, the Futurescape Forum, brought together six of the industry's most influential leaders to forecast what lies ahead as technological breakthroughs, changing consumer tastes, and sustainability concerns continue to reshape the gem and jewelry landscape. You'll want to read pages 348–349 for a recap of this lively and thought-provoking panel discussion.

This event would not have been possible without the thousands of hours of planning by the Symposium steering committee and the dedicated efforts of dozens of GIA volunteers, all of whom are recognized on the front and back inside covers of this issue. I am especially grateful to Kathryn Kimmel, GIA's senior vice president and chief marketing officer, for once again chairing the Symposium and bringing to it her own signature style.

To all those who came to Carlsbad to attend the Symposium, we simply cannot thank you enough for being part of this event. We hope that you came away from it informed and inspired to embrace the future of our great industry.

A handwritten signature in black ink that reads "Susan M. Jacques". The signature is fluid and cursive, with a long horizontal flourish underneath the name.

Susan M. Jacques
President and CEO, Gemological Institute of America





SPEAKER PRESENTATIONS

Colored Stones and Pearls

Tourmaline: A Gemstone's Guide to Geologic Evolution of the Earth's Crust

Barbara L. Dutrow

Louisiana State University, Baton Rouge



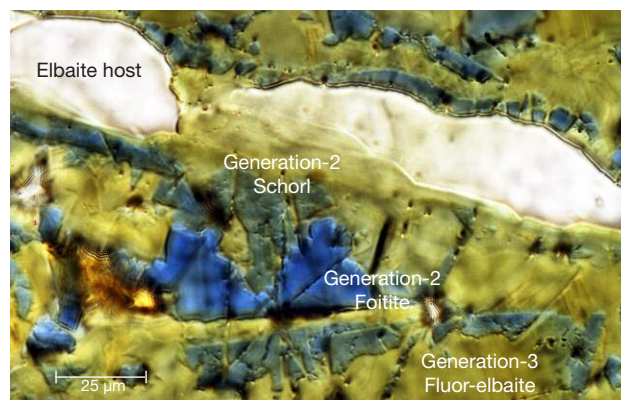
Tourmaline is recognized as an important gemstone and a stunning collector's item, and each crystal contains geochemical fingerprints that can elucidate an astonishing array of geological processes. Through field, experimental, analytical, and theoretical studies, the rich chemical signature encapsulated in tourmaline is being unraveled and revealed. Because of its widely varying chemistry, tourmaline is particularly adept at recording the host-rock environment in which it grew, be it a melt, a marble, or a former subduction zone. In addition, it can record the thermal and baric conditions of its growth, acting as a geothermometer or geobarometer. A crystal that exhibits sector zoning can provide the complete temperature history of its growth, serving as a single-mineral thermometer. Other tourmaline compositions may reveal the absolute age of a geologic event that produced tourmaline formation.

Tourmaline also excels at recording the evolution of the fluids with which it interacts. Its essential ingredient is boron (B), a fluid-mobile element. Thus, tourmaline is nature's boron recorder. Tourmaline formation and growth reflects the availability of boron to the rock system. Fluids can be sourced internally from the melt or from the breakdown of other B-bearing minerals, or fluids with boron can infiltrate the rock system from external sources. In each case, tourmaline preserves signatures of these events in the form of new growth, dissolution of preexisting tourmaline with growth of a new tourmaline composition (tourmaline cannibalizing itself to form anew), or replacement of another mineral. Tourmaline species may hint at fluid compositions. For example, species ranging from oxy-dravite to povondraite are typically found in saline, oxidizing environments and are indicators of these fluids in the geologic past. The deep green chrome (Cr) tourmalines reflect an unusual environment enriched in both Cr and B. Similarly, tourmaline compositions may reflect specific components of the fluid phase and, in some cases, provide quantitative estimates of fluid compositions (figure 1). Fitting data to tourmaline–fluid partitioning experiments permits calculation of the sodium (Na) concentrations in the coexisting fluid phase, and

suggests that the alkali species of tourmaline—elbaite, dravite, and schorl—form in fluids with greater than 0.30 mol/L Na, whereas the vacancy-dominant species, foitite and oxy-foitite, are stable in fluids with less than 0.25 mol/L Na. Once formed, tourmaline resists attack by corrosive acidic fluids.

Combining these features, tourmaline is a mineral containing unparalleled information on the environment in which it grew and the geologic processes responsible for it. An advantage of tourmaline as a geologic record keeper is that once these signals are incorporated, they are retained throughout the “lifetime” of the grain due to its slow volume diffusion. In some extraordinary cases, a single tourmaline grain can record its complete “life cycle,” from its original crystallization from a cooling magma deep within the crust through the rock's uplift, cooling, and partial destruction during erosion to

Figure 1. A single tourmaline fiber contains three distinct chemical zones, each recording the fluid composition at the time of growth. Between zones, fluids dissolved preexisting tourmaline to provide components for the new species in equilibrium. This overall compositional trend mimics the fractionation trend in a pegmatite.



deposition and reburial followed by heating and regrowth in a new geologic environment. The oldest known tourmaline dates back about 3.7 billion years, and it retains the chemical growth zones from its formation in early Earth, thus elucidating the presence of boron-bearing fluids and continental crust during that time.

The totality of this embedded geologic history is the result of tourmaline's flexible crystal structure, which incorporates a substantial number of chemical elements and isotopes, across a wide array of sizes and valence states, and in quantities from major to trace amounts. Such variable chemistry not only produces a kaleidoscope of colored gemstones but also permits tourmaline to be stable over nearly all pressure and temperature conditions found in Earth's crust, and to develop in all major rock types, from solidified igneous melts and pegmatites to metamorphic and sedimentary rocks. This chemical variability classifies tourmaline as a

mineral supergroup, currently consisting of 33 different species, each with a different and unique story.

Telling tourmaline's story typically requires chemical compositions to be obtained. New methods involving laser ablation–inductively coupled plasma–mass spectrometry (LA-ICP-MS) and infrared and Raman spectroscopy, along with well-established techniques such as electron microprobe analysis, provide such information to gemologists and geologists. For tourmaline, a mineral with one of the most exquisite arrays of color, geologists tease apart the complex clues it harbors, and gemologists can use these to tell the story of each gemstone. The widespread occurrence of the tourmaline minerals and their ability to imprint, record, and retain information make them a valuable tool for investigating Earth's geological processes. Tourmaline is the ultimate keeper of geologic information, a geologic DVD.

“Boehmite Needles” in Corundum Are Rose Channels

Franck Notari¹, Emmanuel Fritsch² (presenter), Candice Caplan¹, and Thomas Hainschwang¹

¹GGTL-Laboratories Switzerland, Geneva, and Balzers, Liechtenstein

²Institut des Matériaux Jean Rouxel and University of Nantes, France

Crystallographically oriented, linear inclusions in corundum are often referred to as “boehmite needles” or “polycrystalline boehmite” (boehmite is the orthorhombic aluminum hydroxide γ -AlOOH). These inclusions are oriented along the edges of the rhombohedral faces and form angles of about 90°. They are always found at the intersection of twin lamellae, formed by twinning along the rhombohedral faces. They contain apparently polycrystalline material tentatively identified (at least in some cases) as boehmite. These are common in natural corundum and sometimes used as a criterion to separate natural from synthetic corundum.

Boehmite can be recognized through its infrared absorption. The great majority of the “needle”-containing gem corundum showed no boehmite infrared absorption, thus leading us to believe that these inclusions have a different origin. Microscopic observation reveals three aspects: some are lath- or ribbon-shaped, others are clearly negative crystals, and sometimes

they appear as dotted lines. At the outcrop of the feature on the gem's surface there is most commonly a void that can be followed into the gem, so the “needle” is essentially empty. This feature was also documented in a flux-grown synthetic ruby with no boehmite infrared signal. These channels are favored during titanium diffusion and take on color first, as diffusion is much faster in the empty space.

It is known that in a small number of materials—some metals, calcite, and diamond—hollow channels may form at the intersection of twin lamellae, caused by deformation twinning. This was discovered by Gustav Rose (1868) in calcite, and thus the features are called “Rose channels” (figure 1). We believe that “boehmite needles” are in fact Rose channels. Even when very small, these channels would explain the optical relief observed, without a change in chemistry or infrared absorption. They fit the crystallographic nature of the structures observed.

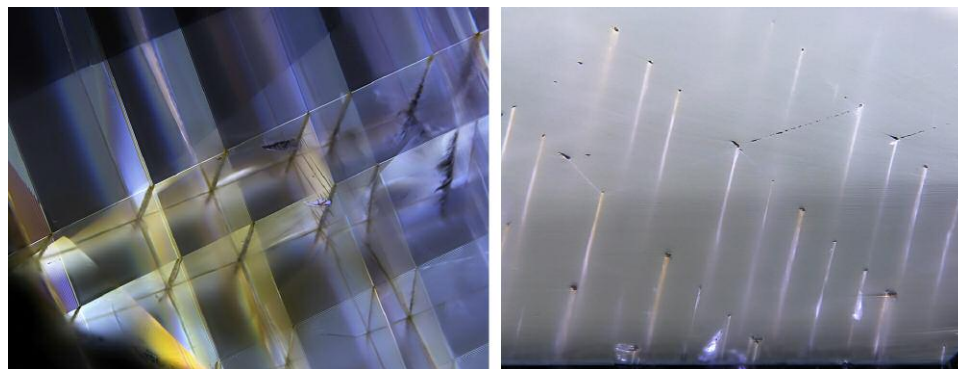


Figure 1. Left: Rose channels at the intersection of twin lamellae in a 7.17 ct color-change sapphire from East Africa, viewed in partially polarized light. Right: Detail of the same zone in reflected light, illustrating the fact that these channels are empty. Photos by Franck Notari; fields of view approximately 5.66 mm (left) and 2.83 mm (right).

Gemstones and Photoluminescence

Claudio C. Milisenda

DSEF German Gem Lab, Idar-Oberstein

Laser- and ultraviolet-excited luminescence spectroscopy and imaging are important techniques for gemstone testing, as they are among the most sensitive spectroscopic methods (see Hainschwang et al., 2013). They are able to identify optically active crystallographic defects such as vacancies and substitutions that are present in such small amounts that they cannot be detected by any other analytical method. Photoluminescence (PL) analysis became particularly important in the last decade for the separation of natural from synthetic diamonds and the detection of treatments. Today the availability of specially designed and reasonably priced portable equipment enables the rapid *in situ* identification of mounted and unmounted natural diamonds.

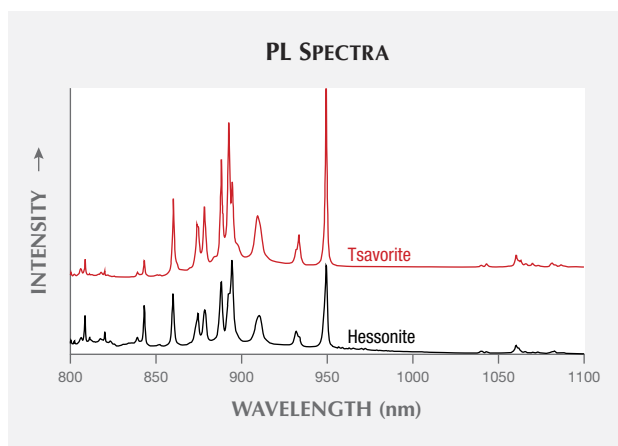
Although PL spectroscopy is most commonly used for diamond identification, it can also be applied to colored stones. Some stones exhibit unique luminescence patterns, which can be used to identify the material. Other examples are the separation of natural from synthetic spinel and the detection of heat-treated spinel. Since chromium is a typical PL-causing trace element, it is also possible to separate chromium-colored gems such as ruby and jadeite from their artificially colored counterparts. The color authenticity of specific types of corals and pearls can also be determined.

The rare earth elements (REE) are among the main substituting luminescence centers in Ca^{2+} -bearing minerals (Gaft et al., 2005). Recently, REE photoluminescence has been observed in cuprian liddicoatite tourmalines from Mozambique (Milisenda and Müller, 2017). When excited by a 785 nm laser, the stones showed a series of bands at 861, 869, 878, 894, and 1053 nm, consistent with the

PL spectra of other calcium-rich minerals (Chen and Stimets, 2014). LA-ICP-MS analysis confirmed the REE enrichment in this type of tourmaline compared to cuprian elbaïtes from Brazil and Nigeria. As a result, photoluminescence can be used as a further criterion for origin determination of Paraíba-type tourmalines.

We have extended our research on other calcium-rich gems, including various grossular garnet varieties such as hessonite and tsavorite (figure 1), uvarovite garnet, apatite, titanite, and scheelite, as well as a number of high-refractive-index glasses and color-change glasses, respectively.

Figure 1. 785 nm laser-induced REE photoluminescence spectra of tsavorite and hessonite garnets. Spectra are offset for clarity.



REFERENCES

- Chen H., Stimets R.W. (2014) Fluorescence of trivalent neodymium in various materials excited by a 785 nm laser. *American Mineralogist*, Vol. 99, No. 2-3, pp. 332–342, <https://doi.org/10.2138/am.2014.4311>
- Gaft M., Reisfeld R., Panczer G. (2005) *Modern Luminescence Spectroscopy of Minerals and Materials*. 2nd edition, Springer, Heidelberg, Germany, 606 pp.
- Hainschwang T., Karampelas S., Fritsch E., Notari F. (2013) Luminescence

spectroscopy and microscopy applied to study gem materials: a case study of C centre containing diamonds. *Mineralogy and Petrology*, Vol. 107, No. 3, pp. 393–413, <https://doi.org/10.1007/s00710-013-0273-7>

Milisenda C.C., Müller S. (2017) REE photoluminescence in Paraíba type tourmaline from Mozambique. *35th International Gemmological Conference*, Windhoek, Namibia, pp. 71–73.

An Overview of Asteriated Gems: From Common Star Sapphire to Rare Star Aquamarine to One-of-a-Kind Star Zircon

Martin P. Steinbach

Steinbach-Gems with a Star, Idar-Oberstein, Germany

Rays of angel's hair in a star-like shape, beams of light hovering over the surface of a gem—gems with stars have fascinated people of all cultures, continents, and religions since ancient times.

Asteriated gems have been known for more than 2,000 years, starting with Periegetes' description of "Asterios" in the first century BCE. Other historical names were *asteria*, *asterius*, *astrion*,

astrodamas, and *astriotes*. From Pliny the Elder (first century CE) to the Middle Ages, to De Boodt (1609) and Brueckmann (1783), asterism was known only in corundum and some feldspar varieties.

Currently, about 60 different gem varieties display asterism, whereas 15 gemstone varieties show a “trapiche” star. The well-known commercial examples include star ruby, sapphire, quartz, almandine garnet, moonstone (orthoclase feldspar), and the four-rayed black star diopside from India. Rare or less well-known varieties include star aquamarine, beryl, bronzite, calcite, chrysoberyl (A.G.S. Research Service, 1937), enstatite, hypersthene, kyanite, peridot, scheelite, scapolite, spinel, and sunstone (oligoclase feldspar). The extremely rare one-of-a-kind stars consist of star alexandrite, amazonite (Steinbach, 2016), cordierite, apatite, “star diamond,” ekanite, emerald (Liddicoat, 1977), kornerupine, kunzite, labradorite, opal, parisite, prehnite, rhodochrosite (figure 1), rhodonite, rutile, serandite, fibrolite (sillimanite), spessartine, taaffeite, tanzanite, topaz, tourmaline, and zircon.

Some of the 60 different star stones introduced in this colorful presentation can also show double stars; 12-, 18-, or 24-rayed stars; a network of stars; and trapiche varieties.

REFERENCES

A.G.S. Research Service (1937) Star chrysoberyl. *G&G*, Vol. 2, No. 8, p. 130.
Liddicoat R.T. (1977) Comments on the Hixon Collection. *G&G*, Vol. 15, No. 9, p. 1.



Figure 1. This 15.51 ct star rhodochrosite is from the Sweet Home mine in the state of Colorado. Photo by Martin P. Steinbach.

One new source of star rose quartz (China) and two new sources of almandine star garnet (China and Russia) will also be presented.

Steinbach M.P. (2016) *Asterism—Gems with a Star*. MPS Publishing and Media, Idar-Oberstein, Germany, 896 pp.

Quantitative Identification of Green Nephrite from Five Major Origins In Asia and North America

Zemin Luo, Andy H. Shen, and Meihua Chen
China University of Geosciences, Wuhan

Green nephrite (serpentine-related) has been generating substantial interest in the gem market. The primary sources are China, Russia, and Canada. Preliminary observations of mineral impurities and chemical components can help separate some dolomite-related nephrite from serpentine-related material. We have developed a novel classifier that can automatically identify the geological origin of random green nephrite samples on the market with 95% prediction accuracy. The technique behind this classi-

fier is based on a trace-element database for green nephrite and a machine learning algorithm.

The green nephrite database was built from 34 samples from five major geological origins (Manasi and Hetian in Xinjiang, China; Taiwan; British Columbia, Canada; and Siberia, Russia; representative samples are shown in figure 1). Trace-element information was collected by LA-ICP-MS with an average of six points on each sample. The following classification models were

Figure 1. Representative green nephrite samples from the five serpentine-related deposits in Asia and North America: Manasi (A), Hetian (B), Taiwan (C), British Columbia (D), and Siberia (E).





Figure 2. The 10 most important trace elements for green nephrite classification, ranked in descending order, analyzed by the random forest algorithm.

tested: neural network (multilayer perceptron), random forest, logistic regression, naive Bayes, and support vector machine. The random forest model gives the best performance on both training sets and cross-validation sets, with over 90% accuracy (table 1). The random forest model also identified the 10 most important trace elements for green nephrite classification as Sr, Ba, Zn, U, Ti, LREE, Cd, Rb, Mn, and K (figure 2). The geological information about this trace-element “fingerprint” needs further investigation.

We used linear discriminant analysis (LDA) to visually demonstrate the obvious separation of Siberian and Manasi green nephrites from the other origins (figure 3). This result is consistent with our optic and spectra characterization results. Green nephrite from the Manasi mine usually presents a heterogeneous grayish yellow green color, which is quite different from that of other origins. The absence of garnet inclusions in Siberian green nephrite—which distinguishes it from material from the other localities—can be confirmed by Raman spectroscopy. Samples from all origins have been characterized by photomicrography, micro-infrared spectra, and Raman spectra. We can therefore integrate the spectra

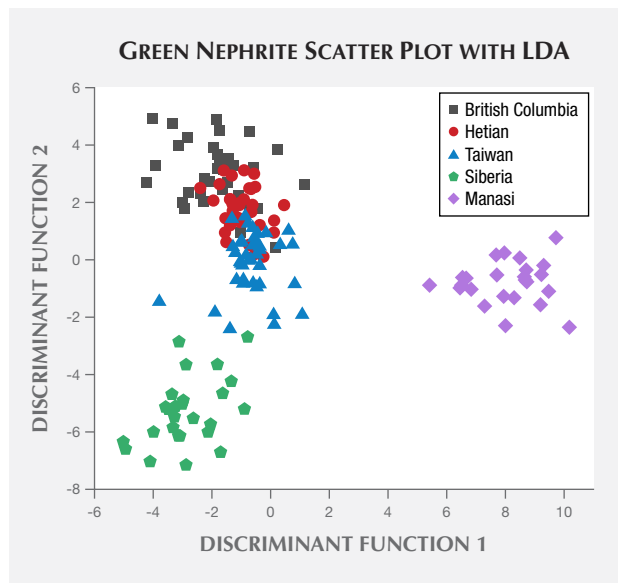


Figure 3. This scatter plot illustrates how an LDA algorithm was used to separate green nephrite. It shows clear separation of Manasi and Siberian nephrite from the other three origins (Hetian, British Columbia, and Taiwan), which show obvious overlap.

TABLE 1. Classification accuracies (%) of the training set and the cross-validation set for the five green nephrite samples using various machine learning algorithms.

Model	Score_train	Score_CV
Random forest	100.0	95.4
Neural network	99.8	92.2
Support vector machine	100.0	85.8
Logistic regression	95.3	83.2
Naive Bayes	88.2	82.6

and trace-element features into our classification model in the next step. We believe that the research method proved in this work is also applicable for other gemstones. It can also be a useful tool to study ancient green nephrite origins.

Radiocarbon Measurements on Pearls: Principles, Complexities, and Possibilities

Gregory Hodgins

University of Arizona Accelerator Mass Spectrometry Laboratory, Tucson

Radiocarbon dating is a method for determining the age of organic remains formed in the past 45,000 years. Also known as carbon-14 or ¹⁴C (figure 1), radiocarbon is a naturally occurring radioactive isotope of carbon with a half-life of 5,730 years. It is continuously formed in the earth’s upper atmosphere and makes

its way into the biosphere via photosynthetic uptake and the food chain. Several radiocarbon dates for pearls have recently appeared in the scientific literature. Mollusks take up radiocarbon during life and incorporate it into shell and pearl carbonate. The aim of this presentation will be to describe the method, identification

complexities, and challenges inherent in dating pearls based upon radiocarbon measurement so that we may plot a path for future research.

There are two variants of the dating method. The first is conventional radiocarbon dating, which applies to organisms that lived before 1955 CE. The second involves the detection of anthropogenic radiocarbon in organisms living between 1955 CE and the present. There are biological, environmental, and experimental complexities in the radiocarbon dating of pearls, and the method will not work in all circumstances. However, some of these complexities—coupled with historic changes in when, where, and how pearls have been produced—mean radiocarbon measurement can provide information unavailable by other means.



Figure 1. The author stands beside the terminus of the accelerator mass spectrometer radiocarbon beam line. Photo by Gretchen Gibbs.

Unconventional Techniques in Pearl Testing: Their Potential and Limitations

Chunhui Zhou
GIA, New York

Current routine pearl testing involves the application of various basic and advanced gemological techniques. These include the use of the gemological microscope, ultraviolet (UV) luminescence, microradiography, computed X-ray microtomography, optical X-ray luminescence, energy-dispersive X-ray fluorescence spectrometry (EDXRF), ultraviolet-visible (UV-Vis) spectroscopy, and Raman spectroscopy. While the majority of pearls may be identified using these existing conventional techniques, in certain cases identification challenges remain.

This talk will discuss the potential and limitations of various unconventional techniques that have been applied to pearl testing over recent years. Some of these techniques have been explored by GIA and resulted in meaningful benefits to the trade, and others referenced in the literature will also be briefly covered. Examples of these techniques include radiocarbon age dating, deoxyribonucleic acid (DNA) bar coding, in-depth trace-element geochemistry and isotope analysis, and 3D reconstruction of internal structures. It is important for gemological and research institutions to continue developing novel techniques for pearl testing in order to achieve the accurate separation between natural and cultured pearls, principally non-bead cultured, as well as other aspects of identification that

might assist in reaching this accurate analysis (e.g., species determination, geographical origin determination, and treatment identification). Despite decades of pearl testing experience, some challenges remain within laboratories, and the application of additional unconventional methods could resolve some of these issues.

Figure 1. The application of unconventional pearl testing methods could be useful in separating difficult pearl samples, such as various types of freshwater pearls shown here. Photo by Diego Sanchez.



ADDITIONAL READING

- Krzemnicki M.S., Hajdas I. (2013) Age determination of pearls: A new approach for pearl testing and identification. *Radiocarbon*, Vol. 55, No. 3, pp. 1801–1809, <http://dx.doi.org/10.1017/S0033822200048700>
- Meyer J.B., Cartier L.E., Pinto-Figueroa E.A., Krzemnicki M.S., Hänni H.A., McDonald B.A. (2013) DNA fingerprinting of pearls to determine their origins. *PLOS One*, Vol. 8, No. 10, pp. 1–11, <http://dx.doi.org/10.1371/journal.pone.0075606>
- Saruwatari K., Suzuki M., Zhou C., Kessrapong P., Sturman N. (2018) DNA

- techniques applied to the identification of *Pinctada fucata* pearls from Uwajima, Ehime Prefecture, Japan. *G&G*, Vol. 54, No. 1, pp. 40–50, <http://dx.doi.org/10.5741/GEMS.54.1.40>
- Zhou C., Hodgins G., Lange T., Saruwatari K., Sturman N., Kiefert L., Schollenbruch K. (2017) Saltwater pearls from the pre- to early Columbian era: A gemological and radiocarbon dating study. *G&G*, Vol. 53, No. 3, pp. 286–295, <http://dx.doi.org/10.5741/GEMS.53.3.286>

What Is Cobalt Spinel? Unraveling the Causes of Color in Blue Spinel

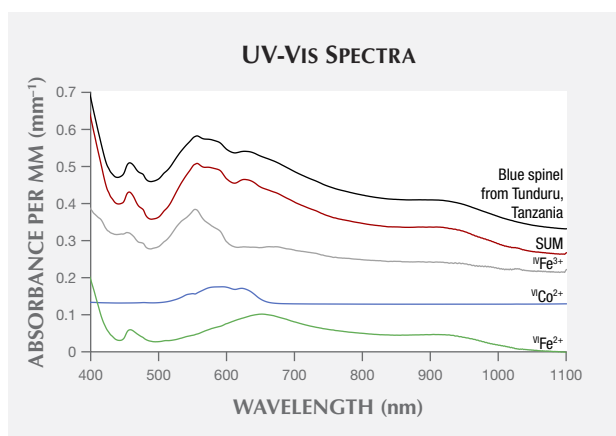
Aaron C. Palke and Ziyin Sun
GIA, Carlsbad, California

Cobalt is known to produce vibrant blue color in both natural and synthetic spinel. In the 1980s and '90s, Vietnam started producing blue spinel with very high concentrations of cobalt and bright, saturated color rivaling that seen in synthetic material. Iron can also cause blue coloration in spinel, although this is typically a duller grayish or greenish blue. So when is a blue spinel worthy of carrying the “cobalt spinel” moniker? With high-sensitivity analytical methods such as LA-ICP-MS, cobalt can be detected in most spinel, even at the sub-ppm level. But sub-ppm concentrations of cobalt do not impact the color of a faceted spinel. In addition, the saturation and quality of blue color will depend on the concentration of iron and its valence state (e.g., Fe^{2+} vs. Fe^{3+}).

In this contribution we will explore the color space of blue spinel and outline the various contributions to their coloration. Using UV-Vis spectrometry and LA-ICP-MS on blue spinel from Vietnam, Sri Lanka, Madagascar, and Tanzania, we have isolated three unique and consistent chromophores (see figure 1). Cobalt in its divalent form (Co^{2+}) has multiple absorption bands between ~510 and 660 nm and produces a bright blue color. Two broad absorption bands at ~650 and 920 nm are related to Fe^{2+} substituting for Al^{3+} in octahedral coordination. Finally, another set of at least three absorption bands occurs at ~500–620 nm and overlaps those from Co^{2+} . Comparison with other Fe-related absorption bands and consideration of the crystal chemistry of spinel suggest that these bands may be related to Fe^{3+} in the tetrahedral site in the spinel structure. This last absorption feature creates a grayish pink coloration, and in combination with Co^{2+} it can be

responsible for blue to violet color change in some spinel. There is clearly a significant interplay between these three chromophores, and a full understanding of the causes of color in blue spinel can only be attained by consideration of all three contributions.

Figure 1. UV-Vis spectra of the individual contributions from three chromophores in blue spinel, octahedral ferrous iron (${}^{\text{VI}}\text{Fe}^{2+}$), octahedral cobalt (${}^{\text{VI}}\text{Co}^{2+}$), and tetrahedral ferric iron (${}^{\text{IV}}\text{Fe}^{3+}$). At the top is the full spectrum of a blue spinel from Tanzania, followed by the sum of the three individual components (SUM). UV-Vis spectra of all blue spinels in this study could be recreated with varying contributions from the three spectra at the bottom.



Diamond Identification

Canary Yellow Diamonds

Wuyi Wang¹ and Terry Poon²

¹GIA, New York

²GIA, Hong Kong

Isolated nitrogen is one of the major defects in producing yellow color in natural diamonds. In regular type Ib yellow diamonds, isolated nitrogen is normally the dominant form, with limited aggregations in A centers (nitrogen pairs). Type Ib diamonds normally experienced strong plastic deformations. In addition to vacancy clusters, many other optic centers were introduced during annealing over their long geological history, such as GRI, NV, and H3 centers. Diamonds from the Zimmi area of West Africa are a

typical example (Smit et al., 2016). As a result, clear brownish and greenish hues are common among these diamonds, so most do not possess true “canary” yellow color. Here we studied more than 2,000 diamonds with real canary yellow color. Their color origin and relationship with type Ib diamonds were explored.

Sizes of the studied diamonds ranged from 0.01 to about 1.0 ct. They showed pure yellow color, with grades of Fancy Intense or Fancy Vivid yellow. Infrared absorption analysis showed that



they were all type IaA with very high nitrogen concentrations, but a very weak absorption from isolated nitrogen at 1344 cm^{-1} was detected in all samples. Concentration of isolated nitrogen was estimated at $\sim 2\text{--}3$ ppm. This isolated nitrogen created smooth absorption in the ultraviolet-visible (UV-Vis) region, increasing gradually to the high-energy side. No other defects were detected using UV-Vis absorption spectroscopy, which explained the pure yellow color we observed. Fluorescence imaging revealed multiple nucleation centers with dominant green color, which was attributed to the S3 defects confirmed through photoluminescence analysis. Compared with natural type Ib diamonds, an outstanding feature of the studied samples is the absence of plastic deformation. For this reason, other vacancy-related defects were not introduced to these diamond lattices over the geological period after their formation.

Sulfide inclusions are common in type Ib diamonds, but they were not observed in these canary stones. Instead, some calcite inclusions were observed. All the observations from this study indicated that the canary diamond samples were formed in a different geological environment than type Ib diamonds.

REFERENCE

Smit K.V., Shirey S.B., Wang W. (2016) Type Ib diamond formation and preservation in the West African lithospheric mantle: Re-Os age constraints from

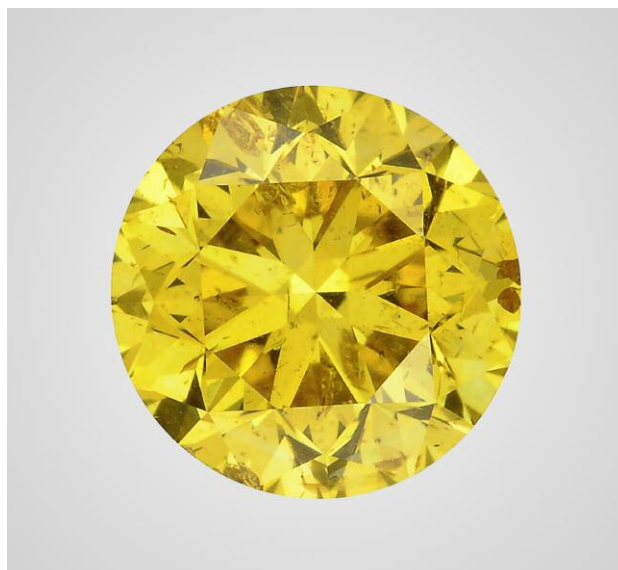


Figure 1. The canary yellow diamonds from this study showed much lower concentrations of isolated nitrogen than regular type Ib yellow diamonds, which usually show brownish and greenish hues linked to plastic deformation. Photo by Sood Oil (Judy) Chia.

sulphide inclusions in Zimmi diamonds. *Precambrian Research*, Vol. 286, pp. 152–166, <http://dx.doi.org/10.1016/j.precamres.2016.09.022>

Addressing the Challenges of Detecting Synthetic Diamonds

David Fisher

De Beers Technologies, Maidenhead, United Kingdom

The dream of growing synthetic diamonds existed for many centuries before it was achieved in the 1950s. The development of techniques to identify synthetic diamonds and enable their reliable separation from natural diamonds has not had the luxury of centuries to work with. Since the early reports on the characteristics of laboratory-grown stones, scientists have been working steadily to establish and improve the means of detection. For many years the De Beers Group has been developing equipment for rapidly screening and testing for potential synthetic and treated diamonds as part of a strategy aimed at maintaining consumer confidence in natural untreated diamonds. This work has been underpinned by extensive research into defects in natural and synthetic diamond, either conducted within De Beers' own facilities or through financial and practical support of research in external institutions.

Key to any detection technique for synthetic diamonds is a fundamental understanding of the differences between them and natural diamonds. This could take the form of differences in the atomic impurity centers or differences in the spatial distributions of these centers brought about by very significant distinctions in the growth

environments. The former was used in the development of the DiamondSure instrument that, among other things, detects variance differences in the absorption spectra due to the presence or absence of the N3 feature. This absorption is from a nitrogen-related defect that is usually only produced in nitrogen-containing diamonds by extended periods at relatively high temperatures—that is, conditions generally experienced by natural diamonds. Growth-related differences in impurity distributions can be very accurately imaged using the DiamondView instrument. Short-wave ultraviolet (UV) light is used to excite luminescence from a very thin layer of diamond near the surface to give images free from the blurring encountered with more common longer-wavelength excitation sources. DiamondView has, since its launch, provided the benchmark for the detection of synthetic diamonds.

A number of approaches involving absorption features have been developed, including the use of almost complete absorption in the ultraviolet region of the spectrum to indicate that a diamond is not synthetic. The UV absorption is produced by the A center (two adjacent nitrogen atoms) and is rarely encountered in as-

grown synthetic diamonds. The main form of nitrogen in synthetic diamonds is a single substitutional nitrogen atom that absorbs in both the ultraviolet and visible regions to produce yellow color. The combination of UV absorption and no strong yellow color is therefore restricted to natural diamond. However, treatment of nitrogen-containing synthetic diamonds is capable of generating A centers, but generally does not produce a colorless stone. This effect accounts for the careful color ranges often applied to instruments relying on UV absorption for screening. This also highlights one of the limitations of absorption spectroscopy: When smaller stones are tested, the amount of absorption decreases and the technique becomes less reliable. In recent years we have seen a shift to smaller sizes (below 0.01 ct) in the synthetic diamonds being offered for sale to the jewelry market, and screening techniques have had to evolve to address this situation and the limitations of absorption-based approaches.

Testing melee-sized diamonds, as well as introducing technical challenges around the measurement technique, has also led to the introduction of greater automation. In 2014 the De Beers Group introduced the first automated melee screening instrument (AMS1), which combined the measurement technique from DiamondSure with automated feeding and dispensing of stones in the range of 0.20 to 0.01 ct. While this instrument was well received and effectively addressed concerns around synthetic melee-sized stones in the trade at the time, there soon came calls for improvements—a faster instrument capable of measuring smaller stones, no restrictions on cut, and a lower referral rate for natural diamonds. These requirements proved impossible to meet with the limitations imposed by absorption measurements, and a new technique based on time-resolved spectroscopy was developed. This resulted in the AMS2 instrument, launched in March 2017. The AMS2 processes stones at a speed of one stone per second, 10 times faster than the AMS1. It measures round brilliants down to 0.003 ct (0.9 mm diameter) and can be used on other cuts for stones of 0.01 ct and above. The measurement technique itself has been incorporated into the SYNTHdetect (figure 1, left), an instrument launched in September 2017 that allows manual observation of the time-resolved emission. Besides providing the same testing capability as AMS2 (figure 1, right) for loose stones, various holders allow testing of mounted stones in a wide range of configurations. The benefit of this approach is that stones tested loose using AMS2 will generate a broadly consistent result when mounted on SYNTHdetect.

Changes in growth processes for synthetic diamonds have also led to the gradual introduction of new characteristics. High-pressure, high-temperature (HPHT) synthetics have tended to be fairly consistent in their growth-related luminescence patterns, while significant variations in the features associated with chemical vapor deposition (CVD) synthetics have been observed. These continue to be well documented and have led to the gradual evolution of the DiamondView instrument and the way in which it is used.



Figure 1. The De Beers Group instruments SYNTHdetect (left) and AMS2 (right) provide screening capability for melee-size diamonds as small as 0.3 points. Photo courtesy of Danny Bowler © De Beers Group.

Post-growth treatment of synthetic diamonds can be applied for a number of reasons: improvement in the color, modification of the atomic defects to make the stones look more like a natural diamond, and removal of a characteristic that could be used to identify a synthetic diamond. The motivation for the latter two treatments can only be described as fraudulent. The challenge in developing detection instruments and techniques is to ensure that they are as robust as possible in the face of such challenges. Treatment techniques will rarely have any effect on the growth patterns associated with synthetic diamonds, and it is therefore very difficult to treat synthetics in a way that would make them undetectable using the DiamondView. Screening instruments tend to be based on a single technique, and it is important that the approach adopted not be vulnerable to simpler forms of treatment. This has been of primary concern to the De Beers Group in the development of our own screening instruments. It has also been necessary in certain cases to withhold detailed information about detection techniques where disclosure of this would lead to undermining of the detection technique itself.

The De Beers Group continues to invest heavily in growth and treatment research in order to develop the next generation of instruments and techniques that will assist the trade in maintaining detection capability to support consumer confidence. The Group is uniquely placed in the industry to address these challenges due to its collaboration with Element Six (world leaders in synthesis of diamond for industrial and technical applications) and its in-depth knowledge of the properties of natural diamonds with known provenance from its own mines.

Diamond at the Diffraction Limit: Optical Characterization of Synthetic Diamond

Phil L. Diggle^{1,2}, Ulrika F.S. D'Haenens-Johansson³, Wuyi Wang³, and Mark E. Newton^{1,2}

¹Department of Physics, University of Warwick, Coventry, United Kingdom

²EPSRC Centre for Doctoral Training in Diamond Science and Technology, Warwick, United Kingdom

³GIA, New York

Diamond, known for its splendor in exquisite jewelry, has been synthesized since the 1950s. In the last six decades, the perfection of laboratory-grown single-crystal diamond has vastly improved through the research and development of two main synthesis techniques. One replicates Earth's natural process, where the diamond is grown in the laboratory under conditions of diamond stability at high temperature and high pressure (HPHT). The other technique relies on the dissociation of methane (or other carbon-containing source gas) and hydrogen and the subsequent deposition of diamond at low pressures from the gaseous phase in a process known as chemical vapor deposition (CVD). In the latter case, diamond is not the stable form of carbon, but the kinetics in the CVD process are such that diamond wins out. Large gem-quality synthetic diamonds are now possible, and a 6 ct CVD (2018) and a 15.32 ct HPHT (2018) have been reported.

It is of course possible to differentiate laboratory-grown from natural diamond based on how extended and point defects are incorporated into the crystal. Furthermore, treated diamond can be identified utilizing knowledge of how defects are produced and how they migrate and aggregate in both natural and synthetic diamond samples. Room-temperature confocal photoluminescence microscopy can be used to image the emission of light from defects in diamond with a spatial resolution limited only by the diffraction limit; a lateral spatial resolution approaching 300 nm is routinely achieved (figure 1). It is possible with this tool to identify point defects with concentrations less than 1 part per trillion (10^{11} cm^{-3}).

This talk will outline the experimental setup, how this tool has been used to identify the decoration of dislocations with point defects in CVD lab-grown diamond, and how different mechanisms for defect incorporation operate at growth sector boundaries in HPHT synthetic diamond.

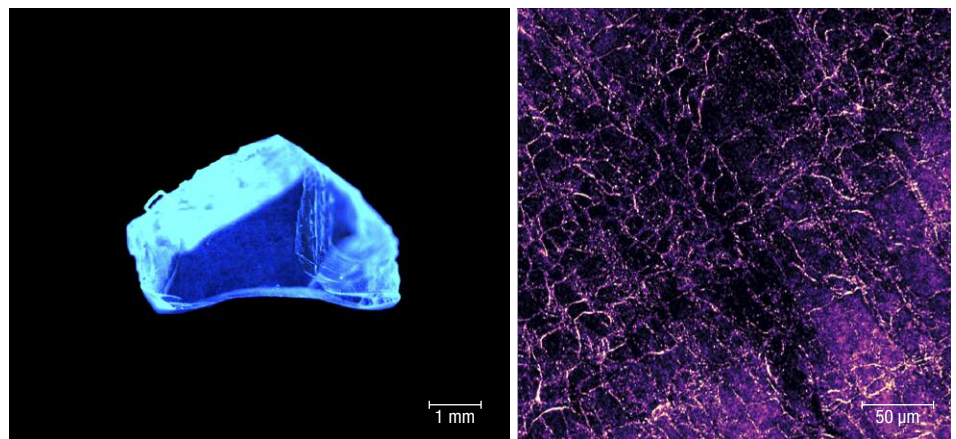


Figure 1. Left: DiamondView fluorescence imaging shows dislocation networks in a natural type IIa diamond. Right: A room-temperature confocal photoluminescence image taken with 488 nm excitation shows H3 defects following a dislocation network pattern within the diamond. Some of the fluorescent spots are single H3 centers.

Fluorescence in Diamond: New Insights

Ans Anthonis, John Chapman, Stefan Smans, Marleen Bouman, and Katrien De Corte
HRD Antwerp, Belgium

The effect of fluorescence on the appearance of diamonds has been a subject of debate for many years (Moses et al., 1997). In the trade, fluorescence is generally perceived as an undesirable characteristic. Nearly 80% of diamonds graded at HRD Antwerp receive a “nil” fluorescence grade, while the remainder are graded

as “slight,” “medium,” and “strong,” their value decreasing with level of fluorescence.

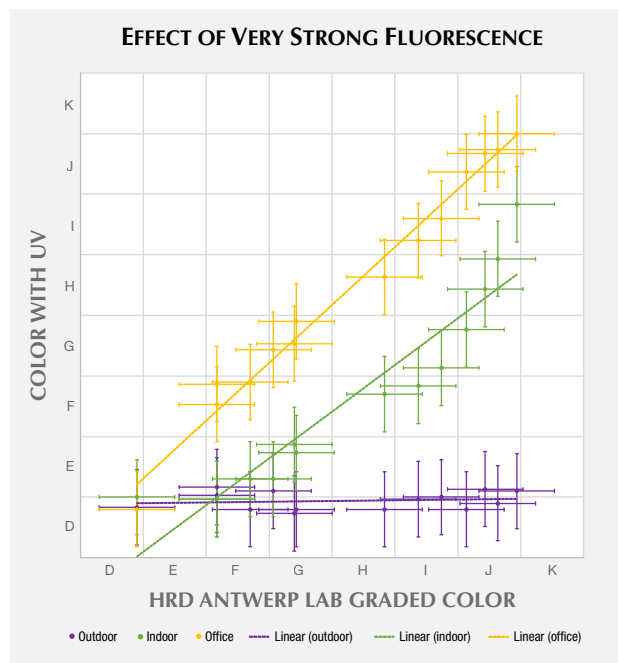
To understand how fluorescence might change diamond appearance, a selection of 160 round brilliant-cut diamonds were investigated in detail. This study focused on the effect of

fluorescence on diamond color. The aim was to determine under what lighting conditions the color of a diamond could change and the magnitude of that effect. We also investigated a smaller selection of diamonds with multiple spectroscopic absorption techniques to study the origin of their fluorescence.

The lighting arrangement we used combined the UV from light-emitting diode (LED) lamps with the light from a daylight-equivalent (grading) fluorescent lamp that had its UV component filtered out. With controlled UV output and after calibrations, it was possible to simulate different illuminations, including outdoors, indoors near a window, office lighting, and grading environments. The grading environment provided the reference color. Diamonds were presented in both table-down and table-up orientations, with the degree of effect determined by visual comparison with nonfluorescent master stones. For each color, both experienced diamond graders and nonprofessionals examined the possible effect of fluorescence on color appearance.

It was found that the UV level in office lighting was insignificant and did not produce any observable effect even with “very strong” fluorescence. However, with daylight from either outdoors or indoors, near a window, the relative strength of UV was significant, sufficient to create a positive color change. For samples with a “very strong” fluorescence, the results are shown in figure 1. For each color, ranging from D to J, the color shift caused by exposure to different UV levels—represented by the different lighting conditions—is illustrated.

Figure 1. For samples with “very strong” fluorescence, the observed color in different lighting conditions (outdoor, indoor, and office) is shown. These samples were graded through the pavilion (table-down). Note that in an outdoor environment, J colors can appear as D colors.



REFERENCE

Moses T.M., Reinitz I.M., Johnson M.L., King J.M., Shigley J.E. (1997) A contribution to understanding the effect of blue fluorescence on the appearance

of diamonds. *G&G*, Vol. 33, No. 4, pp. 244–259, <http://dx.doi.org/10.5741/GEMS.33.4.244>

Fluorescence, Phosphorescence, Thermoluminescence, and Charge Transfer in Synthetic Diamond

Jiahui (Gloria) Zhao^{1,2}, B.G. Breeze^{1,3}, B.L. Green¹, Phil L. Diggle^{1,2}, and Mark E. Newton^{1,2}

¹Department of Physics, University of Warwick, Coventry, United Kingdom

²EPSRC Centre for Doctoral Training in Diamond Science and Technology, Warwick, United Kingdom

³Spectroscopy Research Technology Platform, University of Warwick, Coventry, United Kingdom

Photoluminescence (PL) and phosphorescence underpin many of the discrimination techniques used to separate natural from synthetic diamond. PL is at the heart of many new quantum technologies based on color centers in lab-grown diamonds. In HPHT synthetic diamond, the phosphorescence observed is explained in terms of donor-acceptor pair recombination. The thermal activation of electrons to neutral boron acceptors shows that boron plays a key role in the phosphorescence process. However, there are a number

of things we struggle to explain. For example, the phosphorescence peak positions are not fully explained, and there is no conclusive link between the emission and charge transfer involving the substitutional nitrogen donor.

Secondly, the origin of the phosphorescence observed in some synthetic diamond samples grown by the CVD process is unclear. Although we now have evidence for unintentional boron impurity incorporation at stop-start growth boundaries in some CVD syn-

thetic samples, it is possible that some of the observed phosphorescence does not involve boron impurities.

In this paper we report on the results of combined fluorescence, phosphorescence, thermoluminescence, and quantitative

charge transfer investigations undertaken on both HPHT and CVD synthetic diamond, with the objective of identifying which defects are involved in the fluorescence and phosphorescence processes.

LPHT-Treated Pink CVD Synthetic Diamond

Hiroshi Kitawaki, Kentaro Emori, Mio Hisanaga, Masahiro Yamamoto, and Makoto Okano
Central Gem Laboratory, Tokyo

Pink diamond is extremely popular among fancy-color diamonds, which has prompted numerous attempts to produce pink diamond artificially. Pink CVD synthetic diamonds appeared on the gem market around 2010. Their color was produced by a multi-step process combining post-growth HPHT treatment to remove the brown hue and subsequent electron irradiation, followed by low-temperature annealing. Pink CVD synthetic diamonds treated only with low pressure and high temperature (LPHT), without additional post-growth irradiation, have also been reported but are rarely seen on the market.

Recently, a loose pink stone (figure 1) was submitted to the Central Gem Laboratory in Tokyo for grading purposes. Our examination revealed that this 0.192 ct brilliant-cut marquise was a CVD synthetic diamond that had been LPHT treated.

Visually, this diamond could not be distinguished from natural diamonds with similar color. However, three characteristics of CVD origin were detected:

1. C-H related absorption peaks between 3200 and 2800 cm^{-1} , located with infrared spectroscopy
2. A luminescence peak at 737 nm, detected with photoluminescence (PL) spectroscopy
3. A trace of lamellar pattern seen in the DiamondView

However, irradiation-related peaks such as at 1450 cm^{-1} (H1a), 741.1 nm (GR1), 594.3 nm, or 393.5 nm (ND1) that are seen in the pink CVD diamonds treated with common multi-step processes were not detected.

The presence of four peaks at 3123, 2901, 2870, and 2812 cm^{-1} between 3200 and 2800 cm^{-1} suggests this stone was LPHT treated; the following observations indicate that it was not HPHT treated:

- The 3123 cm^{-1} peak presumably derived from NVH⁰ disappears after a normal HPHT treatment.
- The 2901, 2870, and 2812 cm^{-1} peaks are known to shift toward higher wavenumbers as the annealing temperature rises. Our own HPHT treatment experiments on CVD-grown diamonds proved that the 2902 and 2871 cm^{-1} peaks detected after 1600°C annealing shifted to 2907 and 2873 cm^{-1} after 2300°C annealing. The peak shift of 2901,

2870, and 2812 cm^{-1} is also related to the pressure during the annealing, as these peaks shifted to 2902, 2871, and 2819 cm^{-1} at the higher pressure of 7 GPa compared to 2900, 2868, and 2813 cm^{-1} at the ambient pressure under the same annealing temperature of 1600°C.

- Absorption peaks at 7917 and 7804 cm^{-1} in the infrared region and at 667 and 684 nm in the visible range were also detected, which coincide with the features seen in LPHT-treated stones. From the combination of the intensity ratios of optical centers such as H3 and NV centers that were detected with PL measurement, this sample is presumed to have been treated with LPHT annealing at about 1500–1700°C as a post-growth process.

In recent years, CVD synthetic diamonds have been produced in a wider range of colors due to progress in the crystal growth techniques and post-growth treatments. Although HPHT treatment has been employed mainly to improve the color in a diamond, LPHT annealing may become widespread as the technique is further developed. Gemologists need to have deep knowledge about the optical defects in such LPHT-treated specimens.

Figure 1. LPHT-treated brownish pink CVD synthetic diamond weighing 0.192 ct. Photo by Hiroshi Kitawaki.



Recent Developments in Detection and Gemology in China, Particularly for Chinese Synthetic Diamonds

Jie Ke, Taijin Lu (presenter), Yan Lan, Zhonghua Song, Shi Tang, Jian Zhang, and Hua Chen
National Gemstone Testing Center (NGTC), Beijing

China is the world's largest producer of HPHT-grown industrial diamonds. Its 2016 production of about 20 billion carats accounted for 98% of the global supply. Since the beginning of 2015, melee-sized colorless HPHT synthetic diamonds have been tested at the National Gemstone Testing Center's (NGTC) Shenzhen and Beijing laboratories in parcels submitted by different clients, which means that colorless HPHT synthetic diamonds have entered the Chinese jewelry market and may be mistaken for natural diamonds.

CVD synthesis technology has grown rapidly in recent years. Large colorless and colored (blue, pink) CVD-grown diamonds have been entering the market, and a few have been fraudulently sold as natural diamonds.

China has independently developed gem-grade HPHT synthetic diamond production technology since 2002, and can grow gem-grade type Ib, IIa, and IIb and high-nitrogen-content synthetic diamonds in volume, depending on market needs. Gem-grade type Ib, IIa, and IIb HPHT synthetic diamonds have been grown using the temperature gradient method, under a cubic press at high pressure (e.g., 5.4 GPa) and high temperature

TABLE 1. Technology and products of some Chinese CVD synthetic diamond companies.

Company	Ningbo Crysdiem Industrial Technology	Hebei Plasma Diamond Technology	Shanghai Zhengshi Technology
Products and quality	Crystal size: 9 × 9 × 4 mm. Mass production of diamonds larger than 1 ct; type IIa and IIb; colorless to near-colorless, pink, and blue.	Crystal size: 11 × 11 × 1–3 mm. Scientific research, industrial production.	Crystal size: 12 × 12 × 3 mm, mainly 1.0–6.0 ct. Mass production available. Type IIa and IIb.
Growth technology	Microwave plasma chemical vapor deposition (MPCVD)	DC arc plasma jet CVD	MPCVD

(1300–1600°C). Driven by a specific temperature gradient, the carbon source from high-purity graphite (>99.9%) located at the high-temperature zone can diffuse into the seed crystals in the cubic press, resulting in the crystallization of synthetic diamonds. Chinese production of melee-sized colorless to near-colorless HPHT synthetic diamonds accounts for about 90% of the global output.

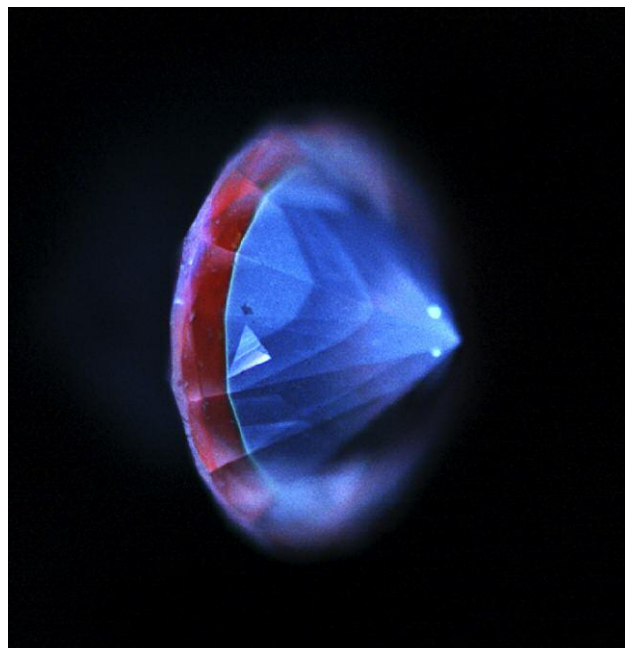
Gem-grade type IIa and IIb CVD synthetic diamonds are grown using the microwave plasma chemical vapor deposition (MPCVD) and direct current (DC) arc plasma methods. Faceted colorless CVD diamonds can be grown in sizes up to 6 ct by at least two Chinese companies (table 1).

After testing and analyzing thousands of natural and synthetic diamonds collected directly from the Chinese companies, NGTC independently developed the GV5000, PL5000, DS5000, and ADD6000 instruments for rapidly screening and identifying the diamonds based on the gemological characteristics obtained.

Besides HPHT and CVD synthetic diamonds, a thickly layered hybrid diamond consisting of both natural and CVD material was identified at the NGTC Beijing laboratory (figure 1). The identification features and properties of regrown CVD synthetic diamonds using natural type Ia diamond crystals as seeds will be reported.

The current status and features of colored stones examined at NGTC laboratories, including several cases studies, will be discussed.

Figure 1. DiamondView fluorescence image of the hybrid natural and CVD-grown diamond. Photo by Shi Tang.



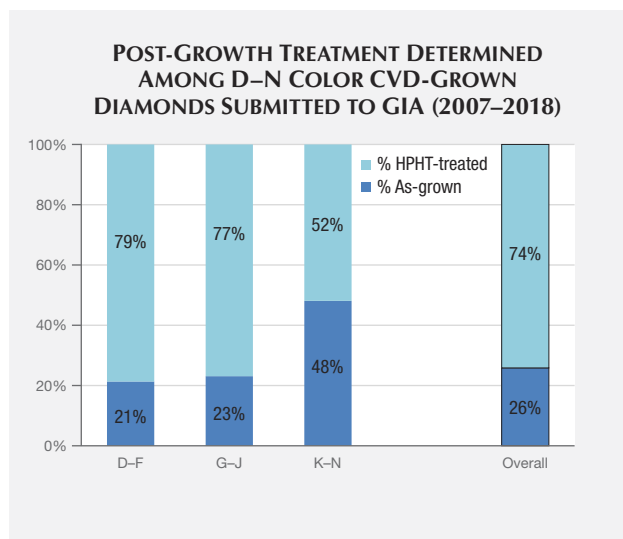
Summary of CVD Lab-Grown Diamonds Seen at the GIA Laboratory

Sally Eaton-Magaña
GIA, Carlsbad, California

While chemical vapor deposition (CVD) diamond growth technology has progressed significantly in recent years, with improvements in crystal size and quality, the use of these goods in the jewelry trade is still limited. Not all CVD-grown gem diamonds are submitted to GIA for grading reports, and they only account for about 0.01% of GIA's annual diamond intake (both D–Z equivalents and fancy color; Eaton-Magaña and Shigley, 2016). The CVD process involves diamond growth at moderate temperatures (700–1300°C) but very low pressures of less than 1 atmosphere in a vacuum chamber (e.g., Angus and Hayman, 1988; Nad et al., 2015). This presentation summarizes the quality factors and other characteristics of the CVD-grown material submitted to GIA (e.g., figure 1) and discusses new research and products.

Today the CVD process is used to produce high-color (as well as fancy-color) and high-clarity type II diamonds up to several carats in size. The majority of the CVD material seen at GIA consists of near-colorless (G–N equivalent) with colorless (D–F equivalent) and various “pink” hues. Additionally, CVD material is constantly setting new size milestones, with the announcement of an approximately 6 ct round brilliant earlier this year (Davis, 2018). However, the attainable sizes among CVD products are dwarfed by those from the HPHT process, with 15.32 ct as the current record for a faceted gem (Ardon and Eaton-Magaña, 2018).

Figure 1. Spectra and fluorescence images of all D–N equivalent CVD-grown diamonds seen at GIA from 2007 to 2018 were analyzed. The vast majority (74%) show features consistent with post-growth HPHT treatment. The percentage of as-grown CVD products increases as the equivalent color progresses from the colorless range (D–F) to near-colorless (G–J) to faint brown (K–N).

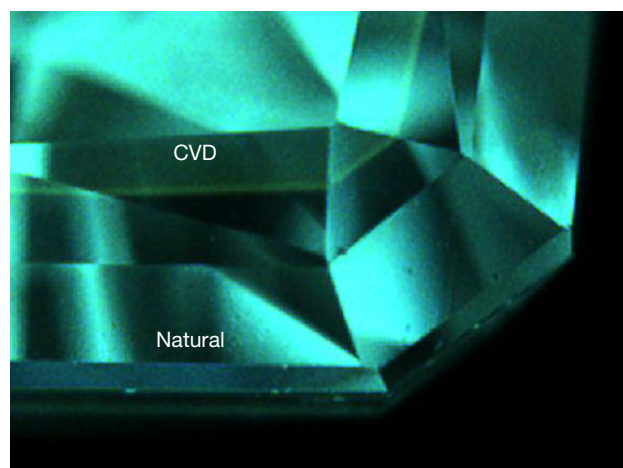


One particular challenge for gemologists (albeit very rarely encountered) comes from the lab-grown/natural hybrids (figure 2) that have been submitted to and documented by gemological laboratories (e.g., Moe et al., 2017; Tang et al., 2018). In these specimens, the grower places a *natural* diamond into the CVD reactor as the seed plate, with both components retained in the faceted gem. If the manufacturer is using a colorless natural type Ia diamond as a seed plate for near-colorless CVD growth, the hybrid cannot undergo any post-growth HPHT treatment, as this would radically alter the natural seed by turning the natural diamond yellow. If the manufacturer is creating a CVD overgrowth layer on a faceted natural diamond, the intent is to either add weight to a diamond that may be near a weight boundary or to achieve a color change, typically to blue. These hybrid products also make it more difficult to infer a diamond's history based solely on its diamond type.

The CVD process has also created some unique gems that have not been duplicated among natural, treated, or HPHT-grown diamonds. These include CVD-grown diamonds with a high concentration of silicon impurities, which create a pink to blue color shift. In those samples, a temporary effect was activated by UV exposure, which precipitated a charge transfer between negative and neutral silicon-vacancy centers (D'Haenens-Johansson et al., 2015).

Also recently seen are type IIb CVD goods. Some that were submitted by clients had a low boron concentration (3 ppb, with G-equivalent color and 1.05 carat weight). Meanwhile, some research samples produced by a manufacturer in China and fashioned as flat plates had dark bluish coloration and very high boron

Figure 2. This 0.33 ct CVD-grown/natural diamond composite with a color equivalent to Fancy blue was previously described (Moe et al., 2017). DiamondView illumination clearly shows the interface between the lab-grown and natural components.



concentration (2500 ppb and higher). Also among that suite of flat-plate CVD samples was one with a black color caused by extremely high amounts of nitrogen-vacancy centers.

REFERENCES

- Angus J.C., Hayman C.C. (1988) Low-pressure, metastable growth of diamond and diamondlike phases. *Science*, Vol. 241, No. 4868, pp. 913–921.
- Ardon T., Eaton-Magaña S.C. (2018) Lab Notes: 15 carat HPHT synthetic diamond. *G&G*, Vol. 54, No. 2, pp. 217–218.
- Davis A. (2018) Washington, D.C., company grows 6-carat diamond. *National Jeweler*, Jan. 31, <https://www.nationaljeweler.com/diamonds-gems/supply/6267-washington-d-c-company-grows-6-carat-diamond>
- D'Haenens-Johansson U.F.S., Ardon T., Wang W. (2015) CVD synthetic gem diamonds with high silicon-vacancy concentrations. *Conference on New Diamond and Nano Carbons*, May 2015, Shizuoka, Japan.
- Eaton-Magaña S.C., Shigley J.E. (2016) Observations on CVD-grown synthetic diamonds: A review. *G&G*, Vol. 52, No. 3, pp. 222–245, <http://dx.doi.org/10.5741/GEMS.52.3.222>
- Moe K.S., Johnson P., D'Haenens-Johansson U.F.S., Wang W. (2017) Lab Notes: A CVD synthetic diamond overgrowth on a natural diamond. *G&G* Vol. 53, No. 2, pp. 237–239.
- Nad S., Gu Y., Asmussen J. (2015) Growth strategies for large and high quality single crystal diamond substrates. *Diamond and Related Materials*, Vol. 60, pp. 26–34, <http://dx.doi.org/10.1016/j.diamond.2015.09.018>
- Tang S., Su J., Lu T., Ma Y., Ke J., Song Z., Zhang J., Liu H. (2018) A thick overgrowth of CVD synthetic diamond on a natural diamond. *Journal of Gemology*, Vol. 36, No. 2, pp. 237–239.

Although new CVD products are continually being manufactured and introduced to the trade, the laboratory-grown diamonds examined to date by GIA can be readily identified.

Diamond Geology

Modern Advances in the Understanding of Diamond Formation



D. Graham Pearson

University of Alberta, Edmonton, Canada

For the past 50 years, the majority of diamond research has focused on diamonds derived from the lithospheric mantle root underpinning ancient continents. While lithospheric diamonds are currently thought to form the mainstay of the world's economic production, the continental mantle lithosphere reservoir comprises only ~2.5% of the total volume of Earth. Earth's upper mantle and transition zone, extending from beneath the lithosphere to a depth of 670 km, occupy a volume approximately 10 times larger.

Diamonds from these deeper parts of the earth—"superdeep diamonds"—are more abundant than previously thought. They appear to dominate the high-value large diamond population that comes to market. Recent measurements of the carbon and nitrogen isotope composition of superdeep diamonds from Brazil and southern Africa, using *in situ* ion probe techniques, show that they document the deep recycling of volatile elements (C, N, O) from the surface of the earth to great depths, at least as deep as the uppermost lower mantle. The recycled crust signatures in these superdeep diamonds suggest their formation in regions of subducting oceanic plates, either in the convecting upper mantle or the transition zone plus lower mantle. It is likely that the deep subduction processes involved in forming these diamonds also transport surficial hydrogen into the deep mantle. This notion is supported by the observation of a high-pressure olivine polymorph—ringwoodite—with close to saturation levels of water. Hence, superdeep diamonds document a newly recognized, voluminous "diamond factory" in the deep earth, likely producing diamonds right up to the present day. Such diamonds

also provide uniquely powerful views of how crustal material is recycled into the deep earth to replenish the mantle's inventory of volatile elements.

The increasing recognition of superdeep diamonds in terms of their contribution to the diamond economy opens new horizons in diamond exploration. Models are heavily influenced by the search for diamonds associated with highly depleted peridotite (dunites and harzburgites). Such harzburgitic diamonds were formed in the Archean eon (>2.5 Ga) within lithospheric mantle of similar age. It is currently unclear what the association is between these ancient lithospheric diamonds and large, high-value diamonds, but it is likely a weak one. In contrast, the strong association between superdeep diamonds and these larger stones opens up a new paradigm because the available age constraints for superdeep diamonds indicate that they are much younger than the ancient lithospheric diamonds. Their younger age means that superdeep diamonds may be formed in non-Archean mantle, or mantle that has been strongly overprinted by post-Archean events that would otherwise be deemed unfavorable for the preservation of ancient lithospheric diamonds.

An additional factor in the search for new diamond deposits is the increasing recognition that major diamond deposits can form in lithospheric mantle that is younger than—or experienced major thermal disruption since—the canonical 2.5 billion years usually thought to be most favorable for diamond production.

This talk will explore these new dimensions in terms of the potential for discovering new diamond sources in "unconventional" settings.

Diamond Precipitation from High-Density CHO Fluids

Thomas Stachel¹, Robert W. Luth¹, and Oded Navon²

¹University of Alberta, Edmonton, Canada

²Hebrew University, Jerusalem

Through research on inclusions in diamonds over the past 50 years, a detailed picture has emerged of the mineralogical and chemical composition of diamond substrates in Earth's mantle and of the pressure-temperature conditions during diamond formation. The exact diamond-forming processes, however, are still a subject of debate.

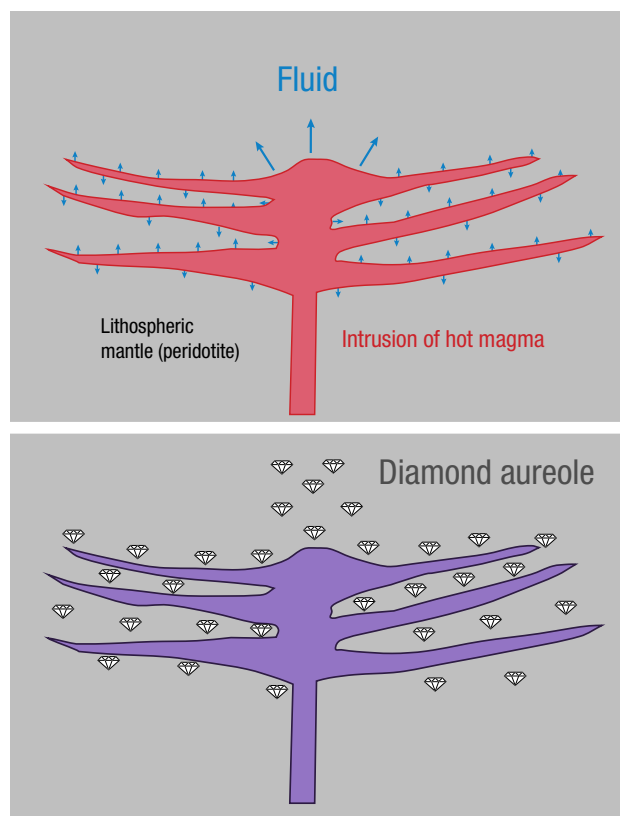
One approach to constrain diamond-forming processes is through model calculations that aim to obtain the speciation and the carbon content of carbon-hydrogen-oxygen (CHO) fluids at particular O/(O+H) ratios and pressure-temperature conditions (using GFluid of Zhang and Duan, 2010, or other thermodynamic models of fluids). The predictions of such model calculations can then be tested against carbon and nitrogen stable isotopes and nitrogen content fractionation models, based on *in situ* analyses across homogeneously grown diamond growth layers. Based on this approach, Luth and Stachel (2014) proposed that diamond precipitation occurs predominantly from cooling or ascending CHO fluids, composed of water with minor amounts of CO₂ and CH₄ (which in response to decreasing temperature may react to form diamond: CO₂ + CH₄ → 2C + 2H₂O).

The second approach focuses on constraining the diamond-forming medium by studying submicrometer fluid inclusions in fibrous-clouded and, more recently, gem diamonds. Such studies established the presence of four compositional end members of inclusions: hydrous-saline, hydrous-silicic, high-Mg carbonatitic, and low-Mg carbonatitic (e.g., Navon et al., 1988; Weiss et al., 2009). Although these fluid inclusions only depict the state of the diamond-forming medium after formation, they nevertheless provide unique insights into the major and trace-element composition of such fluids that otherwise could not be obtained.

The apparent dichotomy between the two approaches—models for pure CHO fluids and actual observation of impure fluids (so-called high-density fluids) in clouded and fibrous diamonds—relates to the observation that in high-pressure and high-temperature experiments close to the melting temperature of mantle rocks, hydrous fluids contain 10–50% dissolved solid components (e.g., Kessel et al., 2015). Although at this stage the impurity content in natural CHO fluids cannot be included in numerical models, the findings for clouded and fibrous diamonds are not in conflict with the isochemical diamond precipitation model. Specifically, the fact that observed high-density inclusions are often carbonate bearing is not in conflict with the relatively reducing redox conditions associated with the O/(O+H) ratios of modeled diamond-forming CHO fluids. The model for the minimum redox stability of carbonate-bearing melts of Stagno and Frost (2010) permits fluid carbonate contents of up to about 30% at such redox conditions.

Although additional data need to be obtained to build a thermodynamic model for CHO fluids with dissolved silicates and to better characterize the major and trace-element composition of high-density CHO fluids in equilibrium with typical diamond substrates (the rock types peridotite and eclogite), we already see sufficient evidence to suggest that the two approaches described above are converging to a unified model of isochemical diamond precipitation from cooling or ascending high-density CHO fluids.

Figure 1. This illustration depicts the isochemical precipitation of diamond in Earth's lithospheric mantle. Top: Intrusion of magma (ΔT to peridotitic wall rock is about +200°C) leads to release of hot CHO fluids from the crystallizing melt. As it infiltrates the peridotitic wall rock, the cooling fluid isochemically precipitates diamond. Bottom: After crystallization of the melt is completed, the intrusion is surrounded by an aureole of diamond, with temperature, volume, fluid content, and redox state of the melt all influencing the amount of diamond precipitated.



REFERENCES

- Kessel R., Fumagalli P., Pettko T. (2015) The behaviour of incompatible elements during hydrous melting of metasomatized peridotite at 4–6 GPa and 1000°C–1200°C. *Lithos*, Vol. 236–237, pp. 141–155, <https://doi.org/10.1016/j.lithos.2015.08.016>
- Luth R.W., Stachel T. (2014) The buffering capacity of lithospheric mantle: implications for diamond formation. *Contributions to Mineralogy and Petrology*, Vol. 168, No. 5, pp. 1–12, <https://doi.org/10.1007/s00410-014-1083-6>
- Navon O., Hutcheon I.D., Rossman G.R., Wasserburg G.J. (1988) Mantle-derived fluids in diamond micro-inclusions. *Nature*, Vol. 335, No. 6193, pp. 784–789, <https://doi.org/10.1038/335784a0>
- Stagno V., Frost D.J. (2010) Carbon speciation in the asthenosphere: Experimental measurements of the redox conditions at which carbonate-bearing melts coexist with graphite or diamond in peridotite assemblages. *Earth and Planetary Science Letters*, Vol. 300, No. 1–2, pp. 72–84, <https://doi.org/10.1016/j.epsl.2010.09.038>
- Weiss Y., Kessel R., Griffin W.L., Kiflawi I., Klein-BenDavid, O., Bell D.R., Harris J.W., Navon O. (2009) A new model for the evolution of diamond-forming fluids: Evidence from microinclusion-bearing diamonds from Kankan, Guinea. *Lithos*, Vol. 112 (Supplement 2), pp. 660–674, <https://doi.org/10.1016/j.lithos.2009.05.038>
- Zhang C., Duan Z.H. (2010) GFluid: An Excel spreadsheet for investigating C-O-H fluid composition under high temperatures and pressures. *Computers & Geosciences*, Vol. 36, No. 4, pp. 569–572, <https://doi.org/10.1016/j.cageo.2009.05.008>

How to Obtain and Interpret Diamond Ages

Steven B. Shirey¹ and D. Graham Pearson²

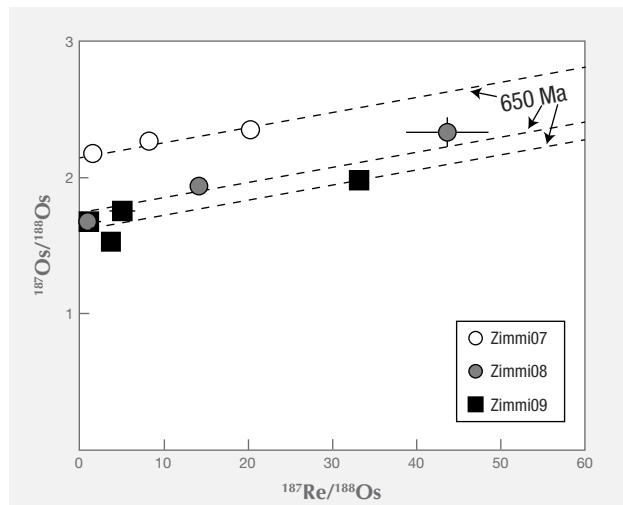
¹Carnegie Institution for Science, Washington, DC

²University of Alberta, Edmonton, Canada

Diamond ages are obtained from radiogenic isotopic analysis (Rb-Sr, Sm-Nd, Re-Os, and Ar-Ar) of mineral inclusions (garnet, pyroxene, and sulfide). As diamonds are xenocrysts that cannot be dated directly, the ages obtained on mineral inclusions provide a unique set of interpretive challenges to assure accuracy and account for preexisting history. A primary source of geological/mineralogical uncertainty on diamond ages is any process affecting protogenetic mineral inclusions before encapsulation in the diamond, especially if it occurred long before diamond formation. In practical application, the isotopic systems discussed above also carry with them inherent systemic uncer-

tainties. Isotopic equilibrium is the essential condition required for the generation of a statistically robust isochron. Thus, isochron ages from multiple diamonds will record a valid and accurate age when the diamond-forming fluid promotes a large degree of isotopic equilibrium across grain scales, even for preexisting (“protogenetic”) minerals. This clearly can and does occur. Furthermore, it can be analytically tested for, and has multiple analogues in the field of dating metamorphic rocks. In cases where an age might be suspect, an age will be valid if its regression uncertainties can encompass a known and plausible geological event (especially one for which an association exists between that

Figure 1. Left: Re-Os isotopic compositions for 10 sulfides from three Zimmi diamonds all fall along 650 Ma age arrays. Each diamond had multiple sulfides that lay on arrays of identical age, giving unequivocal evidence for the age and showing that these diamonds formed in the same episode of diamond formation. Right: Plane polarized light image of a typical sulfide inclusion in a polished Zimmi diamond plate. Note that this diamond only contains one inclusion, whereas analyses of three to four inclusions per diamond are shown in the plot on the left. From Smit et al. (2016), used with permission.



event and the source of diamond-forming fluids) and petroge-
netic links can be established between inclusions on the isochron.

Diamonds can be dated in six basic ways:

1. model ages
2. radiogenic daughter Os ages (common-Os-free)
3. single-diamond mineral isochrons
4. core to rim ages
5. multiple single-diamond isochron/array ages
6. composite isochron/array ages

Model ages (1) are produced by the intersection between the evolution line for the inclusion and a reference reservoir such as the mantle. The most accurate single-diamond age is determined on a diamond with multiple inclusions (3). In this case an internal

isochron can be obtained that not only establishes equilibrium among the multiple grains but also unequivocally dates the time of diamond growth. With extreme luck in obtaining the right diamond, concentric diamond growth zones visible in UV fluorescence or cathodoluminescence can sometimes be shown to constrain inclusions to occur in the core of the diamond and in the exterior at the rim. These single grains can be extracted to give a minimum growth time (4) for the diamond. In optimal situations, multiple inclusions are present within single growth zones, in single diamonds, allowing internal isochrons to be constructed for individual growth zones in single diamonds. If enough diamonds with inclusions can be obtained for study, valid ages for diamond populations can be obtained on multiple single-diamond ages that agree (5) or on composited, mineralogically similar inclusions to give an average age (6).

REFERENCE

Smit K.V., Shirey S.B., Wang W. (2016) Type Ib diamond formation and preservation in the West African lithospheric mantle: Re–Os age constraints from

sulphide inclusions in Zimmi diamonds. *Precambrian Research*, Vol. 286, pp. 152–166, <http://dx.doi.org/10.1016/j.precamres.2016.09.022>

The Lesedi La Rona and the Constellation— The Puzzle of the Large Rough Diamonds from Karowe

Ulrika F.S. D'Haenens-Johansson
GIA, New York

In November 2015, Lucara Diamond's operation at the Karowe mine in Botswana gained notoriety due to the extraction of a series of large colorless diamonds, including the 1,109 ct Lesedi La Rona and the 812 ct Constellation. The Lesedi La Rona marks the largest gem diamond recovered since the Cullinan (3,106 ct) in 1905. The Constellation, considered to be the seventh-largest recorded diamond, attained the highest price ever paid for a rough, selling for \$63.1 million (\$77,649 per carat). Additionally, three other significant colorless diamonds were recovered during the same period, weighing 374, 296, and 183 ct. Due to the similarity in their external characteristics—which include cleavage faces—as well as their extraction locations and dates, it was suspected that these stones might have originated from a larger rough that had broken. Lucara demonstrated that the 374 ct diamond and the Lesedi La Rona fit together, yet a large cleavage plane is still unaccounted for. GIA was able to study several rough and/or faceted pieces of these five diamonds using a range of spectroscopic and imaging techniques to gain insight into the presence and distribution of point defects in these diamonds.

Diamonds are commonly classified according to their nitrogen content measured by Fourier-transform infrared (FTIR) spectroscopy: Type I diamonds contain nitrogen in either isolated (Ib) or aggregated (IaAB) forms, while type II diamonds do not contain detectable nitrogen concentrations (IIa) but may contain boron (IIb). Analysis of faceted stones cut from the Lesedi La Rona indicates that the rough is a mixed-type diamond, containing both type

IIa and pure type IaB regions. These types of diamonds, though exceedingly unusual, have been observed at GIA and reported by De-launay and Fritsch (2017). The Constellation and the 374, 296, and 183 ct diamonds were determined to be type IaB, containing 20 ± 4 ppm B-aggregates (N_4V), in agreement with the concentration for the type IaB pieces of the Lesedi La Rona. Pure type IaB diamonds such as these are actually quite rare, accounting for only 1.2% of a random suite of 5,060 large (>10 ct) D-to-Z diamonds submitted to GIA, whereas 24.6% were type II. Photoluminescence spectra further confirmed analogous defect content for the five large Karowe diamonds, with emissions from H4 ($N_4V_2^0$, 496 nm), H3 (NVN^0 , 503 nm), 505 nm, NV^- (637 nm), and GR1 (V^0 , 741 nm) defects showing similar relative intensities and peak widths. Even for diamonds of the same type, parallel defect content and characteristics across such a variety of defects is unlikely for unrelated stones.

The external morphologies of the diamonds showed primary octahedral, resorbed, and fractured faces, with the Constellation and the 296 ct diamond featuring fractures containing metallic inclusions and secondary iron oxide staining. Deep UV fluorescence (<230 nm) imaging elucidated the internal growth structures of the samples. For the Constellation and the 374, 296, and 183 ct diamonds, at least two growth zones with differing blue fluorescence intensities were observed within single pieces.

Combined with the spectroscopic data, these results provide

compelling evidence that the Lesedi La Rona, the Constellation, and the 374, 296, and 183 ct diamonds from Karowe had com-

parable growth histories and likely originated from the same rough, with a combined weight of at least 2,774 ct.

REFERENCE

Delaunay A., Fritsch E. (2017) A zoned type IaB/IIa diamond of probable “superdeep” origin. *Journal of Gemmology*, Vol. 35, No. 5, pp. 397–399.

Gem Characterization

The Formation of Natural Type IIa and IIb Diamonds

Evan M. Smith and Wuyi Wang

GIA, New York

Many of the world’s largest and most valuable gem diamonds exhibit an unusual set of physical characteristics. For example, in addition to their conspicuously low nitrogen concentrations, diamonds such as the 3,106 ct Cullinan (type IIa) and the Hope (type IIb, boron bearing) tend to have very few or no inclusions, and in their rough state they are found as irregular shapes rather than as sharp octahedral crystals. It has long been suspected that type IIa and IIb diamonds form in a different way than most other diamonds.

Over the past two years, systematic investigation of both type IIa and IIb diamonds at GIA has revealed that they sometimes contain rare inclusions from unique geological origins. Examination of more than 130 inclusion-bearing samples has established recurring sets of inclusions that clearly show many of these diamonds originate in the sublithospheric mantle, much deeper in the earth than more common diamonds from the cratonic lithosphere. We now recognize that type IIa diamonds, or more specifically, diamonds with characteristics akin to the historic Cullinan diamond (dubbed CLIPPIR diamonds), are distinguished by the occurrence of iron-rich metallic inclusions. Less frequently, CLIPPIR diamonds also contain inclusions of majoritic garnet and former CaSiO_3 perovskite that constrain the depth of formation to within 360–750 km. The inclusions suggest that CLIPPIR diamonds belong to a unique paragenesis with an intimate link to metallic iron in the deep mantle (Smith et al., 2016, 2017). Similarly, findings from type IIb diamonds also place them in a “superdeep” sublithospheric mantle setting, with inclusions of former CaSiO_3 perovskite and other high-pressure minerals, although the iron-rich metallic inclusions are generally absent (Smith et al., 2018). Altogether, these findings show that high-quality type II gem diamonds are predominantly sourced from the sublithospheric mantle, a surprising result that has

refuted the notion that all superdeep diamonds are small and non-gem quality. Valuable information about the composition and behavior of the deep mantle is cryptically recorded in these diamonds. CLIPPIR diamonds (figure 1) confirm that the deep mantle contains metallic iron, while type IIb diamonds suggest that boron and perhaps water can be carried from the earth’s surface down into the lower mantle by plate tectonic processes. In addition to being gemstones of great beauty, diamonds carry tremendous scientific value in their unique ability to convey information about the interior of our planet.

Figure 1. Measuring about 7 cm across, this 404.2 ct rough from Angola’s Lulo mine is a good example of the irregular shape and surface texture associated with CLIPPIR diamonds. The unusual characteristics of diamonds like this one are the result of formation in a unique geological setting. Once cut, this rough yielded a 163.4 ct flawless D-color diamond. Photo by Jian Xin (Jae) Liao.



REFERENCES

Smith E.M., Shirey S.B., Nestola F., Bullock E.S., Wang J., Richardson S.H., Wang W. (2016) Large gem diamonds from metallic liquid in Earth’s deep mantle. *Science*, Vol. 354, No. 6318, pp. 1403–1405, <http://dx.doi.org/10.1126/science.aal1303>

Smith E.M., Shirey S.B., Wang W. (2017) The very deep origin of the world’s biggest diamonds. *G&G*, Vol. 53, No. 4, pp. 388–403, <http://dx.doi.org/>

10.5741/GEMS.53.4.388

Smith E.M., Shirey S.B., Richardson S.H., Nestola F., Bullock E.S., Wang J., Wang W. (2018) Blue boron-bearing diamonds from Earth’s lower mantle, *Nature*, Vol. 560, No. 7716, pp. 84–87, <http://dx.doi.org/10.1038/s41586-018-0334-5>



Colored Diamonds: The Rarity and Beauty of Imperfection

Christopher M. Breeding
GIA, Carlsbad, California

Diamond is often romanticized as a symbol of purity and perfection, with values that exceed all other gemstones. However, even the most flawless and colorless natural diamonds have atomic-level imperfections. Somewhat ironically, the rarest and most valuable gem diamonds are those that contain abundant impurities or certain atomic defects that produce beautiful fancy colors such as red, blue, or green—stones that can sell for millions of dollars per carat.

Atomic defects can consist of impurities such as nitrogen or boron that substitute for carbon atoms in the diamond atomic structure (resulting in classifications such as type Ia, type Ib, type IIa, and type IIb) or missing or misaligned carbon atoms. Some defects are created during diamond growth, while others are generated over millions to billions of years as the diamond sits deep in the earth at high temperatures and pressures. Defects may be created when the diamond is rapidly transported to the earth's surface or by interaction with radioactive fluids very near the earth's surface. Each defect selectively absorbs different wavelengths of light to produce eye-visible colors. Absorptions from these color-producing defects (or color centers) are detected and identified using the gemological spectroscope or more sensitive absorption spectrometers such as Fourier-transform infrared (FTIR) or ultraviolet/visible/near-infrared (UV-Vis-NIR; figure 1). Some defects not only absorb light but also produce their own luminescence, called fluorescence. For example, the same defect that produces “cape” yellow diamonds also generates blue fluorescence when exposed to ultraviolet light. In some cases, the fluorescence generated by defects can be strong enough to affect the color of gem diamonds.

Figure 1. Visible-NIR spectra reveal the absorptions and corresponding atomic defects responsible for the color in gem diamonds.

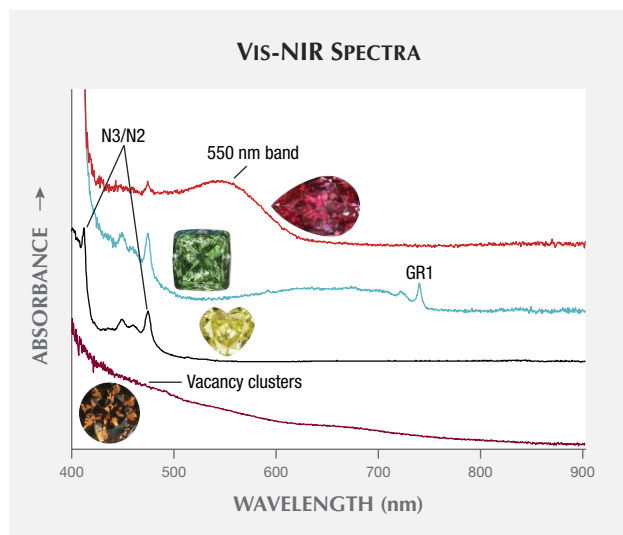


TABLE 1. Most common causes of color in gem diamond.

Color	Cause of color (defect structure)	When imparted
Yellow	N3/N2 “cape” (3NV)	Residence at high T and P
	Isolated nitrogen “C centers” (N)	Growth
	H3 absorption (2NV ⁰)	Residence at high T and P
	Hydrogen (unknown)	Growth
	480 nm band (unknown)	Growth? (unknown origin)
Brown	Vacancy clusters (multiple V)	Transport/residence at high T and P
	Isolated nitrogen “C centers” (N)	Growth
	H3 absorption (2NV ⁰) + 550 nm band (unknown)	Residence at high T and P
	Hydrogen (unknown)	Growth
Orange	H3 absorption (2NV ⁰) + 550 nm band (unknown)	Transport/residence at high T and P
	480 nm band (unknown)	Growth? (unknown origin)
	Isolated nitrogen “C centers” (N)	Growth
Red/Pink	Plastic deformation—550 nm band (unknown)	Transport/residence at high T and P
	Nitrogen-vacancy (NV ⁰ , NV ⁻)	Residence at high T and P
Violet/Purple	Hydrogen (unknown)	Growth
	Plastic deformation—550 nm band (unknown)	Transport/residence at high T and P
Green	Radiation damage—GR1 (V ⁰)	Radioactive fluids—low T and P
	H3 fluorescence (2NV ⁰)	Residence at high T and P
	Hydrogen (unknown)	Growth
	Nickel (Unknown)	Growth
Blue	Boron (B)	Growth
	Radiation damage—GR1 (V ⁰)	Radioactive fluids—low T and P
	Hydrogen (unknown)	Growth

With the exception of most natural white and black diamonds, where the color is a product of inclusions, colored diamonds owe their hues to either a single type of defect or a combination of several color centers. More than one type of defect can produce a particular color, however. Table 1 provides a list of the most common causes of color in diamond.

Subtle differences in atomic defects can drastically affect a diamond's color. For example, isolated atoms of nitrogen impurities usually produce strong yellow color (“canary” yellow diamonds). If those individual nitrogen atoms occur together in pairs, no color is generated and the diamond is colorless. If instead the individual nitrogen atoms occur adjacent to missing carbon atoms (vacancies), the color tends to be pink to red. Rearrangement of diamond defects is the foundation of using treatments to change the color of diamond. Identification of treatments and separation of natural and synthetic diamond requires a thorough understanding of the atomic-level imperfections that give rise to diamond color and value.

Evaluating the Color and Nature of Diamonds Via EPR Spectroscopy

Haim Cohen¹ and Sharon Ruthstein²






¹Ariel University and Ben-Gurion University of the Negev, Israel

²Bar-Ilan University, Israel

Diamond characterization is carried out via a wide variety of gemological and chemical analyses. An important analytical tool for this purpose is spectroscopic characterization utilizing both absorption and emission measurements. The main techniques are UV-visible and infrared spectroscopy, though Raman as well as cathodoluminescence spectroscopy are also used.

We have used electron paramagnetic resonance (EPR) spectroscopy to compare the properties of treated colored diamonds to the pretreated stones. The colors studied were blue, orange, yellow, green, and pink. The EPR technique determines radicals (atoms with unpaired electrons) and is very sensitive, capable of measuring concentrations as low as $\sim 1 \times 10^{-17}$ radicals/cm³. The results, shown in table 1, indicate that all the carbon radicals determined are affected by adjacent nitrogen atoms, with the spectra showing a hyperfine structure attributed to the presence of nitrogen. The highest concentration of radicals and hyperfine structures is observed in pink and orange treated diamonds. The results concerning nitrogen concentration were correlated with

TABLE 1. Distribution of radical concentration in treated colored diamonds.

Blue	40% N	60% C	
Orange	2% N	98% C	
Yellow	8% N	92% C	
Green	2% N	98% C	
Pink	1.8% N	98.2% C	

the infrared spectra, which determine the absorption peaks of the diamonds as well as those of the nitrogen contamination in their crystal structure.

Quantitative Absorption Spectrum Reconstruction for Polished Diamond

Roman Serov (presented by Sergey Sivovolenko)

OctoNus Software, Moscow

Natural diamonds generally exhibit a very wide range of spectra. In polished stones, absorption along with proportions and size define perceived diamond color and thus beauty.

In rough diamonds, the quantitative absorption spectrum (the “reference spectrum” in the context of this article) can be measured using an optical spectrometer through a set of parallel windows polished on a stone, so the diamond can be considered a plane-parallel plate with known thickness.

Polished diamonds lack the parallel facets that might allow plane-parallel plate measurement. That is why polished diamond colorimetry uses one of two approaches that have certain limitations for objective color estimation:

- *Qualitative spectrum assessment with an integrating sphere.* Suppose three diamonds are polished from a yellow rough with even coloration: a round (with short ray paths), a cushion (with high color uniformity and long ray paths), and a “bow tie” marquise (with both long and short ray path areas). The spectra captured from these three stones by an integrating sphere will be completely different because the ray paths are very different. However, the quantitative absorption spectrum will be the same for all three stones, since they are cut

from the same evenly colored rough. Therefore, spectrum assessment with an integrating sphere has very limited accuracy and is practical for qualitative estimations only.

- *Analysis of multiple images of a diamond made by color RGB camera.* This method has low spectral resolution defined by digital camera color rendering. The camera has a smaller color gamut than the human eye, so most fancy-color diamonds are outside the color-capturing range of a digital camera.

However, quantitative absorption data is very valuable for:

- Color prediction and optimization for a new diamond after a recut process
- Objective color assessment and description of a polished diamond

This paper presents a new technology based on spectral light-emitting diodes (LEDs) and high-quality ray tracing, which together allow the reconstruction of a quantitative absorption spectrum for a polished diamond. The approach can be used for any transparent polished diamond. The recent technology prototype has a resolution of 20–60 nm, which is practical for color assessment.

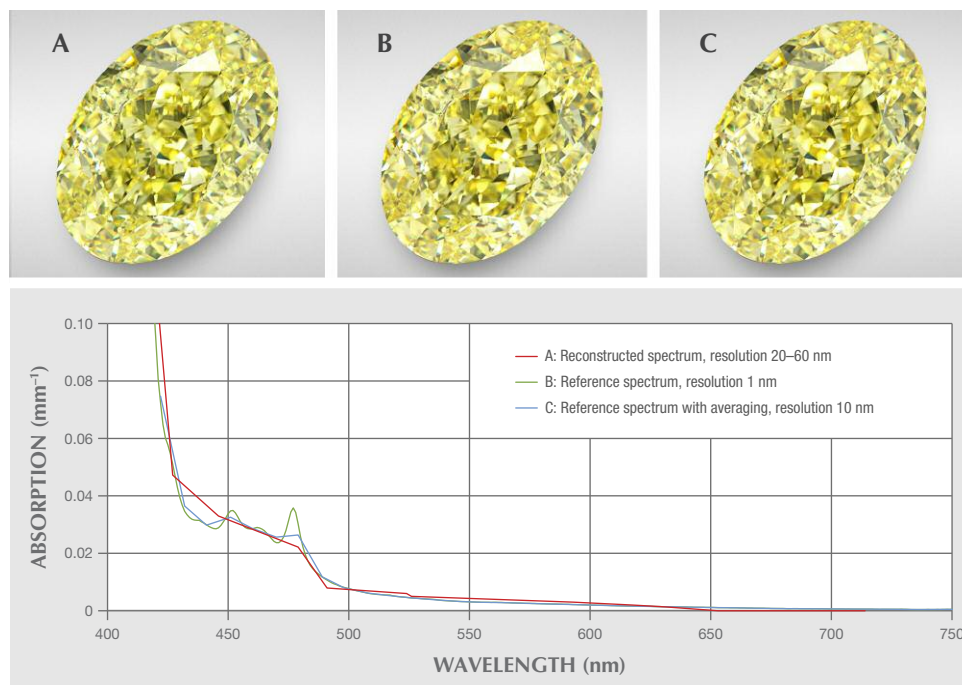


Figure 1. Top: Photorealistic diamond images generated from the reconstructed absorption spectrum (A), the reference spectrum (B), and the averaged reference spectrum (C) of the same stone. Bottom: Quantitative and reconstructed absorption spectra.

Figure 1 (top) presents three photorealistic diamond images: A is based on the reconstructed absorption spectrum collected from a polished diamond, B uses the reference spectrum collected in the rough stage through a pair of parallel windows, and C uses the averaged reference spectrum. Figure 1 (bottom) shows both measured

quantitative absorption and reconstructed absorption spectra.

This technology has the potential to ensure very close to objective color estimation for near-colorless and fancy-color polished diamonds. The reconstructed spectrum resolution can be enhanced to 10–15 nm in future devices.

Gem Localities

Scientific Study of Colored Gem Deposits and Modern Fingerprinting Methods

Lee Groat

University of British Columbia, Vancouver, Canada

Most colored gemstones form near the earth's surface in a wide range of different environments; for example, they can crystallize from igneous magmas or hydrothermal solutions, or via the recrystallization of preexisting minerals during metamorphism. The specific environment determines the types of gem minerals that form, as well as their physical and chemical properties. Field studies of colored gem deposits provide the basis for the scientific understanding of natural gemstone formation and, in turn, the basis for gem identification.

Gem deposits are of scientific interest because they represent unusual geologic and geochemical conditions; for example, emeralds are rare because they require beryllium and chromium (and/or vanadium), which generally travel in very different geochemical circles. Scientists study gem deposits by collecting rock and mineral samples in the field, mapping geological formations and structures, documenting the environment in which the gems

occur, and examining the collected samples back in the laboratory. Such examination yields information on the chemical, temperature, and pressure conditions of gem formation, the associated minerals (often found as distinctive inclusions in the gems themselves), and the age of the deposit. Determining the origin of a gem deposit usually requires a small amount of very specific data. The results are published in publicly available peer-reviewed publications. Such field studies provide clues that can be used to explore for similar types of gem deposits. Challenges include the remoteness of locations that have not been previously studied by geologists, the small size of deposits that precludes study by large mining companies, and the rarity of the gems themselves.

There is much left to do in gem deposit research. For example, despite its growing popularity as a gemstone, there are few studies of gem spinel deposits, especially cobalt-blue spinel (figure 1), for



which only one deposit has been studied. To date we know little about what factors control spinel genesis and color.

Recently there has been another reason to study gem deposits: gem fingerprinting, in which modern methods are used to obtain characteristic information. This information is then compared to information obtained from stones from known localities to estimate where a stone with no locality information originated.

Modern fingerprinting methods analyze the chemistry of the stones (using electron probe microanalysis, isotopic analysis, laser ablation–inductively coupled plasma–mass spectrometry) and/or their solid and fluid inclusions. We know that the chemistry of the stones must reflect the chemistry of the host rock environment; for example, the chromophore in emerald from Lened in Canada is vanadium, and not the typical chromium, because there are no chromium-bearing rocks in the area. With respect to solid inclusions, rubies from Aappaluttoq in Greenland have phlogopite mica inclusions because they recrystallized in a rock at pressures and temperatures where phlogopite is the stable potassium-bearing phase. An example of diagnostic fluid inclusions is the three-phase variety seen in Colombian emeralds (and now also observed elsewhere). New is the use of ICP-MS on fluid inclusions to define part of the fluid assemblage from which the stones were formed; this tells us about the environment of formation, but also may assist in defining a fingerprint for the stone.

Where scientific studies require only very specific data, the more data available from stones of known origin, and the more representative those stones are of the full range of compositions



Figure 1. Cobalt-blue gem spinel from Baffin Island, Nunavut, Canada. Photo by Lee Groat.

and inclusions found in a specific deposit or country of origin, the more accurate the estimation should be. Unfortunately, these data are generally not made public, so every lab doing fingerprinting is essentially working independently, and there is no way to know how accurate their data and the resulting country- or deposit-of-origin estimates are. We also note that a serious problem in origin determination is that some of the best gemstones will be lacking diagnostic inclusions altogether, which then restricts the tools and observations can be used.

Gem Pegmatites of Ukraine, Russia, Afghanistan, and Pakistan: An Update on Recent World-Class Finds

Peter Lyckberg

National Museum of Natural History, Luxembourg

Soviet-era exploration and mining of some 1,900 chamber pegmatites on the western endo-contact of the 1.7 Ga Korosten Pluton in Ukraine for piezo quartz left an underground mine with 110 km tunnels reached by six shafts. Since 1995, increasingly intensified study of old pockets and documentation by Vsevolod Chournousenko, chief geologist of Volhyn Kwarts (Quartz) Samotsvety Company, has revealed new targets. Work on these targets has produced gem-quality beryl and topaz, the latter in record-size crystals up to 230 and 325 kg. Topaz occurred in around 10% of mined pockets.

For the first time in the history of the huge deposit, the “Peter’s Dream Pocket” was found and exploited from January 2013 through January 2014. It contained bicolor topaz still *in situ* growing on cleavelandite, associated with zinnwaldite and smoky quartz. The largest topaz, at 325 kg, was named *dedushka* (grandfather). The Skorkina pocket in the mine was also called “Vsevolod’s Pocket” after

the extraordinary chief geologist who found the topaz mineralization, which yielded a record amount of gem topaz crystals. These came from a depth of 6 to 15 m under the floor, where previous Soviet quartz mining efforts had missed them. The largest of these, the cognac-colored “Sergei” (named after the mine owner), weighs 230 kg and is the largest of its kind. Gem-quality bicolor topaz in large sizes, found particularly in shaft 3 and in open pits in the south and north end of the pegmatite field, is unique to this mine. Extraordinary heliodor crystals were mined in Soviet times, and a smaller quantity mined later yielded faceted stones up to 2,500 ct. A recently mined deep cognac-colored cut topaz weighed 9,000 ct. Natural blue and bicolor topaz (figure 1) have been cut to unique stones, also of large sizes. The color spectrum of topaz and beryl from these pegmatites is amazing.

Lyckberg et al. (2009) noted that gem beryl occurs in only 2% of the approximately 1,900 chamber pegmatites that were mined.

Pegmatite 521 at 90 m depth, accessed from shaft 2, produced over two tons of gem beryl. Over one ton was exploited in 1982 and in 1992, over the course of five days, five miners excavated 900 kg in a green clay zone. Ninety percent of these specimens were of gem quality. In the same pegmatite, a second pocket produced 100 tons of quartz in the 1980s. During the spring of 2018, exploration of this pocket yielded a giant quartz crystal measuring 1.5 m in diameter. The pocket was found to also contain topaz pseudomorphs.

In neighboring Russia, gem aquamarine was produced in 2017 at Sherlova Mountain and sold to China, while in the Ural Mountains only small quantities for collectors were found. Here the last Russian underground gem pegmatite mine, the Kazionnitsa, closed in 1993. In the Malkhansk Mountains, tourmaline-rich lithium pegmatites with quality rubellite crystals were recovered during 2012–2018 at the Sosedka pegmatite. They were a deep red to purplish red color in crystals up to 35 cm in matrix, while gem-quality specimens measured up to 10–15 cm. Many of these crystals are reminiscent of the rubellite from the Jonas mine in Brazil, although the cranberry red color is not quite as intense. Several other pegmatite veins started to produce again, primarily green tourmaline.

The Hindu Kush pegmatites of Afghanistan discovered at Kala and Paprok villages in 1959 and 1969 have again yielded large quantities of gem tourmaline in a rainbow of colors. The huge Mawi and Kanakana pegmatites both produced large quantities of gem kunzite, gem indicolite, and rare morganites. Gem-quality pollucite and other rare species such as manganotantalite were found at Paprok and in the Pech Valley. Kanakana and several other pegmatites produced large morganites with aquamarine cores in crystals up to 25 cm in diameter growing on lepidolite and cleavelandite. The pegmatite field of Waygal produced perhaps the finest single 7 kg kunzite crystal of any find, a flawless 55 cm twinned deep purple crystal with blue 10 cm termination in a pocket with 10 kg other gem-quality crystals.

The Karakorum Mountains of Pakistan have continued to produce large quantities of aquamarine and champagne-colored topaz. Please note that beryl and topaz in these very young 4 to 12 Ma pegmatites have not yet been exposed to radiation from K40 in the feldspars or from U/Th-containing minerals during this short time span. Thus, deeply colored yellow heliodor, blue topaz, and deep or-



Figure 1. This naturally bicolored topaz, measuring 15 cm across, has eye-visible white fluorite inclusions. It was mined from pegmatite 253 (open pit) in 2017. Photo by Albert Russ, courtesy of Volhyn Kwarts (Quartz) Samotsvety Company.

ange topaz are not to be expected here, simply because they have not had a chance to attain those colors (Unpublished data by the author, 1997). Those colors are typical for pegmatites one or two magnitudes older.

Gem-quality rare species mined include large colorless to light lilac gem pollucite (10–40 cm), amblygonite, manganotantalite, various microlites, triplite, green hydroxylherderite, beryllonite in cogwheel crystals up to 35 cm, and värynenite in orange-red gem crystals up to 22 cm long. The area around Shengus and Bulochi, by the Indus River between Nanga Parbat and Haramosh Peak, is the main producer of the rarer species. Since 1985, known hydrothermal mica-lined fissures at Chumar Bakhloor (Unpublished data by the author, 1988; Lyckberg et al., 2013) have been a major source of matrix aquamarine specimens, large crystals for carvings, and much cabochon and bead material, as well as large pink and green gem-quality fluorite, some of which have been faceted.

REFERENCES

- Lyckberg P., Chournousenko V.A., Wilson W.E. (2009) Famous mineral localities: Volodarsk-Volhynsk, Zhitomit Oblast, Ukraine. *The Mineralogical Record*, Vol. 13, No. 6, pp. 11–22.
- Lyckberg P., Chournousenko V., Hmyz A. (2013) Chamber pegmatites of Volodarsk, Ukraine, the Karelia beryl mine, Finland and shallow depth vein peg-

matites of the Hindukush-Karakorum mountain ranges. Some observations on formation, inner structures, rare and gem crystals in these oldest and youngest pocket carrying gem pegmatites on Earth. In *Contributions to the 6th International Symposium on Granitic Pegmatites*, pp. 81–83, http://pegmatology.uno.edu/news_files/PEG2013_Abstract_Volume.pdf

A Multidisciplinary Approach Toward Examining the Sources of Emeralds

Raquel Alonso-Perez¹, Adriana Heimann-Rios², James M.D. Day³, Daniel X. Gray², Antonio Lanzirotti⁴, Darby D. Dyar⁵, and J.C. "Hanco" Zwaan⁶

¹Harvard University, Cambridge, Massachusetts

²East Carolina University, Greenville, North Carolina

³Scripps Institution of Oceanography, La Jolla, California

⁴The University of Chicago, Argonne, Illinois

⁵Mount Holyoke College, South Hadley, Massachusetts

⁶Naturalis Biodiversity Center (National Museum of Natural History), Leiden, The Netherlands

Modern analytical capabilities now allow the combination of non-destructive geochemical and structural studies of emeralds, in addition to detailed studies of their inclusions, to enhance our knowledge of their genesis. Here we present a combination of (1) X-ray absorption near-edge structure (XANES), to determine local coordination environment and oxidation state of the main emerald chromophores Fe, V, and Cr; (2) Raman spectroscopy, with special emphasis on the correlation between H₂O molecules and alkali site occupancy; and (3) inductively coupled plasma–mass spectrometry (solution-ICP-MS) to examine the role of major, minor, and trace elements during emerald formation. Our aim is to develop a systematic approach to characterizing emeralds by identifying key geochemical and structural features that enable provenance and geological origin of emerald deposits to be determined.

In this study, we analyzed 31 emeralds from the Mineralogical & Geological Museum, Harvard University. Preliminary XANES results indicate that chromium is present as Cr³⁺, although crystal orientation dependence and beryl crystal structural behaviors need to be assessed in detail. Raman spectroscopy results of the OH-stretching vibrations at higher frequencies (3500–3700 cm⁻¹), corresponding to H₂O type II and type I, respectively, display an orientation dependence. For a given orientation, there is an increase in intensity of the OH-stretching vibration, and therefore H₂O concentration, from Colombian to Zambian emeralds. A strong correlation of peak shape and position of the OH-stretching vibration with three major geochemical indices is also observed. Vanadium concentrations correlate positively with Ge, Rb, Cs, and Lu, and they can be used to distinguish three emerald groups based on their geochemistry: (1) Colombia; (2) South Africa, Nigeria, and Egypt; and (3) Brazil, Madagascar, and Zambia. Whereas a smooth transition occurs from group 2 to group 3, group 1 Colombian emeralds are highly distinctive. The distinctiveness of Colombian emerald indicates the potential for using trace-element abundances to examine geological formation (see figure 1). For example, ratios such as Ga/Rb versus Hf/Ta are also characteristic of each different emerald formation. The combination of XANES, Raman spectroscopy, and ICP-MS studies offers significant utility for not only refining the crystal structure of emeralds but also defining markers for different sources.

For a given orientation, there is an increase in intensity of the OH-stretching vibration, and therefore H₂O concentration, from Colombian to Zambian emeralds. A strong correlation of peak shape and position of the OH-stretching vibration with three major geochemical indices is also observed. Vanadium concentrations correlate positively with Ge, Rb, Cs, and Lu, and they can be used to distinguish three emerald groups based on their geochemistry: (1) Colombia; (2) South Africa, Nigeria, and Egypt; and (3) Brazil, Madagascar, and Zambia. Whereas a smooth transition occurs from group 2 to group 3, group 1 Colombian emeralds are highly distinctive. The distinctiveness of Colombian emerald indicates the potential for using trace-element abundances to examine geological formation (see figure 1). For example, ratios such as Ga/Rb versus Hf/Ta are also characteristic of each different emerald formation. The combination of XANES, Raman spectroscopy, and ICP-MS studies offers significant utility for not only refining the crystal structure of emeralds but also defining markers for different sources.

REFERENCE

Rudnick R.L., Gao S. (2004) Composition of the continental crust. In H.D. Holland and K.K. Turekian, Eds., *Treatise on Geochemistry. Vol. 3, The Crust*, Elsevier-Pergamon, Oxford, UK, pp. 1–64.

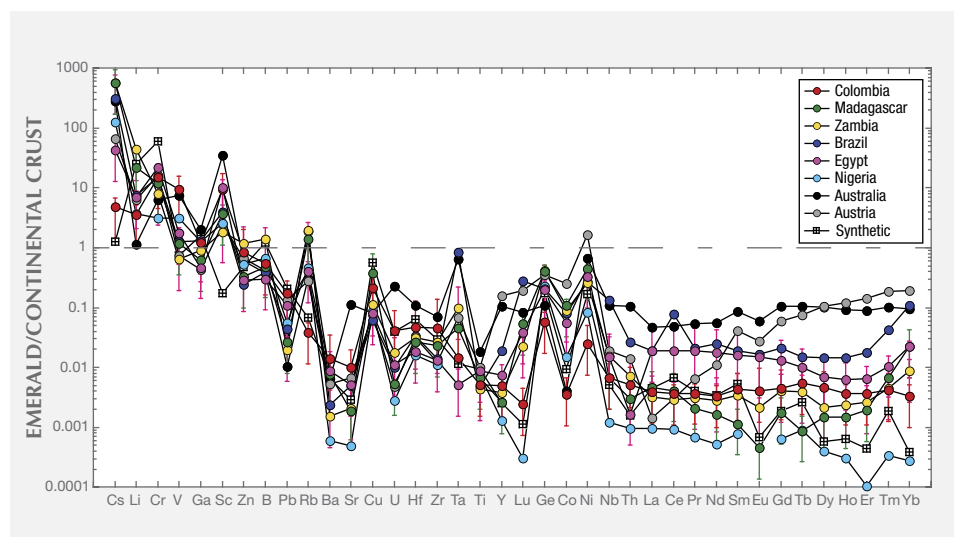


Figure 1. Multi-incompatible trace element plot normalized to bulk continental crust (Rudnick and Gao, 2004) for emeralds from Colombia, Madagascar, Zambia, Brazil, Egypt, Nigeria, Australia, and Austria, as well as synthetic emeralds.

The Proof of Provenance

Klemens Link

Gübelin Gem Lab, Lucerne, Switzerland

Consumers now demand more transparency on the provenance of the goods and services they purchase, an expectation that also applies to luxury products such as gemstones. Yet the gemstone trade has a reputation of being opaque. The Gübelin Gem Lab has kicked off a long-term initiative dedicated to closing this gap. Under the label Provenance Proof, technologies are developed that allow gemstones to be traced back to specific mines in order to provide more transparency throughout the chain of custody. The Provenance Proof initiative is independent of the traditional lab work, and all technologies are made available to the entire industry.

The first technology developed under the Provenance Proof initiative is referred to as the Emerald Paternity Test. The Gübelin Gem Lab has developed a physical tracer using nanolabels to suit the needs of the gemstone industry. These nanolabels are based on DNA fragments encapsulated in silica; with a diameter of 100 nm, they are invisible even to the most powerful optical micro-

scope. The identity of the mine and the miner, the exact location, the time period, and possibly further information are encoded into the DNA. The use of such labels allows the miner to tap the full potential of storytelling about specific provenance, including the possibility of independent proof of this source.

The nanotracers allow the tracing of a gemstone from the end consumer back to the original mine. Nevertheless, the other steps along the value chain remain nontransparent. To shed light on the entire value chain, we developed a digital logbook that allows the user to document all steps and transactions linked to a particular gemstone on its way from the mine to the end consumer. The backbone of this logbook is a hyperledger-based, community-controlled blockchain that is open to the entire industry and accessible with a smartphone. All data is securely encrypted and decentralized and only available to the holder or custodian of a specific gemstone.

General Gemology and Jewelry

Gemstones and Sustainable Livelihoods: From Mines to Markets



Saleem H. Ali

Gemstones and Sustainable Development Knowledge Hub, University of Delaware, Newark

Colored gemstone supply chains are highly fragmented. The large variety of gemstones found in the trade, each with different mining and manufacturing issues and production cycles, adds to this complexity. Yet this fragmentation also creates opportunities for diffuse positive impacts in livelihood formation across the supply chain. Gemstones are predominantly mined through artisanal and small-scale mining (ASM) operations, and many of those who mine the stones remain in poverty. Furthermore, the mining is often undertaken without any mechanism for environmental remediation that can sustain livelihoods beyond the mining phase. In a sector that ranges over 50 producing countries, with a multitude of cultures, environments, and minerals, much research remains to be done on how sustainability can be improved and catalyzed between mines and markets. The benefits that could flow from the sale and beneficiation of colored gemstones remain elusive and often accrue in favor of corrupt interests that could also exacerbate security concerns in fragile states. This sector is a neglected area for research and training and has also largely eluded international mechanisms for accountability such as the United Nations–mandated Kimberley Process for diamonds.

The gemstone industry can play a vital role in sustaining livelihoods and national economies following the cessation of mining. Thailand, formerly a gemstone mining nation, has succeeded in transforming its industrial sector to become the major international hub for the processing (treatment, cutting, and polishing) and trading of gemstones within a few decades. Thailand had a long tradition in gemstone manufacturing and has successfully moved up the gemstone supply chain. The country has achieved this transformation by transmitting know-how, fostering innovation in gemstone refinement, and embodying proactive governance structures. Case lessons like these must be understood and adapted to other geographies as far as realistically possible. The beneficiation of gemstones in their country of origin is a great challenge facing countries across the globe, but especially in Africa. Despite the value and the beauty of the stones, those who mine them and those in the first steps of the value chain often live in poverty. There are encouraging developments—for example, Tanzania has successfully created a gemstone cutting and jewelry-making hub, and the Ethiopian opal sector has had some promising developments in cutting and polishing.

Thus, from mines to markets, colored gemstones provide important opportunities for contributing to development and thereby improving the brand and value of the sector for consumers. However, an integrated mechanism for linking business imperatives with social development dimensions of the sector is essential. This pres-

entation will summarize some of the key research lessons gleaned through the Gemstones and Sustainable Development Knowledge Hub established in 2017 and the nascent educational program that is being developed through a network of international university partners on “Minerals, Materials and Society.”

Challenges of a Twenty-First Century Gem Trader

Edward Boehm

RareSource, Chattanooga, Tennessee

The gem trade looks much different than it did at the end of the last century. Previously the focus was on disclosure of synthetics and treatments, but in the last two decades it has evolved to include greater concern for sustainability, environmental conservation, and transparency in ethical sourcing. Country of origin has always played an important role in high-end gems, and this trend continues today, but the added element of traceability is changing the impact and importance of third-party verification. The country-of-origin pedigree associated with fine-quality gems from sources such as Myanmar (figure 1) and Kashmir has historically translated into desirability and higher value. However, today’s concerned consumer views a

country mired in sociopolitical conflict, war, genocide, or terrorism as an undesirable source, potentially leading to boycott by not only consumers but also NGOs and large or publicly traded jewelry companies. These challenges, while daunting, should also be viewed as opportunities for the entire gem trade.

Reputable gem dealers focus on finding quality gems sourced from reliable producers while competing for the best prices. Ethical sourcing is a main focus for many dealers, but recent sustainability and transparency requirements from larger retail chains are adding layers of responsibility that gem traders and gem trade organizations are working diligently to address. The American Gem Trade Association (AGTA), the International Colored Gemstone Association (ICA), and the World Jewellery Confederation (CIBJO) have been leaders in clear communication and disclosure to the consumer. Despite the demands of additional transparency, they face these challenges as opportunities to differentiate themselves by addressing the issues with positive and active policies. Membership in one of these organizations focused on ethical sourcing provides trade professionals with identifiable goals and guidelines to adhere to.

Modern tools to help gem traders adapt to these principles are becoming more available as demand increases. Professionals no longer have to rely only on their own gemological knowledge and contacts. Laboratory reports and now nanotechnology and blockchain tracking all provide potential third-party options for identifying and tracing the flow of gem material. Gemological laboratory reports and recent technological breakthroughs provide avenues for addressing some of the issues facing the trade, but they are not foolproof panaceas for the issues at hand. It will also take active good faith initiatives that involve the entire supply chain, from miners to retailers. As these technologies evolve and others are discovered, the trade will have even more ways to provide accurate information and confidence to consumers.

Figure 1. A gem miner holds a traditional brass plate of corundum, spinel, and peridot rough and crystals from Mogok, Myanmar. Photo by Edward Boehm.



San Diego Gemstones and Gem Localities

William Larson

Pala International, Fallbrook, California

For over 125 years, San Diego County has produced famous gemstone treasures. This talk will explore the history and famous localities from the original finds of the nineteenth century, as well as the connection to Chinese Empress Dowager Cixi (1835–1908). Her enthusiasm for San Diego gems led to an estimated 90 tons of tourmaline shipped to China before 1910 and the “type” locality finds of kunzite (figure 1) and morganite.

Of special interest, this presentation will detail the revival of San Diego gem mining starting in the 1950s and continuing to this day by looking at the three most important districts: Ramona for spessartine garnet and topaz; Mesa Grande for tourmaline; and Pala for tourmaline, morganite, and kunzite.

The author has been directly involved with 16 gem mining projects in San Diego County since the 1960s and has locally mined 36,000 feet of underground tunnel, resulting in many successful finds. The talk will also delve into current and future challenges for gem mining in San Diego County and elsewhere, including high mining costs—involving governmental, environmental, and safety regulations—and land-use restrictions. Possible bright spots for future gem mining localities include geophysical exploration techniques and underground radar, new mining techniques, and advances in explosives.

Figure 1. This 40.34 ct pink-lavender kunzite is from Pala, California. Photo by Mia Dixon/Pala International.



GIA's Field Gemology Program: A Modern Approach to Origin Determination

Wim Vertriest

GIA, Bangkok

Nowadays, origin determination is an undeniable part of gemology. For many high-end colored gemstones, country of origin is considered an important aspect that can significantly influence price. GIA realized early on that delivering trustworthy scientific studies on gemstone origin is a complex affair. It requires advanced technology, well-trained scientists, years of experience, and above all dependable reference samples.

Since the establishment of its field gemology department in 2008, GIA has built and maintained a reliable reference collection. The best way to collect samples is to cut out all intermediaries, thus removing any misinformation, and visit the mining areas in person to collect gemstones at the source, or as close to it as possible. GIA gemologists have observed and documented many of the most important ruby, sapphire, and emerald mining areas over the last decade (figure 1). Over 90 expeditions, over

20,000 reference samples—more than one million carats—have been collected.

The samples collected are integrated into GIA's colored stone reference collection. Each sample is accompanied by information detailing its sourcing, such as collection date, gem species, known treatment, previous owner details, GPS coordinates of mining and/or buying locations, and purchase price. All the data is subsequently available in an internal database that is accessible to GIA gemologists globally. When data (e.g., inclusion photos, trace element chemistry, and spectra) are collected on the samples, they are added to the database. This becomes an important resource to GIA colored stone gemologists in every location. In a video on scientific research collections, Sir David Attenborough noted:

a research library associated with collections is almost of greater importance than the objects themselves. Unless you know where it came

from *exactly*, and when it came from *exactly*, you are missing a lot of very, *very* important information. That information can not only come from the object itself, but from the circumstances, documentation, that should accompany every scientifically collected specimen. (“Sir David Attenborough on Museum Collections - 360,” American Museum of Natural History, posted August 31, 2017)

While in the field, GIA team members also document the local situation. This covers mining techniques, trading activity, traditional jewelry making, gemstone history, and local gem cutting. Videos, photos, and interviews are then used to create articles and supplement course content for GIA’s educational programs. In this way, the information gathered during field expeditions becomes an invaluable resource to multiple departments within GIA and serves as a historical record of gem mining sites around the globe.

Figure 1. Greenland ruby samples in matrix collected for GIA’s field gemology program. Photo by Wim Vertriest.



Closing the Knowledge Gap Across the Supply Chain: A Case Study of GIA and Pact’s Field Collaboration in Tanzania

Cristina Villegas

Mines to Markets Program, Pact, Washington, DC

For years, field gemologists and international development experts across disciplines have noted that colored stone supply chains are lopsided in terms of stakeholder knowledge about stone types, quality and grading, handling know-how, and what happens after the stone leaves the mine and its journey begins in the global jewelry supply chain. Those who mine the stones—typically at great personal risk—are usually the most likely to know the least about them. One stone can change a life if it is of especially high quality, while others may be “tourist grade” (local parlance for lower-value stones). Many artisanal and small-scale miners (ASM) simply do not realize the difference.

In 2017, the Gemological Institute of America and Pact, an international nonprofit social development organization with a specialty in developing and delivering ASM economic and social programs, joined forces to test a simple idea: Can a simple guidebook make a difference, and how?

The project, originally conceived by GIA distinguished research fellow Dr. James Shigley, is part of the Institute’s mission-driven effort to share information and skills throughout the gem

Figure 1. Miriam S. Mshana, an artisanal sapphire miner, is chairwoman of the Tanga chapter of the Tanzanian Women Miners Association (TAWOMA), a field partner that facilitated access to the remote mining sites. TAWOMA comprises more than 3,000 women working across the mining sector producing gold, colored gemstones, diamonds, and industrial materials. The Tanga chapter alone has 600 members. Photo by Cristina Villegas.



and jewelry industry supply chain and with the public. An area in Tanzania's Umba Valley was identified, and the program rolled out in 2017 with the Tanga chapter of the Tanzania Women Miners Association (TAWOMA; figure 1). The results were fascinating and validated the need for the guidebook. Of particular note: For every \$1 the project invested in artisanal and small-scale miners, there was a \$12 social return on the investment. Both male and female miners commented that they believe these changes they have experienced will last for more than five years.

This presentation will focus on how the project was implemented, monitored, and measured, and will engage the audience to help identify answers to these questions:

- How can the gemological research sector, and other parts of the jewelry supply chain, help advance local economic and social development agendas in sub-Saharan Africa?
- What other knowledge could be imparted in a context of low literacy? Are there other ways that learning programs could be structured to maximize impact in a given province? In other words, how can we improve in the future and also inspire others to act?

In reporting on her June 2018 trip to the region, the author will provide an update on the 2017 project participants.

New Technologies and Techniques

Synthetic CVD Diamond—30 Years On

Daniel J. Twitchen

Element Six, Global Innovation Centre, Harwell, Oxford, United Kingdom

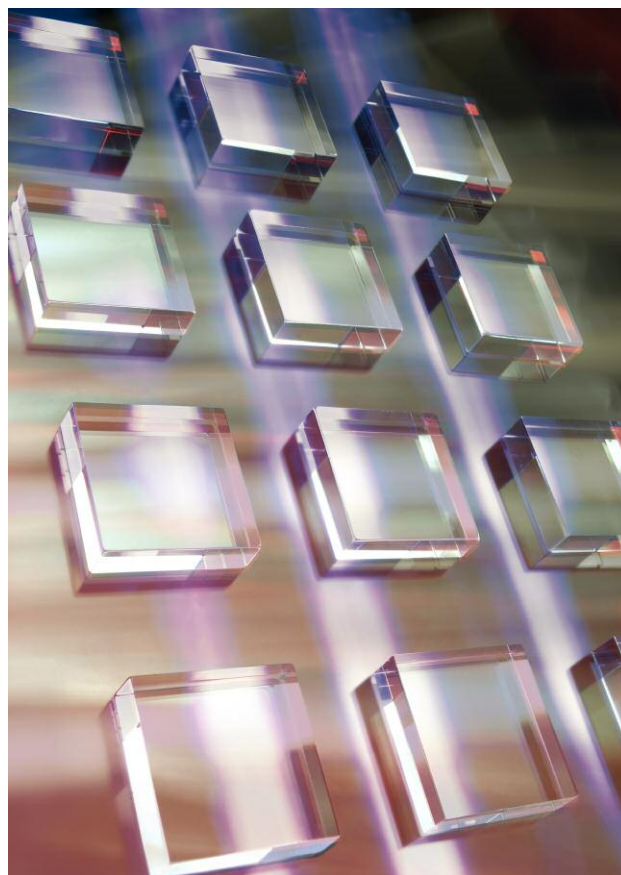
Element Six first started its chemical vapor deposition (CVD) synthetic diamond program in 1988. Thirty years on, this talk will review notable high and low points, flagging some lessons learned.

Volume synthesis of diamond by CVD (figure 1) has not only contributed to reducing the cost of the material but also enabled the superlative properties of diamond to be more fully utilized. It has long been recognized that, aside from its extreme hardness, diamond is a remarkable material with many properties—optical, thermal, electrochemical, chemical, and electronic—that outclass competing materials. When combined, these properties offer the designer an engineering material with tremendous potential to create solutions that can shift performance to new levels or enable completely new approaches to challenging problems.

Components routinely fabricated using CVD synthetic diamond now span tweeters for loudspeakers, radiation detectors and sensors, optical components for lasers, windows for radio frequency and microwave transmission, blades and cutting tools, and electrodes for electrochemical sensing, ozone generation, and direct oxidation of organic matter.

Lightbox, a new De Beers company, has recently announced jewelry using white, blue, and pink lab-grown CVD diamonds. As crystal growers and materials scientists know, intrinsic undoped diamond is colorless in the visible range, but its absorption properties can be modified by defects, often referred to as “color centers,” formed either during the CVD growth process or through post-growth treatments such as irradiation and annealing. This presentation briefly summarizes some of the tools used to engineer CVD diamond. For example, controlling the nitrogen level (yellow CVD) to obtain particular thermal and optical properties,

Figure 1. Single-crystal CVD diamond. Courtesy of Element Six.



doping with boron (blue) to make electrically conducting diamond used to produce ozone for sanitization and for thermal management in telecommunications, and growing in nitrogen-vacancy centers (pink) to make magnetic sensors.

The diverse applications of diamond that harness its exceptional properties and the impact of color centers touch our lives in unexpected ways: Diamond is used to create the high-quality mirror finish on your smartphone and to produce the 170 miles of copper wiring in the aircraft that takes you on vacation, and it

is also enables new higher-power lasers used in welding our cars together. It is even used in the quality control of food and in pharmaceutical manufacturing.

In summary, there has been considerable progress in the fabrication and commercialization of CVD-grown diamond over the last 10 years by a number of producers. This progress, coupled with the broad range of applications, shows that perhaps a new age of industrial diamond has truly begun—the age of CVD synthetic diamond.

Beyond Gemstones: The Medical, Industrial, Scientific, and Computational Applications of Lab Diamonds

Jason Payne

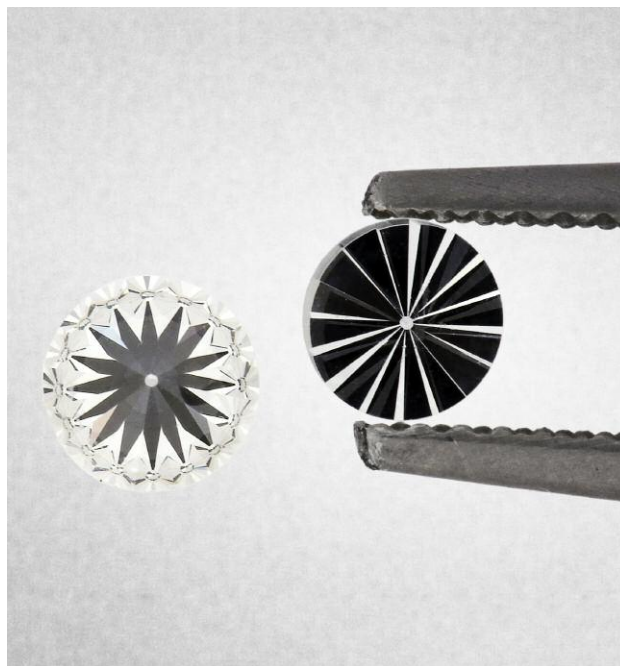
Ada Diamonds, San Francisco

Many gemologists know that there are important technological applications for laboratory-grown diamonds; however, it is less understood how broad the nongemological uses really are or why diamond is the ideal material for each use. This presentation will review modern industrial applications of laboratory-grown diamonds, including surgical tools, tumor detection, orthopedic implants, water purification, industrial tooling, compound refractive energy focusing, Fresnel lenses, high-pressure anvils (figure 1), sound reproduction, deep space communication, high-power electronics, quantum computing, long-term data storage, AC/DC conversion, and electrical vehicle efficiency.

These applications are rooted in the less frequently discussed gemological properties of diamonds that make it a “supermaterial.” The biological, thermal, mechanical, optical, acoustic, and electrochemical properties of diamond will be introduced. Specific properties discussed will include thermal conductivity, Young’s modulus, breakdown field, band gap, and saturated electron drift velocity. Furthermore, the utility of diamond defects such as nitrogen vacancies and boron will be explored.

In addition to discussions about functional monocrystal diamonds, two unnatural forms of functional diamond will be discussed: polycrystalline diamond (PCD) and diamond-like carbon (DLC). Many of the functional diamonds discussed, including PCD and DLC, will be available for hands-on examination as part of the presentation.

Figure 1. Laboratory-grown diamond anvils, capable of generating 1 terapascal of pressure, enable high-pressure experiments for physics, chemistry, materials science, and industry. Photo courtesy of New Diamond Technology.



Big-Data Analysis and Insights in the Online Gem and Jewelry Trade

Menahem Sevdermish and Guy Borenstein
Gemewizard, Ramat Gan, Israel

Big-data analytics is the process of collecting, organizing, and analyzing large volumes of data to reveal hidden patterns and unfamiliar correlations, identify market trends, and extract other useful information that might otherwise be invisible—even for the data manager.

Big-data analytics is seldom used within the gem and jewelry trade. The gem and jewelry sector is kept with general fixed inquiries that block the category from characterizing its inventory and users, and by that, identifying new opportunities.

Another challenge is that in most online marketplaces, the “What You See Is What You Get” experience is hindered by two main factors: improper disclosure and misrepresentation of images (e.g., digitally enhanced photos).

The research and development team of Gemewizard has devised and digitized a fully automatic big-data analysis system for large-scale gem and jewelry marketplaces, based on color and contextual search engine and image analysis (figure 1). This system generates unique market analytics and a fraud detection and prevention service.

Since 2016, the Gemewizard team has had the opportunity to examine the validity of the system using vast amounts of data from a world-leading online retail marketplace. The information gathered from this survey, together with additional volumes of information collected from the Internet, provided some important insights regarding the online gem and jewelry trade. Some of these insights, which we consider fruitful and eye-opening for any marketplace or e-tailer, will be revealed.

The gem-related information contains insights regarding common fraudulent activities and practices for 128 varieties, species, and series of merchandisable gems. The gathered data includes anomalies in attributes such as:

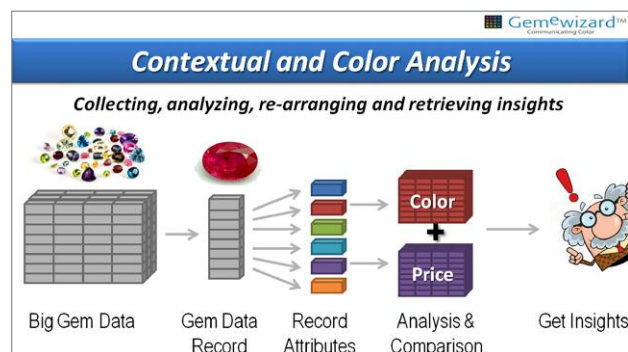
- Gem type: Mineralogical, gemological, and trade names, as well as misnomers. Analysis includes accepted word

combinations (e.g., “ruby” and “zoisite”) versus problematic ones (e.g., “diamond” and “moissanite”).

- Color (e.g., “yellow emerald”)
- Synthetic wording and nicknames (e.g., “heating with light elements”)
- Treatment wording, ranked and analyzed according to severity (e.g., “heating” versus “diffusion” in ruby)

The trade-related information provides powerful forecasting tools for the marketplace administrator. These include sales and trends history, defined by attributes such as type, color, geography, seasonality, and price, and the ability to identify tendencies (e.g., “Prices of untreated ruby gems between 2 and 3 carats are on the rise in Europe..”) and pricing opportunities (e.g., “Currently, there is a high demand for pale-colored Paraíba tourmaline gems in Far East markets”).

Figure 1. The system algorithm crawls the HTML pages of gem websites for big data. For each gem, it condenses the item page to its attribute components and records useful data. The collected data is then compared against the entire database to identify insights and peculiarities.



Diamond Impression: The Key to Sustainable Competitiveness

Sergey Sivovolenko¹, Roman Serov², and Janak Mistry³ (presenter)

¹OctoNus Finland Oy, Tampere, Finland

²OctoNus Software, Moscow

³Lexus SoftMac, Surat, India

People are impressed with the uniqueness of diamond, which incorporates factors such as brilliance and fire. When the trade commoditized the category through the Four Cs, it was partly due to

the technical inability to promote diamond’s impressive optical effects, including optical illusions. This common trade practice inhibited diamond’s competitiveness against other goods in the

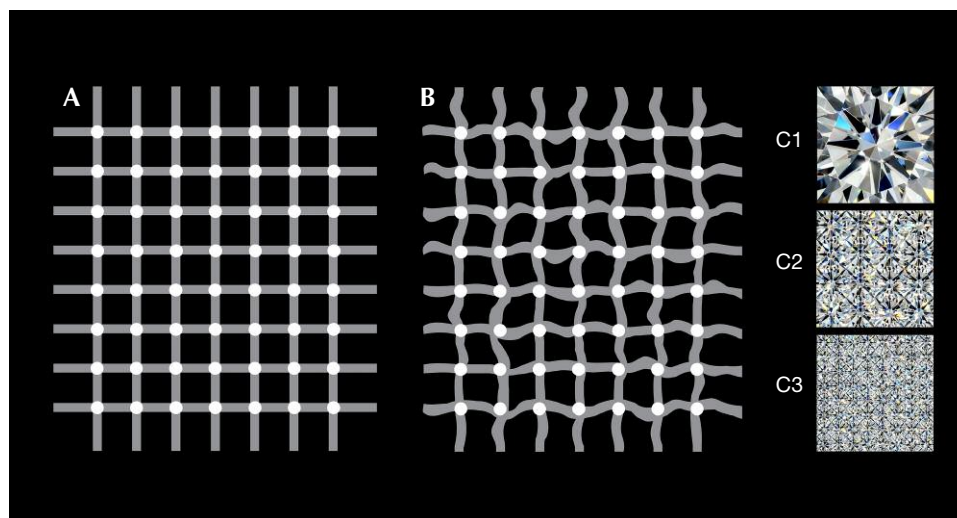


Figure 1. A scintillation grid (A), a scintillation grid with a wavy pattern (B), and squares covered by round brilliant-cut diamonds in different sizes (C).

luxury sector. But from now on, emerging technology will allow demonstration of diamond's magic on a large scale with fine details.

Modern algorithmic craftsmanship creates the category of high-vibrancy diamonds, referred to here as Hi-Vi: exceptional diamonds with superior consumer benefits such as brilliance, fire, table color, symmetry, and spread, compared to others of the same shape, size, and pavilion color. The triple excellent round, which took centuries for the industry to craft, was the first Hi-Vi diamond.

Diamond vibrancy is a combination of optical effects and illusions. For example, brilliance, fire, scintillation, and spread depend on both objective parameters such as cut design and stone size, as well as subjective aspects of human vision, such as space-temporal sensitivity and stereo perception. Figure 1A demonstrates the scintillating grid illusion: The intersections seem to flicker white and black, generating additional brightness and contrast when the observer's glance wanders. Distortion of pattern ruins this effect (figure 1B). Certain patterns produce higher perceived brightness. This example is a 2D effect; more astonishing optical illusions result from human stereo vision.

The phenomenon of diamond brilliance has a similar origin—human vision peculiarity—as the scintillating grid illusion

described above. The impact of optical illusions on both Hi-Vi diamond patterns and jewelry designs (e.g., melee) are to be considered, so Hi-Vi optimization is made for not just single diamond cuts, but also for each diamond jewelry piece as a whole.

Figure 1C shows squares with round brilliant-cut (RBC) patterns that differ only in size. The integral colored and colorless areas are exactly the same, while the perceptions of fire and brilliance in each image are quite different. It is impossible to maximize two performance parameters (both fire and brilliance, for example) simultaneously. The consumer's final choice should be based on subjective preferences and rely on performance benchmarks.

Hi-Vi diamonds should be demonstrated with an optical performance digital “loupe,” which allows even inexperienced buyers to easily appreciate the performance difference at the highest levels of brilliance, fire, and scintillation. The “loupe” is critically important for mass marketing of relatively small diamonds. For sustainable market development, diamond impressiveness and vibrancy born of masterly designed optical illusions and visual effects is the selling proposition to craft, demonstrate, and explain.

For online access to all issues of GEMS & GEMOLOGY from 1934 to the present, visit:

gia.edu/gems-gemology





Photo Montage
2018 GIA International Gemological Symposium
October 7-9, 2018











Photos by Denise Conrad, Richard Deomampo, Joyce Wing Yan Ho, Emily Lane, Kevin Schumacher, and Eric Welch



Colored Stones and Pearls

3D Reconstruction of the Internal Structures of Pearls

Emiko Yazawa and Chunhui Zhou
GIA, New York

Pearl testing involves a variety of tools and techniques, most notably X-ray imaging. GIA applies both real-time X-ray micro-radiography (RTX) and computed X-ray microtomography (μ -CT) to reveal the internal structures of pearls and draw conclusions on their identity. These images help gemologists determine whether a pearl is natural, bead-cultured, non-bead cultured (NBC), and so forth. The identification of some pearls remains challenging for even the most well-equipped laboratories. Researchers sometimes find surprises hidden within—a piece of shell or some other interesting object that is difficult to visualize with two-dimensional images.

Here, we present a range of interesting internal three-dimensional structures (figure 1), using specialized software and μ -CT slice images for the reconstruction. These include unusual internal growth features such as bivalve and gastropod shells, foraminifera, flower-shaped bead nuclei, and plastic bead nuclei, as well as non-bead-cultured features such as voids and linear structures. This powerful research tool makes it possible to virtually explore, manipulate, extract, and reconstruct specific areas inside a pearl for analysis. It also gives the operator the ability to enhance the existing μ -CT data to view the details more clearly, thus revealing the fascinating world within pearls that gemologists routinely encounter.

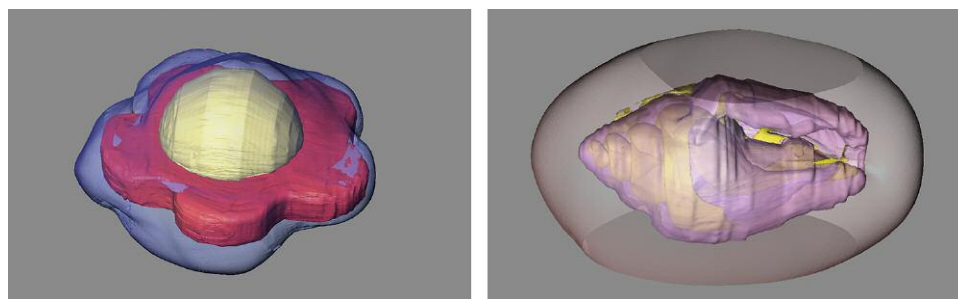


Figure 1. 3D reconstructions of the internal structures of two bead-cultured pearls with atypical nuclei. Left: A flower-shaped bead nucleus. Right: A small gastropod shell used as a nucleus.

Atypical “Bead”-Cultured *Pinctada Maxima* Pearls Nucleated with Freshwater Non-Bead-Cultured Pearls

Promlikit Kessrapong and Kwanreun Lawanwong
GIA, Bangkok

At present, most of the freshwater shell bead nuclei used in the cultured pearl industry originate from mussels from the Mississippi River in the United States. However, shell beads are not the only material used as nuclei in the culturing process. Cultured

freshwater pearls have also been used as nuclei to produce atypical bead-cultured (aBC) South Sea pearls (Scarratt et al., 2017).

GIA researchers sourced several aBC samples from Orient Pearl Ltd. in Bangkok. Two samples were selected, one “golden” and one



Figure 1. Photographs of the “golden” (left) and white (right) atypical bead-cultured pearls. Photos by Kwanreun Lawanwong.

white (figure 1), both showing an unmistakable saltwater appearance. Standard testing methods as well as macro photography, microradiography, X-ray luminescence (Hänni et al., 2005; Kessrapong et al., 2017), Raman and photoluminescence (PL) spectroscopy and ultraviolet-visible spectrophotometry (UV-Vis) were applied to the samples prior to cutting them in half. After they were sawn, further data was collected through photomicrography, X-ray fluorescence (XRF) images, and laser ablation–inductively coupled plasma–mass spectrometry (LA-ICP-MS) analysis.

As expected, the results of the examination confirmed their aBC nature. While their appearance, baroque shapes, and white to strong yellow (golden) colors indicated they were typical saltwater *Pinctada maxima* pearls, their internal structures revealed clear boundaries where the outlines of freshwater NBC pearl nuclei could be seen in the microradiographs. Raman, PL, and UV-Vis spectra for the golden sample indicated it formed within a *P. maxima* mollusk. Also, in keeping with their freshwater NBC nuclei structure, a weak to moderate fluorescence was observed, which would not be the case to such a degree if they were entirely saltwater in origin. The golden pearl showed a yellow-orange fluorescence to X-ray luminescence, while the white sample exhibited a yellow-green reaction, similar to the result one would expect to see in cultured saltwater pearls incorporating freshwater mussel shell nuclei.

REFERENCES

Hänni H.A., Kiefert L., Giese P. (2005) X-ray luminescence, a valuable test in pearl identification. *Journal of Gemmology*, Vol. 29, No. 5/6, pp. 325–329.
 Kessrapong P., Lawanwong K., Sturman N. (2017) *Pinctada maculata* (pipi) bead-cultured blister pearls attached to their shells. *GIA Research & News*, Apr. 25, <https://www.gia.edu/gia-news-research/pinctada-maculata-bead-cultured-blister-pearls-shells>

Examining the halves, we observed more detail: the demarcation between the two parts (nuclei and surrounding nacre overgrowth), small void/linear features (proving the NBC origin of the nuclei), the different colors/structures between the saltwater and freshwater nacre components, and some other indications of their cultured origin (i.e., small voids within the demarcation zones). The X-ray luminescence reactions were similar to those seen in the whole samples, only more intense since the inner freshwater nuclei were now directly exposed to the X-rays and not masked by the saltwater nacre that covered them prior to cutting. LA-ICP-MS analysis clearly revealed the nature of the outer saltwater layers and inner freshwater pearls, through significant differences in the concentrations of Sr and Mn among other elements. The Mn levels in the center were higher while the Sr levels were lower compared to the overgrowth layers, where the opposite was true, as expected in saltwater material.

Although cutting the pearls in half was a nice way to reveal the features in more detail, it is worth noting that gemologists do not need to go to such extremes to prove the identities of such pearls in laboratory conditions. Standard testing methods permit the straightforward identification of aBC pearls. Cutting them in half is a useful exercise to carry out for scientific examination of their structures and to allow more detailed analysis that would not otherwise be possible.

Scarratt K., Sturman N., Tawfeeq A., Bracher P., Bracher M., Homkrajac A., Manustrong A., Somsard N., Zhou C. (2017) Atypical “beading” in the production of cultured pearls from Australian *Pinctada maxima*. *GIA Research & News*, Feb. 13, <https://www.gia.edu/gia-news-research/atypical-beading-production-cultured-pearls-australian-pinctada-maxima>

Chinese Freshwater Cultured Pearl Industry at a Crossroads

Qishen Zhou and Ren Lu

Gemmological Institute, China University of Geosciences, Wuhan

During the past 15 years, China has made tremendous progress in the quality and output of freshwater cultured pearls (see figure 1). Innovative technologies have facilitated a variety of colors and high-quality nacre within a shorter culturing cycle. Large-scale culturing

has boosted the annual output to a high of 2,200 tons, and China has become an undisputed freshwater pearl empire.

However, the expanded production has been accompanied by considerable damage to the environment. With a more forceful im-

plementation of the Chinese government's environmental policy, there have been many strict bans in the main producing areas of freshwater cultured pearls during the past three years. The pearl culturing area decreased from approximately 250 km² in 2005 to 100 km² in 2016, and output has also dropped from a peak annual output of over 2,200 tons to less than 1,300 tons in 2017. Production is predicted to decline by about 50 percent in the next year or two.

The number of Chinese lakes with Grade IV–V water quality (Grade IV water is used in general industrial and recreational water areas and Grade V water is employed in agricultural and general landscape water areas; see New York Water Quality Standards, 2016) increased from 16.67% in 2000 to 58.5% in 2016. It is worth emphasizing that about 20% of all lakes are still Grade V. At the same time, water eutrophication has become a common phenomenon. It is caused by the discharge of excess nutrients (mainly nitrogen and phosphorus), resulting in abnormal reproduction and growth of various aquatic organisms and plants. Since 2003, the proportion of eutrophic lakes and reservoirs in China has increased from 50% to an average of 77.93%, while the proportion of eutrophic reservoirs alone has nearly doubled from 15.05% to 28.8%. Among the lakes monitored by the government in 2013 and 2015, many of the eutrophic lakes are also leading areas for pearl culturing.

As a result of the Chinese government's strict environmental regulations, the extensive feeding model with massive fertilization is no longer permitted. The government has carried out the forced demolitions of some pearl culturing areas during the past three years, and the three largest freshwater pearl-culturing provinces/regions also have implemented strict bans on cultured pearls. Meanwhile, the central and eastern provinces such as Hubei and Zhejiang began compulsory demolition of freshwater pearl culturing in 2017, which caused a dramatic decline in pearl output.

This has been a major setback for freshwater pearl farmers, aquaculture companies, and pearl workers. The Chinese government at all levels has subsidized the farmers who have suffered from demolition, though most are still reported to have suffered serious losses because of culturing bans.

At the same time, the new environmentally friendly and standardized aquaculture models will usher in a new era for Chinese freshwater cultured pearls. The Chinese Academy of Agricultural Sciences and various enterprises have developed many new culturing



Figure 1. Tea set decorated with Chinese freshwater pearls from the 2016 G20 Summit held in Hangzhou, China. Courtesy of Angeperle Corp.

methods. For example, fish-clam mixed cultivation has been shown to improve water quality and increase output value, and the three-part aquaculture model of fish, clam, and poultry can balance ecological concerns and generate considerable income. Environmentally friendly aquaculture will become the new standard for freshwater cultured pearls, and it will take about 5 to 10 years to adopt automated aquaculture technology across mainland China.

To summarize, wholesale and retail prices of Chinese freshwater pearls will fluctuate significantly in the next two to five years based on the freshwater pearl culturing cycle. China's freshwater cultured pearl industry has formed a complete and relatively mature supply chain over the past decade. It is still facing new challenges, new development opportunities, and critical decisions for a sustainable industry under the government's new policy and the promotion of new aquaculture technologies. At the same time, the increasing demand for high-quality freshwater cultured pearls in China and around the world is prompting the upgrade and transformation of the product.

REFERENCES

Akamatsu S., Li T.Z., Moses T.M., Scarratt K. (2001) The current status of Chinese freshwater cultured pearls. *G&G*, Vol. 37, No. 2, pp. 96–113, <http://dx.doi.org/10.5741/GEMS.37.2.96>

New York Water Quality Standards (2016) <https://www.epa.gov/sites/production/files/2014-12/documents/nywqs-section1.pdf>

Comparison of Laser Ablation and Solution ICP-MS Analyses of Emeralds

Ruan Hattingh¹, Raquel Alonso-Perez², Aaron C. Palke³, Lee Groat⁴, and James M.D. Day¹ (presenter)

¹Scripps Institution of Oceanography, La Jolla, California

²Harvard University, Cambridge, Massachusetts

³GIA, Carlsbad, California

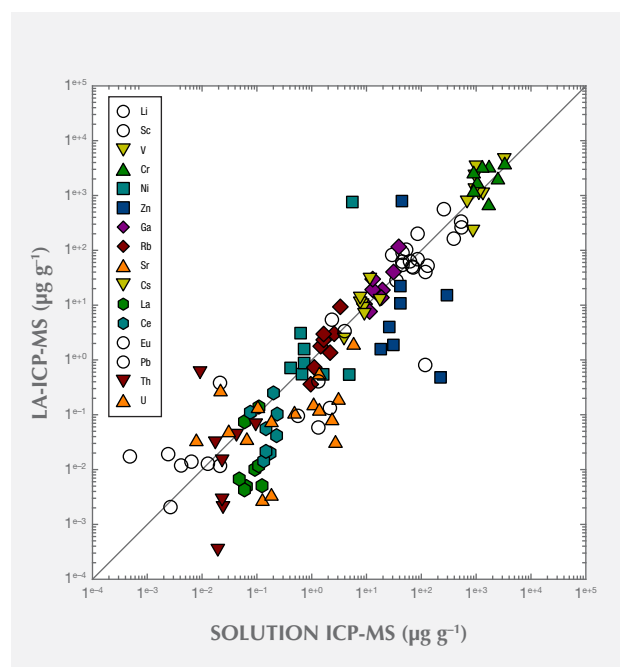
⁴University of British Columbia, Vancouver, Canada

Geochemical studies of emeralds can confirm their provenance and improve our understanding of deposit origin. LA-ICP-MS is a minimally destructive and relatively high-throughput technique that allows determination of more than 30 major, minor, and trace elements simultaneously using small spot sizes (20–100 μm). A reliable and consistent LA-ICP-MS protocol requires good standardization, including the use of matrix-matched standard reference materials. Here we provide a robust assessment of the quality of LA-ICP-MS analysis of emeralds, utilizing a set of natural and synthetic gem-quality emeralds housed within the Mineralogical and Geological Museum at Harvard University. Our goals were to identify large emeralds as potential standard reference materials and to examine the robustness of certain trace elements in emeralds for provenance and for petrogenetic models of their origin.

In this study, we have analyzed more than 45 emeralds using both LA-ICP-MS and solution ICP-MS techniques. For solution ICP-MS, between 5 and 10 mg of individual emeralds was digested in HF-HNO₃ prior to analysis of Be by standard addition and all other elements by comparisons with standard reference materials spanning a range of major-, minor-, and trace-element compositions (see also the oral presentation by R. Alonso-Perez from this conference, p. 280). Some emeralds that we analyzed contained small inclusions, but the majority were inclusion-free. For comparison, portions of the same emeralds were also measured by LA-ICP-MS using 100 μm spot sizes on a New Wave Research UP213 (213 nm) laser ablation (LA) system coupled to a ThermoScientific iCAPq ICP-MS. In general, we found excellent agreement for major-, minor-, and trace-element data between the solution ICP-MS and LA-ICP-MS techniques (figure 1), finding reliable results by LA-ICP-MS for Li, Be, Na, Mg, Al, Si, K, Sc, Ti, V, Cr, Fe, Ni, Zn, Ga, Rb, Cs, and Pb. Less reliable results were

generated for Sr and the rare earth elements, due to the generally low abundances of these elements in emeralds. During this study, we identified natural emeralds as potential standard reference materials for future inter-laboratory LA-ICP-MS comparison, as well as a synthetic emerald (Harvard ID 109678) that is enriched in the key elements outlined above and in Mo.

Figure 1. Comparison of selected trace-element abundances in emeralds measured using both solution- and laser-ablation ICP-MS.



Fluid Effervescence: A New Process for Natural Color Variation In Gems

Dan Marshall

Simon Fraser University, Burnaby, British Columbia, Canada

The emeralds from the Emmaville-Torrington deposit in Australia are commonly zoned (figure 1) and display alternating bands of emerald green and colorless growth zones within individual crys-

als at the millimeter scale. The zoning is seen optically but can be observed via imaging techniques such as backscattered electron and cathodoluminescence, and detected chemically via electron

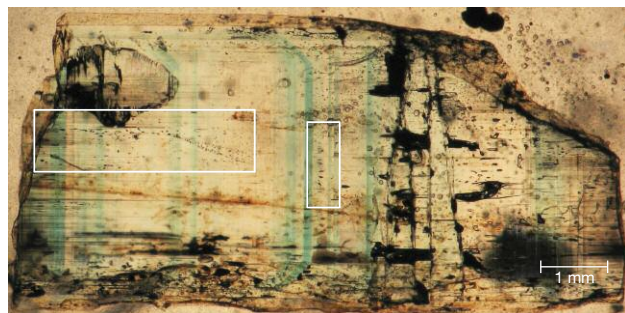


Figure 1. Internal features of a zoned emerald crystal from the Emmaville-Torrington deposit. Photomicrograph by Dan Marshall.

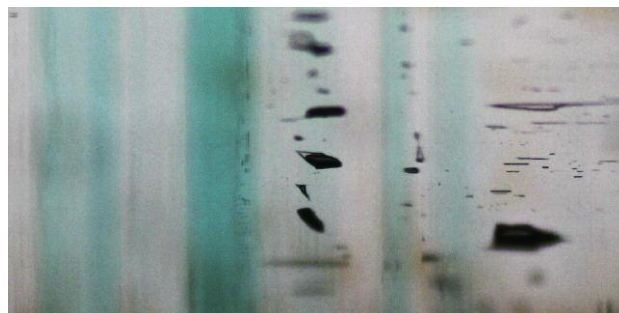


Figure 2. Enlarged area of the photomicrograph of the primary fluid inclusions from figure 1 showing alternating colored and clear areas in the zoned emerald crystal. The clear zones correspond to growth zones dominated by primary vapor-rich fluid inclusions. The field of view is approximately 650 microns. Photomicrograph by Dan Marshall.

microprobe analyses. Additionally, there is a correlation between the presence of a population of primary vapor-rich fluid inclusions within the clear growth zones (figure 2) and a second population of highly saline three-phase (liquid + vapor + halite) fluid inclusions in the darker or colored growth zones.

The two fluid inclusion populations appear to represent conjugate sets of a boiling or effervescent system, with the three-phase fluid inclusions having an average salinity of approximately 33 wt.% NaCl equivalent. This population undergoes total homogenization into the liquid and probably represents fluids trapped in the liquid system of a two-phase (effervescent) system. The vapor-rich population of fluid inclusions (again, see figure 2) have

an average salinity of approximately 6 wt.% NaCl equivalent and homogenize into the vapor phase at higher temperatures.

The correlation of color versus clear growth zones—corresponding to high-salinity liquid-dominant and vapor-dominant low-salinity primary fluid inclusions, respectively—indicates that the color banding within the Emmaville-Torrington emerald is related to emerald precipitation in the liquid or vapor portion of an effervescing fluid system. Other emerald deposits worldwide display similar growth banding, as do some other deposits of gem topaz and gem varieties of quartz.

The Heat Treatment of Basalt-Related Blue Sapphires

Wasura Soonthorntantikul, Ungkhana Atikarnsakul, Charuwan Khowpong, and Sudarat Saeseaw
GIA, Bangkok

Heat treatment is the most common method used to improve the color and/or clarity of corundum. Basalt-related blue sapphires typically have an unattractive dark blue color due to their high iron content, and low-temperature heat treatment can be applied to lighten this material (Nassau, 1981; Hughes et al., 2017). The main factors that influence the changes in corundum are the temperatures employed, the conditions in which they are heated, and the duration of the treatment process. However, it is difficult to distinguish between naturally heated and heat-treated blue sapphires from basalt-related deposits using only standard gemological testing and microscopic examination. In this study, basalt-related blue sapphires from various locations (Thailand, Cambodia, Australia, and Nigeria) were heat treated at low temperatures, ranging from 700 to 1050°C, for durations of 1.75, 7, and 28 hours in air (oxidizing atmosphere). The changes in color appearance, UV fluorescence, internal features, and spectroscopic properties were investigated.

The results indicated a negligible change or a slight lightening of the blue color after treatment at 700°C, while an obvious

lightening of the blue color resulted from heating at 900°C and 1050°C (figure 1). Some solid inclusions, iron stains, and partially healed fractures showed signs of alteration during the heating experiments, while needles and minute particles did not show any signs of change. Unheated samples were inert to short-wave ultraviolet (UV) radiation. After heating, most basalt-related blue sapphires remained inert under short-wave UV, but a few samples exhibited a very weak chalky green fluorescence. Fourier-transform infrared (FTIR) spectra obtained from the samples varied considerably, with differences between the peak intensities recorded before each heat treatment process and also after each unique temperature and time treatment combination. In most cases, unheated blue sapphires from basalt-related deposits revealed the characteristic 3309 cm^{-1} series of peaks in the FTIR spectrum (the intensity of 3232 cm^{-1} being much lower than that of 3309 cm^{-1}). After heating at 700°C and 900°C, the intensity of the 3309 cm^{-1} peak decreased and the 3232 cm^{-1} peak increased, respectively. However, some samples that initially

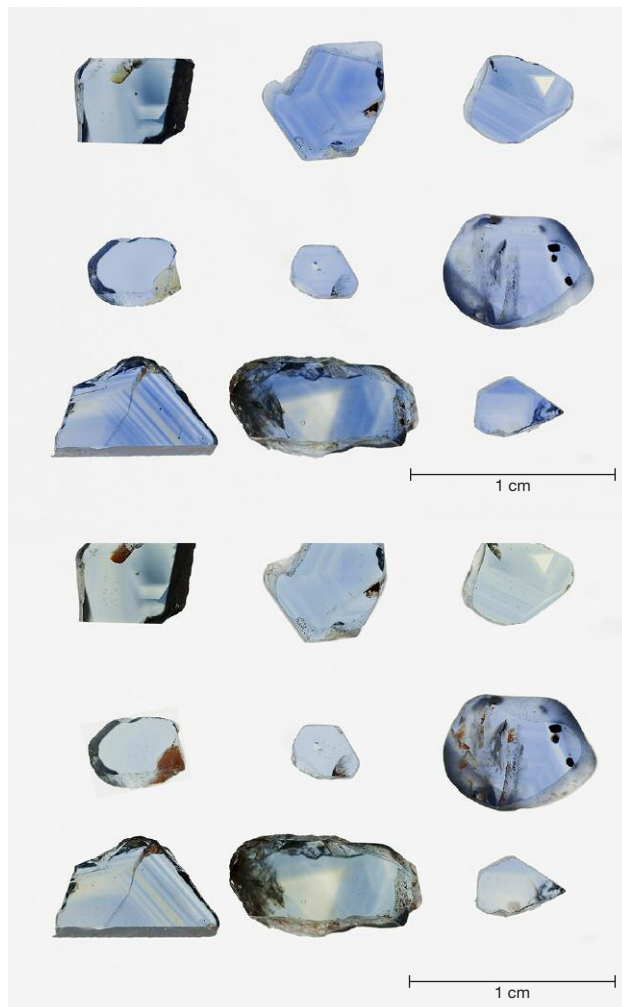


Figure 1. Color-calibrated photos of basalt-related blue sapphires before (top) and after heating at 1050°C for 28 hours (bottom). Photos by Sasithorn Engniwat.

showed a relatively intense 3232 cm^{-1} peak in the series before treatment exhibited a more intense 3309 cm^{-1} peak and a less intense 3232 cm^{-1} peak post-treatment. After heating at 1050°C for 1.75 hours, we recorded a decrease in the intensity of the 3309 cm^{-1} peak and an increase in the 3232 cm^{-1} peak, to the point where they were of almost comparable intensity. When subsequently heated for 7 and 28 hours, the intensity of 3309 cm^{-1} peak increased and that of the 3232 cm^{-1} peak decreased (figure 2). The ultraviolet/visible/near-infrared (UV-Vis-NIR) spectra obtained from the samples heated at 900°C and 1050°C for 1.75, 7, and 28 hours showed a reduction in the height/in-

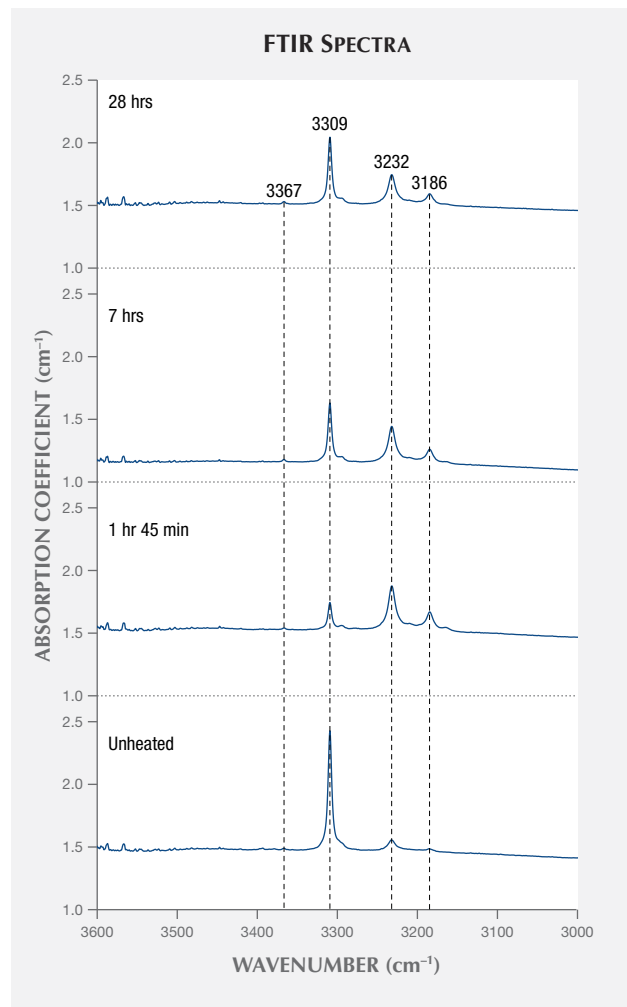


Figure 2. FTIR spectra of the sample before and after heating at 1050°C for up to 28 hours.

tensity of the broad band centered at 580 nm related to an Fe^{2+} - Ti^{4+} intervalence charge transfer. This reduction is the root cause of the lighter color after heat treatment.

The results of this study show that even with advanced data, it is very challenging to separate basalt-related stones that have been heated from those that have not undergone any post-mining heat treatment, owing to the variable results associated with the experimental temperatures and durations used. Inclusion studies may provide sufficient evidence in some cases, but even when comparing the inclusions scene before and after treatment, separation often remains challenging.

REFERENCES

- Hughes R.W., Manorotkul W., Hughes E.B. (2017) *Ruby & Sapphire: A Gemologist's Guide*. RWH Publishing/Lotus Publishing, Bangkok, pp. 146–148, 200–201.
- Nassau K. (1981) Heat treating ruby and sapphire: Technical aspects. *G&G*, Vol. 17, No. 3, pp. 121–131, <http://dx.doi.org/10.5741/GEMS.17.3.121>

“Low-Temperature” Heat Treatment of Mozambican Ruby

Sudarat Saeseaw, Charuwan Khowpong, and Ungkhana Atikarnsakul
GIA, Bangkok

Mozambique is one of the most important sources of ruby today, with the Montepuez mine producing material ranging from light to dark purplish red. To improve their color, Montepuez rubies are heated at low temperatures to remove the purplish component—caused by blue color zoning—and create a more attractive and desirable red color. For this study, 47 samples were selected for heat treatment in air (oxidizing environment) at different temperatures and varying durations. The samples were heated to 600, 700, 800, and 900°C for 2 hours and 40 minutes, 8 hours, or 24 hours. The results showed no significant change to the blue color zoning when heated to 600 or 700°C over any of the time frames chosen; however, the blue component was reduced when heated to a minimum of 800°C for 2 hours and 40 minutes (figure 1).

Observing any changes to inclusions can be challenging when examining material subjected to lower-temperature heating, since

there is less chance inclusions will be affected (Pardieu, 2015). Inclusions in Mozambican rubies are limited to needles, platelets, and other fine particles. When any alteration takes place, the evidence is very subtle. During treatment, spots can form on these platelets (figure 2), although this is not always the case. When crystalline inclusions are present, it is easier to identify heat treatment because fractures often develop around them, especially in larger crystals. Some gems contain fractures with associated iron staining or fingerprints, and their appearance may change drastically during treatment (Sripoonjan, 2016). Inclusion studies are not always conclusive, however, and advanced techniques such as FTIR spectroscopy are needed to assist in detecting low-temperature heat treatment. The presence of the 3309, 3232, and/or 3185 cm^{-1} peak(s) appears related to heat treatment, since they were only observed in heated stones.

Figure 1. Color-calibrated photos of a Montepuez ruby before (left) and after (right) heat treatment at 800°C for 8 hours. The stone’s blue color component clearly decreased after heating. Photos by Sasithorn Engniwat.

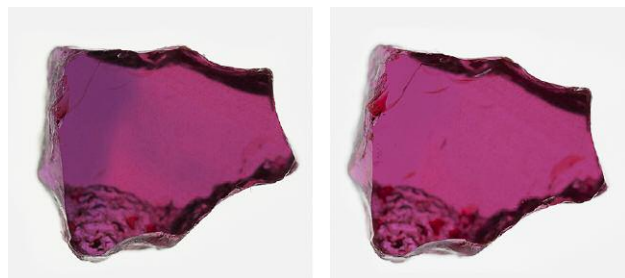


Figure 2. Mozambican ruby with spotted platelets that indicate heat treatment. Brightfield and fiber-optic illumination. Photo by Charuwan Khowpong; field of view 1.0 mm.



REFERENCES

Pardieu V., Saeseaw S., Detroyat S., Raynaud V., Sangsawong S., Bhusrisom T., Engniwat S., Muiyal J. (2015) GIA lab reports on low-temperature heat treatment of Mozambique ruby. *GIA Research News*, Apr. 28, <https://www.gia.edu/gia-news-research-low-temperature-heat-treatment-mozambique-ruby>

Sripoonjan T., Wanthanachaisaeng B., Leelawatanasuk T. (2016) Phase transformation of epigenetic iron staining: indication of low-temperature heat treatment in Mozambique ruby. *Journal of Gemmology*, Vol. 35, No. 2, pp. 156–161.

Pearl Classification: GIA’s Approach

Joyce Wing Yan Ho and Sally Chan Shih
GIA, New York

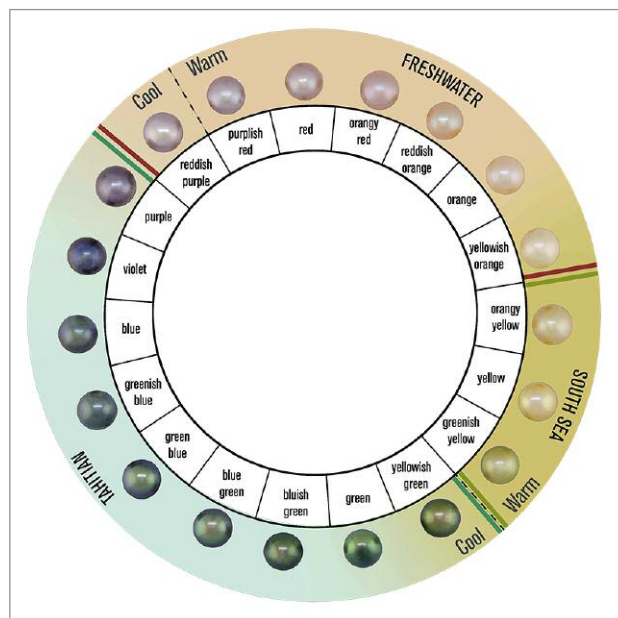
Pearls form in a wide variety of sizes, shapes, and colors. As a result, they are among the most popular materials in the jewelry industry. Their unique appearance and the affordability of many types of

cultured pearls on the market have allowed them to gain a greater audience. Throughout the ages, pearls have been associated with class, grace, and beauty by many cultures. Such a diverse range of

pearl types has meant that a way of grading or classifying them was required, and as a consequence, a number of different grading systems have been developed. The differences make the comparison of grades between systems difficult to align, and agreeing on a universal grading system has remained one of the many challenges facing the pearl industry.

GIA created the “7 Pearl Value Factors” (figure 1) for the same reason it developed the 4Cs of diamond quality: to establish a standard terminology for describing quality using language everyone can understand. Each value factor is important in determining a pearl’s overall quality. This poster reviews each value factor, starting with size and then looking at shape, color, luster, surface, nacre quality, and matching. GIA has developed a modernized color scale for all types of pearls (saltwater and freshwater) and physical master sets to ensure a pearl is graded with a degree of consistency. Every GIA laboratory worldwide uses the same grading system to produce consistent results. Adopting GIA’s standard pearl classification terminology throughout the gem and jewelry industry would foster improved communication within the trade and, by default, bridge the communication gap between buyers and sellers through easily understandable terminology.

Figure 1. Color is one of GIA’s 7 Pearl Value Factors. This hue circle depicts generalized color distribution by pearl type.



A Pearl Identification Challenge

Nicholas Sturman¹, Laura M. Otter^{2,4}, Artitaya Homkrajae³, Areeya Manustrong¹, Nanthaporn Nilpetploy¹, Kwanreun Lawanwong¹, Promlikit Kessrapong¹, Klaus Peter Jochum⁴, Brigitte Stoll⁴, Herman Götz⁵, and Dorrit E. Jacob²

¹GIA, Bangkok

²Macquarie University Department of Earth and Planetary Sciences, Sydney

³GIA, Carlsbad, California

⁴Max Planck Institute for Chemistry, Mainz, Germany

⁵Johannes Gutenberg University, Mainz, Germany

Pearl testing in laboratory conditions usually follows a set routine. The pearls are examined to obtain a preliminary idea of their type and identification, and then a series of steps (e.g., trace-element geochemical analysis, optical X-ray luminescence, microradiography, and X-ray computed microtomography) are undertaken to confirm the initial examination. With experienced gemologists it is possible, in many cases, to reach the same conclusion that was arrived at after the initial examination. However, all experienced gemologists have encountered situations—whether handling pearls or other gems—where the final result does not match the initial opinion.

This poster illustrates the trace-element characteristics of pearls in general, but focuses on two nacreous pearl samples in particular that revealed “atypical” properties not encountered in any pearls tested previously by GIA gemologists. On initial examination, the pearls did not show clear indications of being ei-

ther freshwater or saltwater. Nor was it clear whether they were likely to be natural or cultured. In most cases, these two questions would be resolved very quickly after some of the initial examination procedures were completed. This was not the case with these two examples, however, since the energy-dispersive X-ray fluorescence (EDXRF) results conflicted with the optical X-ray luminescence observations. This led to additional LA-ICP-MS analysis, a procedure not often required in routine pearl testing. The situation appeared even more perplexing after RTX work revealed inconclusive structures, which led to additional analysis using μ -CT. The pearls were so unusual in a number of ways, especially with regard to their trace-element chemistry, that we decided to seek a second opinion on this aspect in particular. Hence, the pearls were sent to the Max Planck Institute for Chemistry (MPIC) in Mainz, Germany.

The results of the work by GIA and MPIC showed that the pearls consisted of layer-like zones with distinct trace-element signatures associated with both saltwater and freshwater environments, as confirmed by the spot analysis undertaken by three different LA-ICP-MS units in three different locations operated by three different groups of scientists. While the pearls were in Germany, the opportunity was also taken to perform μ -CT analysis on both samples. The results were in keeping with those obtained by GIA, though the interpretation of the structures was

not straightforward and together with the trace-element chemistry led to various questions about the producing mollusk and the origin/type.

In summary, the pearls were found to be a mixture of saltwater and freshwater layers. While the pearls are likely non-bead cultured, their true identity remains a puzzle owing to their complex chemistry and questions raised concerning the producing mollusks. To our knowledge, these pearls with mixed trace-element patterns are the first of their type recorded in the literature.

The Study of Tanzanite's Gemological and Color Characteristics

Jinding Yu and Ren Lu

Gemmological Institute, China University of Geosciences, Wuhan

Tanzanite was discovered in the Merelani Hills in the Arusha region of northeastern Tanzania during the 1960s. It first became popular with a promotional campaign by Tiffany & Co. in the late 1960s. The fact that there is only one deposit in the world further raised its value. Never before had a newly discovered gemstone gained so much success within such a short time.

Natural, unheated blue tanzanite is rare and known for its trichroic colors: bluish violet, violetish blue, and yellow-green. To best realize the hidden beauty, natural tanzanite, often showing a brown hue, is heated to achieve a predominantly blue coloration before reaching the market. It has been previously reported that

heated tanzanite will convert from trichroic to dichroic, but there have been few details and virtually no quantitative UV-Vis absorption coefficient data to support that claim.

Tanzanite exhibits metachromatism, a color change, when illuminated by cold and warm light sources. In addition, tanzanite also exhibits the Usambara effect. The only form of zoisite to have its Usambara effect studied until now was epidote. If these two color phenomena are also recognized, it will raise tanzanite's status and value.

For this study we chose several brown zoisites, a violet tanzanite, a pink zoisite and a green zoisite from Merelani, and a green zoisite

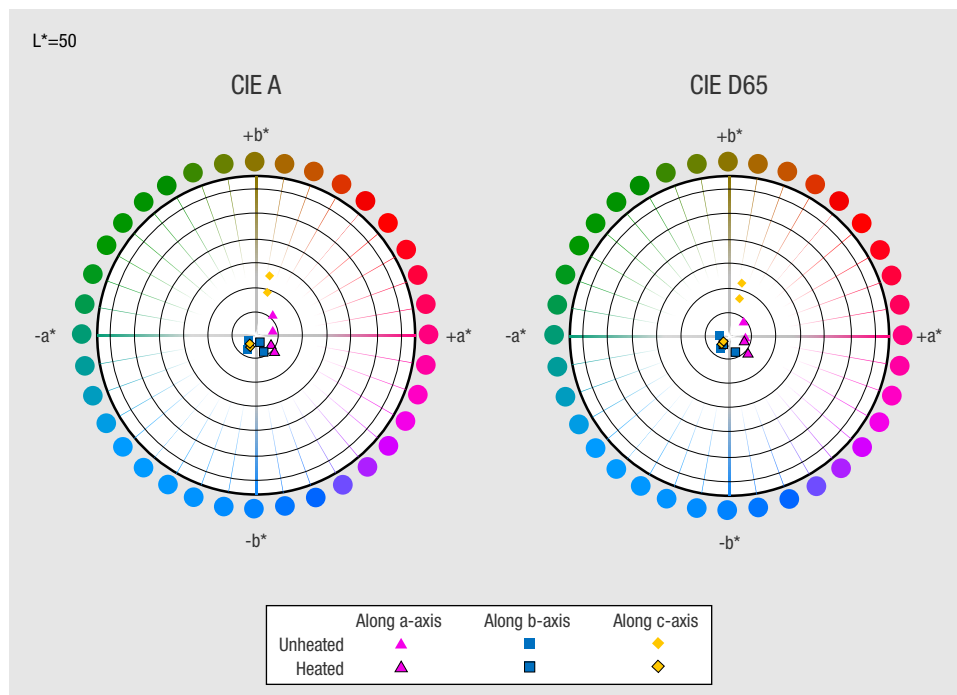


Figure 1. Colorimetric parameters for three axes of an unheated and a heated tanzanite sample are shown in CIELAB color space under standard A illuminant (left) and standard D65 illuminant (right). See Liu et al. (1999), Schmetzer et al. (2009), and Sun et al. (2015).

from Afghanistan. We conducted a systematic and quantitative analysis of the tanzanite sample using XRF and LA-ICP-MS, as well as FTIR, Raman, and UV-Vis spectroscopy. We attempted to quantitatively analyze the tanzanite's color before and after heating.

The results showed that tanzanite changed from trichroic to nearly—but not completely—dichroic after heating. The differ-

ence between these two types of blue was eye visible but also indicated by the spectrum and the photos. The study revealed tanzanite's color-change quantitative data and the method for taking photos of its color-change effect. We also found that the brown zoisite displayed the Usambara effect. Lastly, we concluded that the tanzanite's blue level is probably related to vanadium.

REFERENCES

Liu Y., Shigley J.E., Halvorsen A. (1999) Colour hue change of a gem tourmaline from the Umba Valley, Tanzania. *Journal of Gemmology*, Vol. 26, No. 6, pp. 386–396.

Schmetzer K., Bernhardt H.-J., Bosshart G., Hainschwang T. (2009) Colour-change garnets from Madagascar: Variation of chemical, spectroscopic and colorimetric

properties. *Journal of Gemmology*, Vol. 31, No. 5-8, pp. 235–282.

Sun Z., Palke A.C., Renfro N. (2015) Vanadium- and chromium-bearing pink pyrope garnet: Characterization and quantitative colorimetric analysis. *G&G*, Vol. 51, No. 4, pp. 348–369, <http://dx.doi.org/10.5741/GEMS.51.4.348>

Diamond Identification

Complex Charge Transfer in Chameleon Diamonds: A Model of the Color-Change Process

James E. Butler^{1,2}, Keal S. Byrne², Wuyi Wang³, and Jeffrey E. Post²

¹Cubic Carbon Ceramics, Washington, DC

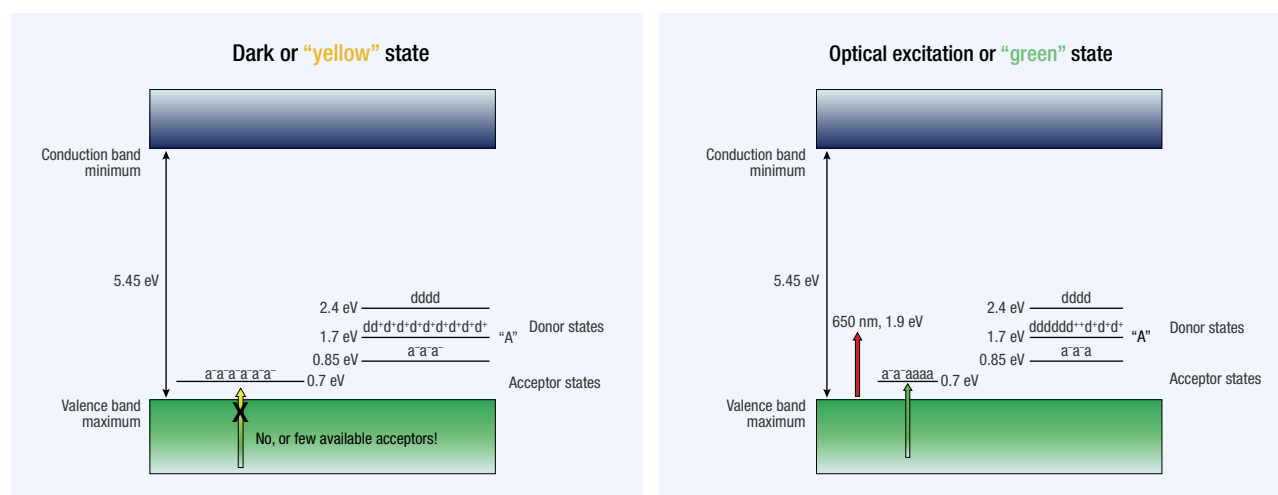
²Department of Mineral Sciences, Smithsonian Institution, Washington, DC

³GIA, New York

A group of natural diamonds known as chameleon diamonds change color from green to yellow based on their exposure to light and heat. These diamonds also emit long-lived phosphorescence after UV excitation. We have observed the optical response of these diamonds to optical and thermal excitation and developed a model

to explain the observed phenomena. A principal element of the model is the proposal of an acceptor state (figure 1), which should be observable in the near-infrared (NIR) region. Subsequently, we have observed the NIR absorption to this acceptor state, supporting our model of charge-transfer processes in these diamonds.

Figure 1. A schematic of the model for each color state of a chameleon diamond based on absorption from valence band states to the proposed acceptor state being blocked by full compensation (the “yellow” state) or incomplete compensation when exposed to room lighting (the “green” state).



Melee Diamonds: Metal Defects and Treated Color

Shoko Odake
GIA, Tokyo

Gem-quality laboratory-grown diamonds are manufactured in large quantities. With frequent reports of the mixing of melez-sized synthetic diamonds with natural stones, demand for melee diamond screening is increasing. During melee diamond screening at GIA's Tokyo lab, two notable types of samples with uncommon characteristics have been found.

1. *Natural melee diamonds with silicon and nickel defects.* Luminescence peaks derived from Si- and Ni-related defects are often observed in colorless melee grown by the HPHT method. The silicon-related defect, once considered proof of CVD-grown diamond, is now known to exist naturally as well (Breeding and Wang, 2008). Several colorless melee diamonds having both silicon- and nickel-related emissions have been found in GIA's Tokyo lab; olivine inclusions were found in one of these samples. Spectroscopic and gemological features confirmed that the samples were grown in nature.
2. *Irradiated laboratory-grown diamond melee found among irradiated natural melee diamonds.* Several thousand

greenish blue melee diamonds have been submitted by various clients to the Tokyo lab for testing. Each diamond's color was attributed to a strong GR1 defect caused by irradiation treatment. Fourier-transform infrared (FTIR), photoluminescence (PL), and DiamondView analysis revealed that most of them were irradiated natural diamonds. Eight were irradiated CVD-grown diamonds, and one was an irradiated HPHT-grown specimen. The infrared spectrum of all the CVD samples showed a peak at 3123 cm^{-1} , while their PL spectrum showed a doublet peak at 596/597 nm. Those peaks are specific to as-grown CVD diamonds, as annealing removes the peaks. From their spectra, these CVD specimens were considered irradiated without pre-annealing.

REFERENCE

Breeding C.M., Wang W. (2008) Occurrence of the Si-V defect center in natural colorless gem diamonds. *Diamond and Related Materials*, Vol. 17, pp. 1335–1344, <http://dx.doi.org/10.1016/j.diamond.2008.01.075>

Nitrogen in CVD-Grown Diamond

Alexander M. Zaitsev^{1,2}, Kyaw Soe Moe², and Wuyi Wang²
¹College of Staten Island, City University of New York
²GIA, New York

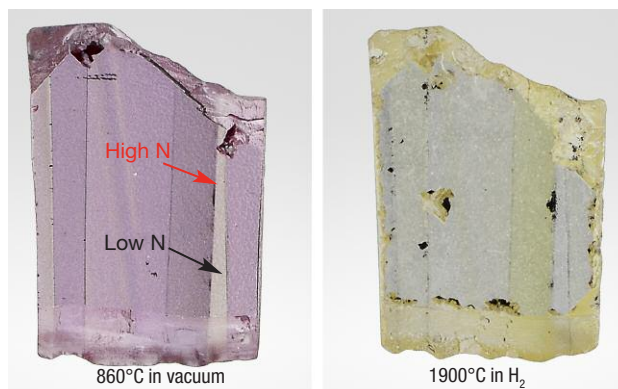
In diamond grown by the CVD method, nitrogen behaves differently than it does in natural and HPHT-grown diamond. The most striking peculiarities are low efficiency of doping, formation of unique optical centers over a wide spectral range from the ultraviolet (UV) to the IR regions, and formation of unusual defects related to aggregated nitrogen. In order to gain a better insight into this problem, several nitrogen-doped specimens grown in GIA's CVD diamond lab and a few commercial yellow CVD-grown diamonds have been studied in their as-grown (as-received) state and after electron irradiation and annealing at temperatures up to 1900°C (low-pressure, high-temperature treatment).

We found that the brightest pink color of electron-irradiated nitrogen-doped CVD-grown diamond is produced by the NV⁻ center after annealing at temperatures of about 1000°C . Annealing at temperatures over 1600°C destroys the irradiation-induced pink color (figure 1).

The most prominent optical centers in the IR spectral region (figure 2, left) produced absorptions at 2828, 2874, 2906, 2949,

3031, 3107, 3123, and 3310 cm^{-1} (latter two not shown). These are ascribed to nitrogen-hydrogen complexes. Two characteristic

Figure 1. The distribution of color in commercial nitrogen-doped CVD-grown diamond after electron irradiation and subsequent annealing at temperatures of 860°C (left) and 1900°C (right).



ABSORPTION SPECTRA

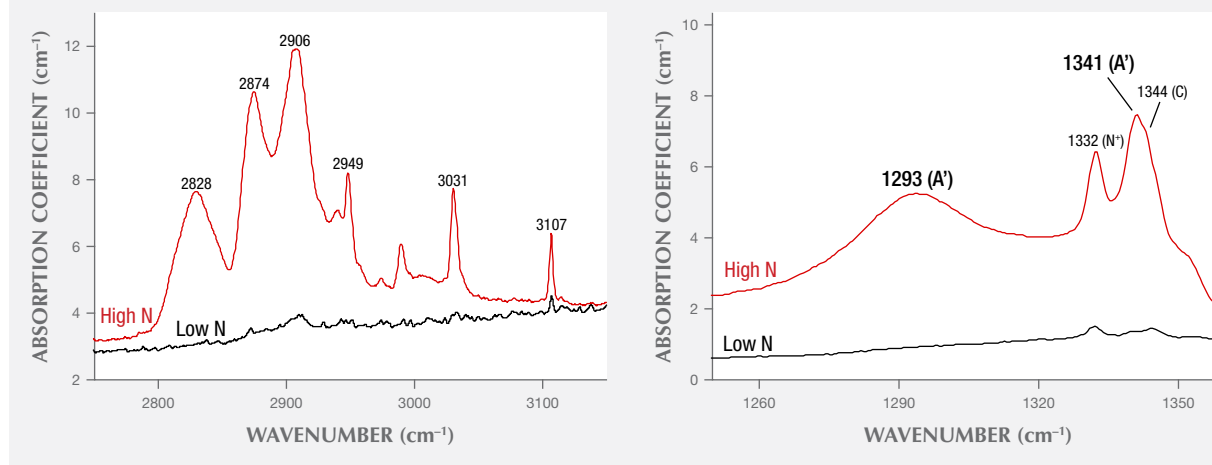


Figure 2. These spectra show specific nitrogen-hydrogen absorption features in the two-phonon spectral range (left) and absorption of modified nitrogen A-aggregates (right) in nitrogen-doped CVD-grown diamond.

absorption features at 1293 and 1341 cm^{-1} (figure 2, right) are unique to CVD diamond. They are tentatively ascribed to a modified form of nitrogen A-aggregates.

In the visible and NIR spectral ranges, characteristic nitrogen-related centers have zero-phonon lines (ZPLs) at 457, 462, 489, 498, 647, 722.5, 852.5, 865.5, 868.5, 908, 921.5, and 924.5 nm. The 489 nm feature is a major color center of electron-irradiated,

nitrogen-doped CVD-grown diamond. This center, together with the GR1 center, is responsible for the green color in this material.

An assumption is made that N atoms may form clusters in highly nitrogen-doped CVD-grown diamonds. These clusters may result in broad-band luminescence at wavelengths of 360, 390, 535, and 720 nm and a strong broadening of the ZPLs of many optical centers.

Steps in Screening and ID of Laboratory-Grown Diamonds with Synthetic Diamond ID Kit

Branko Deljanin¹ and John Chapman²

¹CGL-GRS Swiss Canadian Gemlab, Vancouver, Canada

²Gemetrix, Perth, Western Australia

Laboratory-grown diamonds are created using either high-pressure, high-temperature (HPHT) or chemical vapor deposition (CVD). With the influx of manmade diamonds on the market over the past few years, instrument producers and labs have launched screening and detection instruments to help dealers and jewelers spot HPHT- or CVD-grown specimens.

Most standard instruments are inaccurate testers or just type I and type II screening devices that do not give a definite answer about diamond genesis. Over the last four annual Mediterranean Gemmological and Jewellery Conferences and more than 30 workshops given in 17 countries, we have assembled a portable new Synthetic Diamond Identification Kit. The kit comprises two portable instruments and two booklets:

- A PL inspector (mini UV lamp with magnifier) to inspect laboratory-grown, treated, and natural diamonds

using long- and short-wave fluorescence and phosphorescence

- A 2017 handbook with images and explanation of long- and short-wave reactions of diamonds of all types
- A mini foldable polariscope with portable light to separate natural diamonds using characteristic birefringence patterns from HPHT and CVD diamonds
- A 2010 handbook with images and explanations of cross-polarized filter reactions of diamonds of all types

The combination of this kit with professional training could identify all HPHT-grown diamonds and most CVD-grown diamonds on the market, loose or mounted. Also available are melee and jewelry inspectors consisting of larger UV lamps with magnifiers designed for identification of small loose or mounted diamonds.

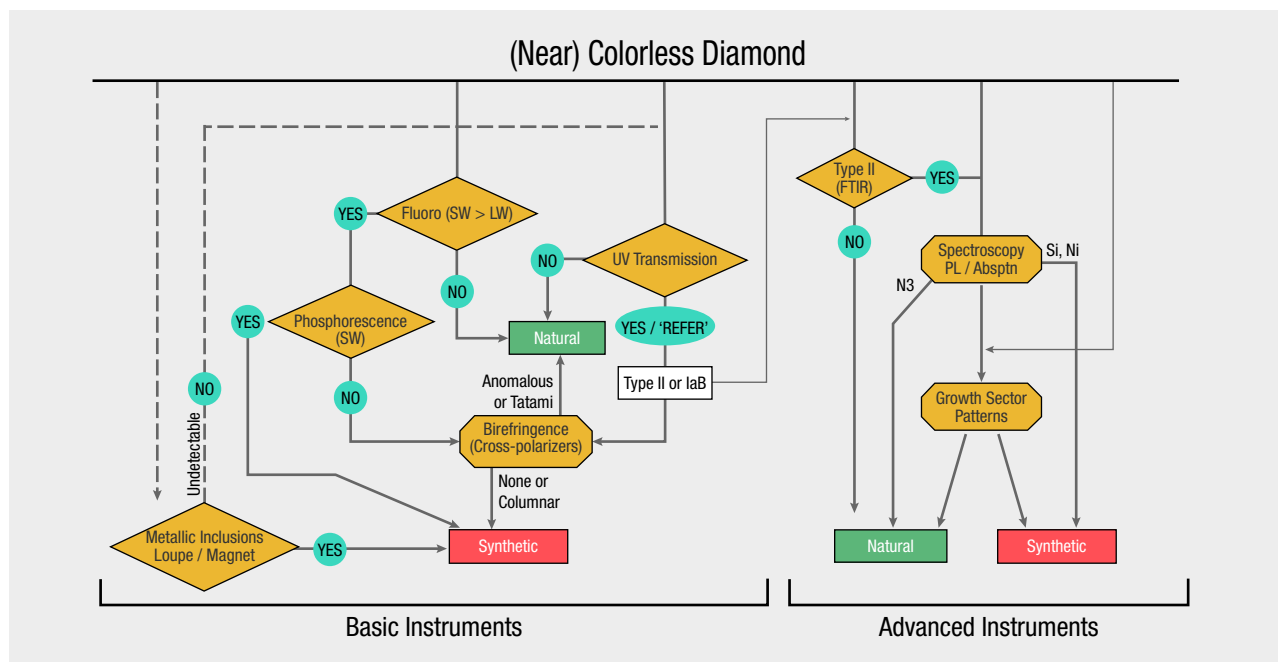


Figure 1. This chart illustrates the steps in the screening and identification of lab-grown diamonds.

Different diamond types and subtypes can exhibit different birefringence under cross-polarized filters. A clear majority of natural diamonds exhibit some degree of internal strain, with type II natural diamonds showing a weak “tatami” pattern. HPHT-grown diamonds are free of such strain, and CVD-grown diamonds show mostly coarse columnar patterns.

Most natural diamonds have a strong reaction to long-wave UV; this reaction is usually weaker (mostly blue) at shorter wavelengths. Laboratory-grown diamonds generally exhibit more intense fluorescence with short-wave UV compared to long-wave UV, with a

chalky coloring tinged with green or yellow. Most HPHT-grown diamonds also phosphoresce. If a diamond is free of inclusions, fluorescence is a reliable screening test to flag suspicious stones that should be further checked under cross-polarized filters (figure 1).

In the case of some rare near-colorless clean CVD-grown diamonds that do not show fluorescence or have a birefringence pattern that is coarse but resembling tatami in type IIa and weak patterns in natural Ia diamonds, additional tests using advanced spectroscopy and strong short-wave UV light to observe growth patterns are needed to confirm diamond genesis.

Diamond Geology

Evidence of Subducted Altered Oceanic Crust into Deep Mantle From Inclusions of Type IaB Diamonds

Tingting Gu¹, John Valley², Kouki Kitajima², Michael Spicuzza², John Fournelle², Richard Stern³, Hiroaki Ohfuji⁴, and Wuyi Wang¹

¹GIA, New York

²Department of Geoscience, University of Wisconsin, Madison

³Canadian Centre for Isotopic Microanalysis (CCIM), Department of Earth and Atmospheric Sciences, University of Alberta, Edmonton

⁴Geodynamics Research Center (GRC), Ehime University, Matsuyama, Japan

Nitrogen is one of the most common impurities in diamond, and its aggregation styles have been used as criteria for diamond classification. Pure type IaB diamonds (with 100% nitrogen in B aggregation) are rather rare among natural diamonds. The occurrence of the B center is generally associated with high temperature and a long

residence time of the host diamond, which would potentially provide information on the earth’s deep interior. Seawater circulation is the unique process that shapes the surface of our planet and potentially has a profound effect on its interior due to slab subduction.

In about 50 type IaB diamonds with detectable micro-inclusions

submitted to GIA for screening, we found that more than 70% of them contained a typical mineral assemblage from the sublithosphere. Jeffbenite (TAPP), majorite garnet, enstatite, and ferropericase have been observed, which could be retrograde products of former bridgmanite. CaSiO_3 -walsstromite with larnite and titanite is the dominant phase present in approximately 40% of all diamond samples. Direct evidence from oxygen isotope ratios measured by secondary ion mass spectrometry, or SIMS, ($\delta^{18}\text{O}_{\text{VSMOW}}$ in the range +10.7 to +12.5‰) of CaSiO_3 -walsstromite with coexisting larnite and titanite that retrograde from CaSiO_3 -perovskite suggest that hydrothermally altered oceanic basalt can subduct to depths of >410 km in the transition zone. Incorporation of materials from subducted altered oceanic crust into the deep mantle produced diamond inclusions that have both lower mantle and subduction

signatures. $\text{Ca}(\text{Si,Al})\text{O}_3$ -perovskite was observed with a high concentration of rare earth elements (>5 wt.%) that could be enriched under P - T conditions in the lower mantle. Evidence from ringwoodite with a hydroxide bond, coexisting tuite and apatite, precipitates of an NH_3 phase, and cohenite with trace amounts of Cl imply that the subducted brines can potentially introduce hydrous fluid to the bottom of the transition zone. In the diamonds with subducted materials, the increasing carbon isotope ratio from the core to the rim region detected by SIMS ($\delta^{13}\text{C}$ from -5.5‰ to -4‰) suggests that an oxidized carbonate-dominated fluid was associated with recycling of the subducted hydrous material. The deep subduction played an important role in balancing redox exchange with the reduced lower mantle indicated by precipitated iron nanoparticles and coexisting hydrocarbons and carbonate phases.

Origin of Rare Fancy Yellow Diamonds from Zimmi (West Africa)

Karen V. Smit¹, Ulrika F.S. D'Haenens-Johansson¹, Daniel Howell², Lorne C. Loudin¹, and Wuyi Wang¹

¹GIA, New York

²Department of Geoscience, University of Padua, Italy, and Diamond Durability Laboratory, New York

Type Ib diamonds from Zimmi, Sierra Leone, have 500 My mantle residency times whose origin is best explained by rapid tectonic exhumation after continental collision to shallower depths in the mantle prior to kimberlite eruption (Smit et al., 2016). Here we present spectroscopic data for a new suite of Zimmi sulfide-bearing type Ib diamonds that allow us to evaluate the link between their rare Fancy yellow colors, the distribution of their spectroscopic features, and their unusual geological history. Cathodoluminescence (CL) imaging revealed irregular patterns with abundant deformation lamellae, as

sociated with the diamonds' tectonic exhumation (Smit et al., 2018). Vacancies formed during deformation were subsequently naturally annealed to form vacancy clusters, $\text{NV}^{0/-}$ centers, and H3 (NVN^0). The brownish yellow to greenish yellow colors observed in Zimmi type Ib diamonds result from visible absorption by a combination of isolated nitrogen and deformation-related vacancy clusters (Smit et al., 2018). Color-forming centers and other spectroscopic features can all be attributed to the unique geological history of Zimmi type Ib diamonds and their rapid exhumation after formation.

REFERENCES

Smit K.V., Shirey S.B., Wang W. (2016) Type Ib diamond formation and preservation in the West African lithospheric mantle: Re-Os age constraints from sulphide inclusions in Zimmi diamonds. *Precambrian Research*, Vol. 286, pp. 152–166, <http://dx.doi.org/10.1016/j.precamres.2016.09.022>

Smit K.V., D'Haenens-Johansson U.F.S., Howell D., Loudin L.C., Wang W. (2018) Deformation-related spectroscopic features in natural type Ib-IaA diamonds from Zimmi (West African craton). *Mineralogy and Petrology*, pp. 1–15, <http://dx.doi.org/10.1007/s00710-018-0587-6>

Type Ib–Dominant Mixed-Type Diamond with Cuboctahedral Growth Structure: A Rare Diamond Formation

Kyaw Soe Moe and Paul Johnson

GIA, New York

Type Ib–dominant mixed-type diamonds (Ib-IaA) can be formed by multiple growth events (Titkov et al., 2015; Smit et al., 2018). In this study, we report on a 0.41 ct Fancy Dark brown gem-quality diamond that formed in a *single* growth event. It is a type Ib-IaA with a C defect (single-substitutional nitrogen atom) con-

centration up to 21 ppm. The Fourier-transform infrared (FTIR) peaks of the H1a and H1b defects (figure 1, left) suggest that this diamond was irradiated and annealed to achieve a Fancy color grade. The cuboctahedral structure can be observed in the DiamondView images (figure 1, right), which show reddish orange

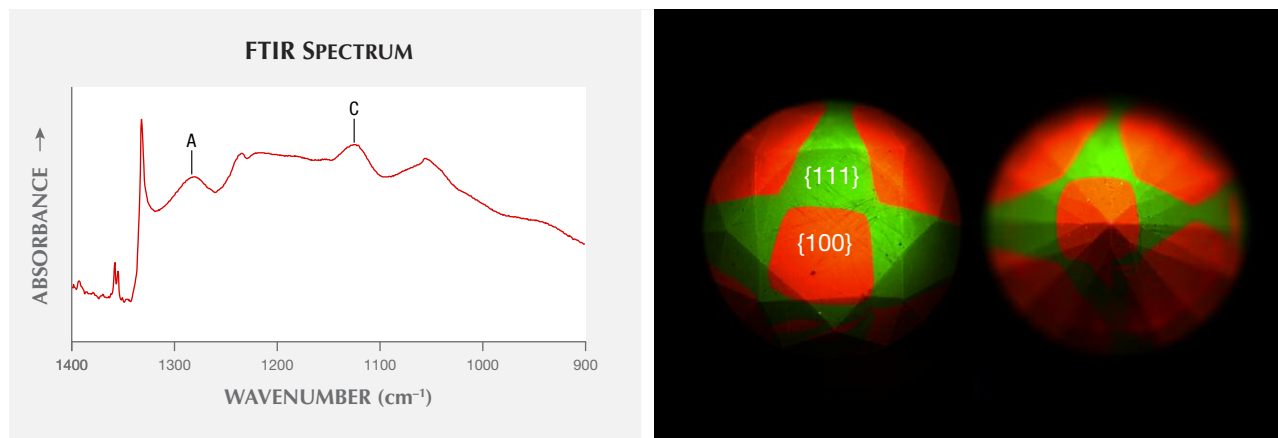


Figure 1. Left: The stone's FTIR spectrum revealed that it is a type Ib-IaA diamond with nitrogen defects, "C" single nitrogen atoms and an "A" pair of nitrogen atoms. Right: DiamondView images show cuboctahedral growth structure containing a {100} sector with reddish orange fluorescence and a {111} sector with green fluorescence. Distinct fluorescence zoning following growth structure is caused by NV centers in {100} sectors and H3 defects in {111} sectors, which were created during the irradiation and annealing processes.

fluorescence in the {100} sector caused by NV centers and green fluorescence in the {111} sector caused by H3 defects. Irradiation treatment helps us to see the cuboctahedral structure. However, the presence of an amber center suggests that it did not undergo HPHT treatment.

Cuboctahedral growth structure can be usually observed in HPHT diamonds that are grown in a laboratory with a fast growth rate (i.e., less than one week per carat) under *P-T* conditions of 5–6 GPa and 1300–1500°C. A natural diamond that grows rapidly in a single growth event would also possess mixed cuboid and octahedral forms.

REFERENCES

Smit K.V., D'Haenens-Johansson U.F.S., Howell D., Loudin L.C., Wang W. (2018) Deformation-related spectroscopic features in natural type Ib-IaA diamonds from Zimmi (West African craton). *Mineralogy and Petrology*, pp. 1–15, <http://dx.doi.org/10.1007/s00710-018-0587-6>

Time and temperature are critical in the aggregation of nitrogen atoms in diamond. Nitrogen atoms are initially incorporated as single atoms during diamond formation. Our sample was rich in C defects associated with A defects (a pair of nitrogen atoms). This suggests that the process of nitrogen aggregation was interrupted by the diamond's ascent to shallower depths in the mantle at lower temperatures by rapid tectonic exhumation (Smit et al., 2018). The cuboctahedral growth structure of this diamond indicated that, prior to ascending to shallower depths of the mantle, it grew in a few days in the diamond stability field (i.e., 150–200 km in depth within the earth) in a single growth event.

Titkov S.V., Shiryayev A.A., Zudina N.N., Zudin N.G., Solodova Y.P. (2015) Defects in cubic diamonds from the placers in the northeastern Siberian platform: Results of IR microspectrometry. *Russian Geology and Geophysics*, Vol. 56, No. 1-2, pp. 354–362, <http://dx.doi.org/10.1016/j.rgg.2015.01.026>

Gem Characterization

3161 cm⁻¹ Infrared Feature in Synthetic Sapphires

Gagan Choudhary and Sandeep Vijay
Gem Testing Laboratory, Jaipur, India

The 3161 cm⁻¹ mid-infrared (IR) spectral feature (figure 1) is an important tool in the identification of unheated sapphires, especially in material from low-iron metamorphic environments such as Sri Lanka. This feature is a series of bands, composed of a strong

peak at ~3161 cm⁻¹ and smaller side bands at ~3075, 3240, and 3355 cm⁻¹. A few researchers have attributed these features to OH groups involved in charge compensation with Si⁴⁺, while some have assigned them to structurally bonded OH, associated with Mg²⁺.

The 3161 cm^{-1} series is more commonly observed in natural-color yellow sapphires than any other color of corundum; occasionally it is encountered in blues and pinks. These authors, however, have encountered a strong feature at $\sim 3161\text{ cm}^{-1}$ in a few specimens of yellow synthetic sapphire grown by the flame-fusion (Verneuil) process. Their synthetic origin was determined on the basis of inclusion study, which revealed the presence of clouds of minute gas bubbles, along with some bomb-shaped gas bubbles, typically associated with corundum or spinel grown by the flame-fusion process. Milky zones of fine pinpoints and a “plato” effect were also present.

The 3161 cm^{-1} mid-IR feature in these synthetic yellow sapphires displayed side bands at approximately 3220 and 3277 cm^{-1} , as opposed to 3240 and 3352 cm^{-1} in natural sapphires.

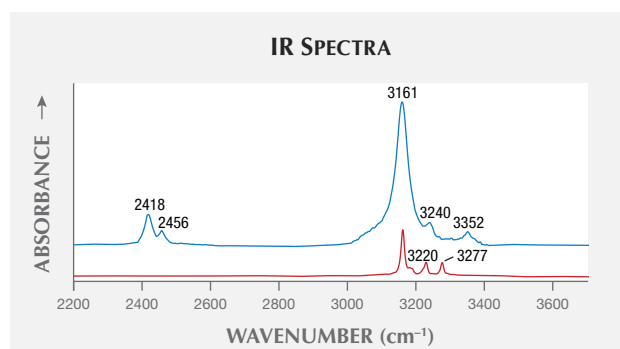


Figure 1. The 3161 cm^{-1} series mid-IR feature, assigned to structurally bonded OH and associated with Mg^{2+} , displays side bands at ~ 3352 and 3240 cm^{-1} in natural sapphires and at ~ 3277 and 3220 cm^{-1} in synthetic material. Natural sapphires also displayed CO_2 -related bands at ~ 2456 and 2418 cm^{-1} .

Agate Analysis by Raman, XRF, and Hyperspectral Imaging Spectroscopy for Provenance

Aaron Celestian¹, Arlen Heginbotham², Rebecca Greenberger³, Bethany Ehlmann³, Bibek Samanta⁴, Alyssa Morgan¹, and Sergey Mamedov⁵

¹Natural History Museum of Los Angeles County

²J. Paul Getty Museum, Los Angeles

³California Institute of Technology, Pasadena

⁴University of Southern California, Los Angeles

⁵Horiba Scientific, Edison, New Jersey

The Getty Institute in Los Angeles recently acquired the Borghese-Windsor Cabinet (figure 1, left), a piece of furniture extensively decorated with agate, lapis lazuli, and other stones. The cabinet is thought to have been built around 1620 for Camillo Borghese

(later Pope Paul V). It was traditionally thought that all agate gemstones acquired during the sixteenth and seventeenth centuries were sourced from the Nahe River Valley near Idar-Oberstein, Germany. While Brazilian agate began to be imported into Germany by the

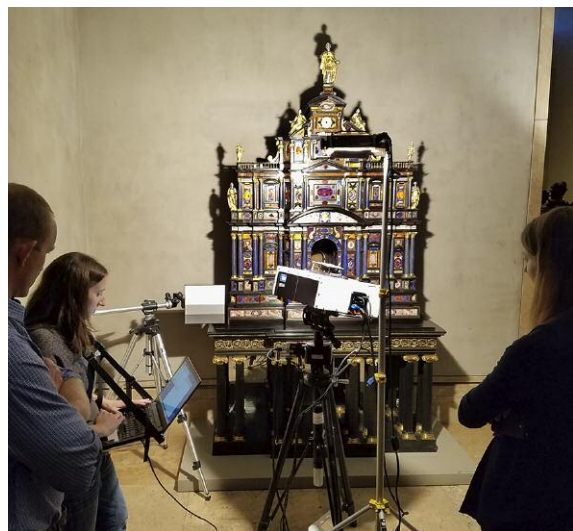


Figure 1. Left: The Borghese-Windsor Cabinet on display at the Getty Center, being imaged by the hyperspectral analyzer (center, on tripod). Right: This Brazilian agate from Rio Grande do Sul is part of the NHMLA collection. Transect A-A' is where the Raman map was collected. Photos by Arlen Heginbotham (left) and Aaron Celestian (right).

1800s, it is possible that some was imported in the eighteenth century or earlier. A primary research goal was to determine if the agates in the Borghese-Windsor Cabinet are of a single origin, or if they have more than one geologic provenance.

Both quartz and moganite will crystallize together as agate forms, but moganite is not stable at Earth's surface and will convert to quartz over tens of millions of years (Heaney, 1995; Gíslason et al., 1997; Moxon and Rios, 2004). Thus, older agate contains less moganite. Agate from Idar-Oberstein is Permian in age (around 280 million years old), while agate from the Brazilian state of Rio Grande do Sul generally formed during the Cretaceous (around 120 million years ago). It is thought that Rio Grande do Sul would have been a primary source of material exported to Europe because it is one of Brazil's oldest and largest agate producers.

When examining the cryptocrystalline parts of agate from comparative collections, Brazilian agates from the collection of the Natural History Museum of Los Angeles County (NHMLA; figure 1, right) had 8% or higher moganite concentration, whereas the Idar-Oberstein agate (on loan from the Smithsonian National Museum of Natural History) had less than 2% moganite. The moganite distribution in the agate is heterogeneous, likely due to different growth stages and changing geological conditions during agate formation. Using the Raman maps, we were able to isolate the areas that contained moganite + quartz and measure the ratios in those specific bands (figure 2). This narrow-band approach to determining quartz to moganite ratio, when compared to broad-brand and whole-sample approaches, was shown to be more reproducible in distinguishing Brazilian from German agates.

These same agates from the Brazilian and German localities were then taken to Caltech to collect hyperspectral imaging data

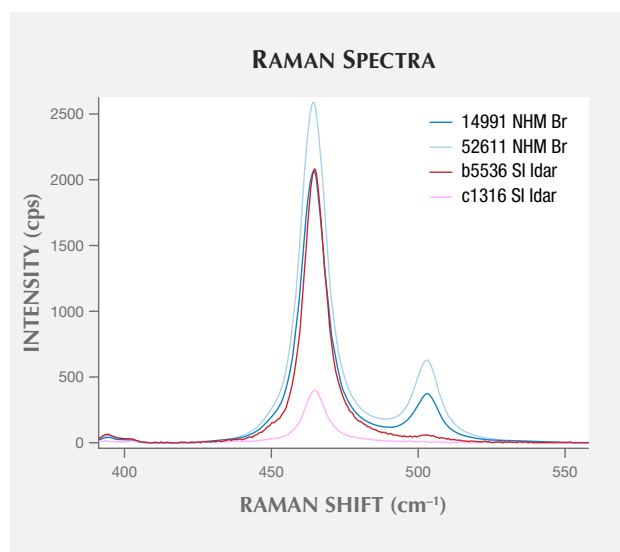


Figure 2. Raman analyses of two Brazilian agates (blue) and two German agates (red) in the diagnostic region between 400 and 550 cm^{-1} show the strongest peaks for quartz at 463 cm^{-1} and moganite at 501 cm^{-1} . These data were taken from narrow-band analysis (summing all spectra in the narrow agate bands that contained quartz + moganite). Each band was used as a separate analysis. Note the strong moganite presence in the Brazilian agates.

(on a custom-built Headwall Photonics co-boresighted visible/near-infrared and shortwave infrared sensor). Imaging data were compared to the NHMLA laboratory Raman and X-ray fluorescence analyses, and correlation analysis of combined datasets from the three different experimental procedures allowed us to establish a unique characterization pattern for the different localities.

REFERENCES

Gíslason S.R., Heaney P.J., Oelkers E.H., Schott J. (1997) Kinetic and thermodynamic properties of moganite a novel silica polymorph. *Geochimica et Cosmochimica Acta*, Vol. 61, No. 6, pp. 1193–1204, [http://doi.org/10.1016/S0016-7037\(96\)00409-7](http://doi.org/10.1016/S0016-7037(96)00409-7)
 Heaney P.J. (1995) Moganite as an indicator for vanished evaporites: A testament reborn? *Journal of Sedimentary Research*, Vol. 65, No. 4A, pp. 633–638,

<http://dx.doi.org/10.1306/D4268180-2B26-11D7-8648000102C1865D>
 Moxon T., Rios S. (2004) Moganite and water content as a function of age in agate: An XRD and thermogravimetric study. *European Journal of Mineralogy*, Vol. 16, No. 2, pp. 269–278, <http://dx.doi.org/10.1127/0935-1221/2004/0016-0269>

Beryllium Heat Treatment of Blue Sapphire from Sri Lanka

Sutas Singbamroong^{1,2}, Panjawan Thanasutthipitak¹, Thawatchai Somjaineuk³, and Nazar Ahmed²

¹Department of Geological Science, Chiang Mai University, Thailand

²Dubai Central Laboratory Department, Dubai, United Arab Emirates

³Chanthaburi Gem and Jewelry Manufacturer Association, Chanthaburi, Thailand

Since at least 2000, corundum has been subjected to a beryllium (Be) heat treatment technique in Chanthaburi, Thailand. For this study, samples of transparent to translucent milky-white to yellow,

purple to violet, and light to medium blue sapphires from Sri Lanka (metamorphic origin) were heat treated with Be in three types of furnaces (gas, electric, and fuel) at various temperatures

and in both oxidizing and reducing atmospheres. The technique of Thai gem heating specialist Thawatchai Somjaineuk was used to intensify blue color, improve clarity, and distribute uneven color. Somjaineuk's technique has been used to enhance Sri Lankan corundum with a milky/silky appearance since 2004, and supplies approximately 50 kg of beryllium-treated blue sapphire per year to the gem market.

The samples were studied after each step of heating for basic gemological properties, spectroscopic properties using ultra-violet/visible/near-infrared (UV-Vis-NIR) and Fourier-transform infrared (FTIR) absorption spectroscopy, and chemical composition using laser ablation–inductively coupled plasma–mass spectrometry (LA-ICP-MS). The corundum samples were first heated in a traditional O₂/LPG mixed-gas furnace to about 1500°C for two hours in an oxidizing atmosphere. The white to yellow and light to medium blue sapphires turned colorless, whereas the purple to violet sapphires became pink. The second step of heating was performed with Be in an electric furnace at about 1700°C for 48 hours in an oxidizing atmosphere. After this process, the milky/silky colorless sapphires became a more transparent yellow, while the pink sapphires turned orange-pink. These stones were enhanced in the final step by reheating in a fuel furnace at about 1700°C for 72 hours in a reducing atmosphere. All samples became blue with light to strong saturation and tone.

The combination of the color appearance, the absorption spectra analyzed after oxidation with Be and reduction heating (figure 1), and the chemical data suggest that Be and/or Mg trapped-hole yellow color centers—created during oxidation heating with Be—were made inactive after reduction heating. The blue

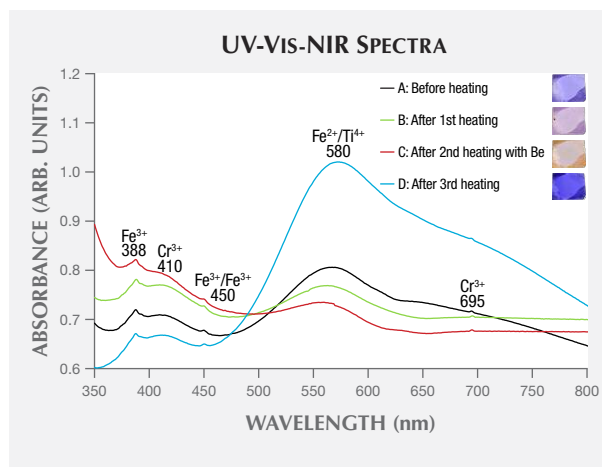


Figure 1. UV-Vis spectra of a violet sapphire before treatment (A), after a first heating in a reducing atmosphere (B), after a second heating with beryllium in an oxidizing atmosphere (C), and after a third heating in a reducing atmosphere (D).

coloration is mainly caused by strong broad absorption bands of Fe²⁺/Ti⁴⁺ intervalence charge transfer (IVCT) mechanism without Fe²⁺/Fe³⁺ IVCT. However, chemical data were analyzed for those samples and showed relatively high Mg and Be concentrations in comparison with the Ti composition, which does not fit well with the model that indicates [Ti⁴⁺] > [Mg²⁺ + Be²⁺] causes blue coloration. This heating technique is still not well understood. Further experiments and analyses are being carried out to confirm the role of beryllium in blue sapphires.

Gemological and Spectroscopic Characteristics of Australian Sapphires

Yafen Xu and Jingru Di

Gemmological Institute, China University of Geosciences, Wuhan

Although Australia has assumed a major role in the production of sapphire, research on this material has not been comprehensive. This study aims to analyze the gemology and spectroscopy of Australian sapphires and provide a theoretical basis for their treatment.

Under the optical microscope and other conventional instruments, hexagonal color zones were blue and yellow. Healing fissures and inclusions were extremely common. Raman spectroscopy showed that the inclusions were two-phase: CO₂ and H₂O with sapphire, rutile, zircon, diaspore, and amphibole, among others. Sulfur on the healing fissures indicated that S was filled during transportation. The IR spectra of the Australian sapphires typically revealed a 3310 cm⁻¹ absorption peak

(figure 1, left). This absorption feature is related to structural OH groups within the sapphire and revealed that these samples grew in reducing conditions. LA-ICP-MS indicated that the Cr/Ga ratio was less than 1 and the Fe/Ti ratio was generally 10–100 (figure 1, right), the typical ratio of magmatic sapphire. The iron content was between 3230 and 9431 ppm. Color varied with the content of Fe, Ti, Si, and Mg. UV-Vis absorption peaks (figure 2) at 377, 387, and 450 nm were caused by the d-d electronic transition of Fe³⁺ and Fe²⁺-Fe³⁺ in the region with less Ti; the absorption band centered at 559 nm in the yellow-green region indicated the charge transfer of Fe²⁺-Ti⁴⁺→Fe³⁺-Ti³⁺ and higher Ti content in this area. Fe²⁺-Fe³⁺ charge transfer

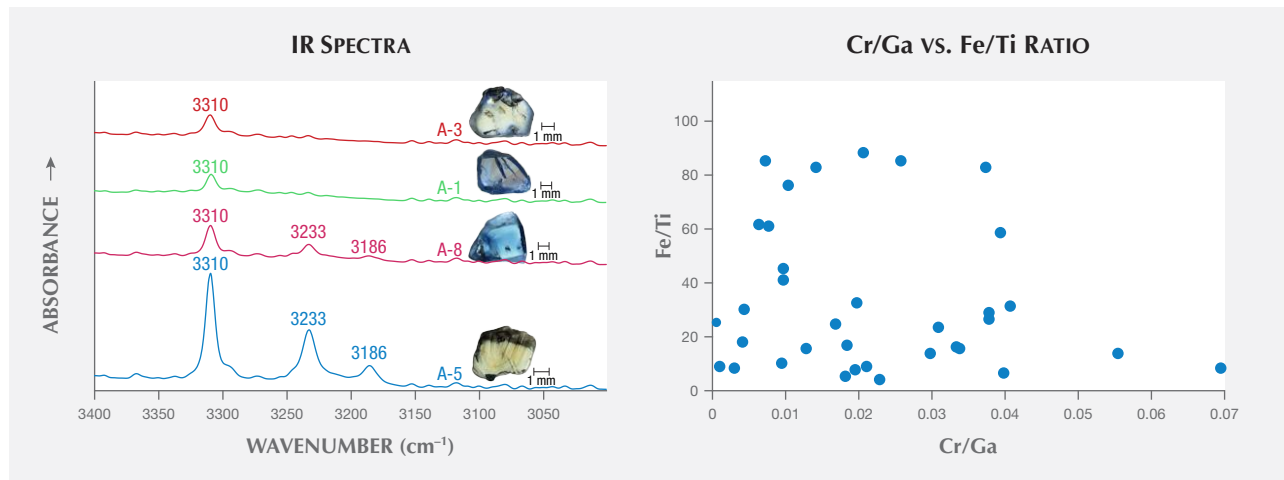


Figure 1. The absorption band of 3310 cm^{-1} in IR spectra (left) and the Cr/Ga versus Fe/Ti ratios (right) indicate that the Australian sapphires are magmatic and grew in a reducing environment.

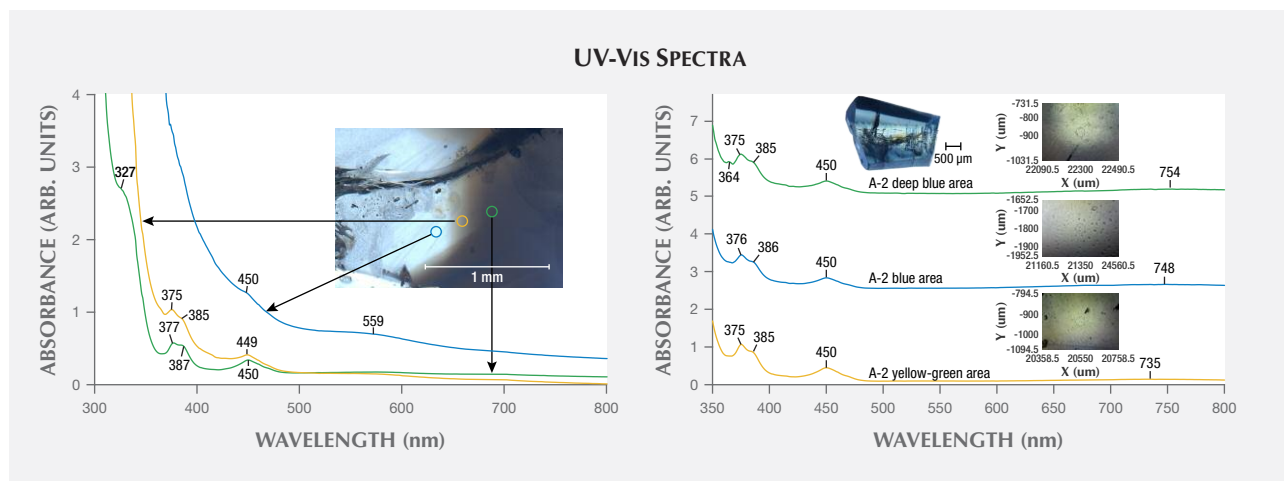


Figure 2. The UV-Vis spectra of the color zones in sapphire A-4 (left) and A-2 (right) are different because of different chromogenic ions (pairs).

often occurs together with $\text{Fe}^{2+}\text{-Ti}^{4+} \rightarrow \text{Fe}^{3+}\text{-Ti}^{3+}$ charge transfer and causes the wide absorption band at 700–800 nm centered

at 754 nm. The center may shift with different ratios of the charge transfer of $\text{Fe}^{2+}\text{-Fe}^{3+}$ and $\text{Fe}^{2+}\text{-Ti}^{4+} \rightarrow \text{Fe}^{3+}\text{-Ti}^{3+}$.

REFERENCES

Kan-Nyunt H.-P., Karampelas S., Link K., Thu K., Kiefert L., Hardy P. (2013) Blue sapphires from the Baw Mar mine in Mogok. *G&G*, Vol. 49, No. 4, pp. 223–232, <http://dx.doi.org/10.5741/GEMS.49.4.223>

Yimiao L., Tao C. (2015) Gemological characteristic of ruby and sapphire from Muling, Heilongjiang Province. *Journal of Gems & Gemology*, Vol. 17, No. 4, pp. 1–7.

A Grading Method of Jadeite Jade Transparency Based on Digital Image Analysis

Danlu Cui

Gemmological Institute, China University of Geosciences, Wuhan

In the jadeite jade market, transparency is an important feature judged by experienced practitioners observing with the unaided eye under reflected light. However, this method is easily influenced by subjective factors.

This research simulates human observation of characteristics that could help in judging jadeite transparency through certain visual information features. This approach could allow gemologists to evaluate transparency rapidly while effectively avoiding subjective factors, especially under the same test conditions used to judge jadeite jade color.

Some promising research results have been obtained, through comparing the lightness value of each image pixel in jadeite jade pictures and then using the maximum between-class variance method (OSTU) to obtain a binarization threshold. Thus, the image data is classified into a relatively bright area and a relatively dark area. When a beam of light is directed across an oval-cut jadeite jade with different degrees of transparency, different results are obtained from the images.

1. In oval-cut jadeite jade with a high degree of transparency, a beam of light arrives at the underside and then converges in the other side of its curved surface, forming a relatively bright area.
2. In oval-cut jadeite jade with a medium degree of transparency, a beam of light is divided into two parts—one part reflected at the point of incidence or absorbed during the light transmission, and the other part arriving at the underside and then converging in the other side of its curved surface. Therefore, the brightness of the whole image is even.
3. In oval-cut jadeite jade with a low degree of transparency, most of the light is reflected at the point of incidence or absorbed. Little light reaches the underside, and therefore a relatively dark area forms at the other side of the curved surface.

Based on these three characters, oval-cut jadeite jade with different degrees of transparency can be judged objectively and automatically.

Inclusion Characteristics of Wax-Like Amber After Hydrothermal Treatment

Yamei Wang^{1,2} and Yan Li¹ (presenter)

¹Gemmological Institute, China University of Geosciences, Wuhan

²Gem Testing Center of China University of Geosciences, Wuhan

Amber products can be hydrothermally treated (figure 1) in order to improve the transparency of the material. In this process, an abundance of tiny nano- or micro-sized bubbles penetrate the amber in the presence of an aqueous solution (with some catalyst) through controlling the temperature and pressure and selecting an inert atmosphere environment (figure 2). After the treatment, the inner layer of the weathered skin of rough amber material will generate a layer with various thickness of a yellowish white or greenish yellow “hydrothermally treated skin” or a corrugated crust containing pores. The finished amber shows residues with white hydrothermally treated spots of various sizes, which may enter into the amber’s inte-

Figure 1. Variations in the appearance of amber samples before and after hydrothermal treatment: sample 1, sample 2, and sample 3. Note that there was no weight change in the amber before and after hydrothermal treatment. Photos by Yamei Wang.



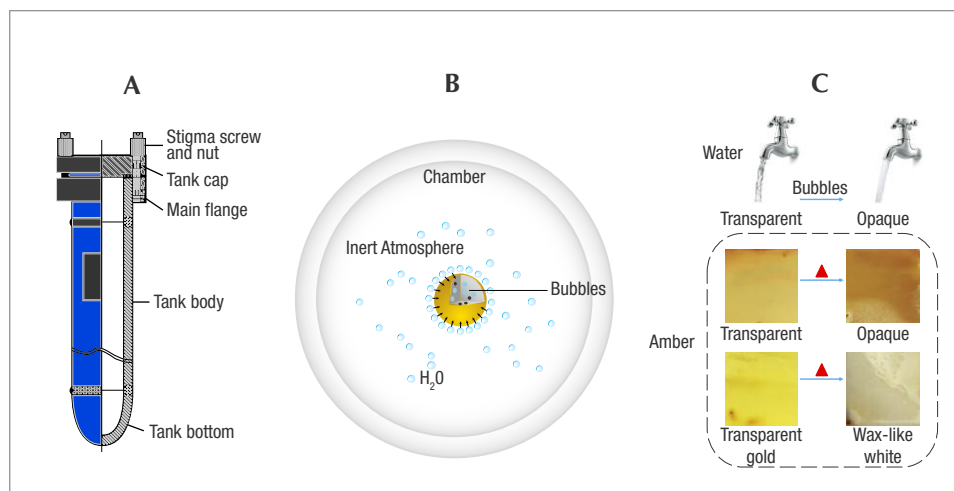


Figure 2. A: Sketch of the pressure furnace used for hydrothermal treatment. B: Evaporation of H₂O steam on amber in the chamber under inert atmosphere. C: Hydrothermal treatment from bubbles in the flowing water. Illustrations by Yan Li.

rior or remain on the finished surface. The treated wax-like amber displays abundant gas-liquid inclusions with small and dense flat or disc-shaped bubbles accompanied by tiny stress fracture patterns. The bubbles are uneven in size and densely distributed, forming a cloud-like effect. Because the infrared spectra data of the experimen-

tal samples before and after the treatment showed little difference, identification required the support of statistical FTIR data. A series of comprehensive tests are needed to identify hydrothermally treated amber, including the diagnostic evidence of the crust-like skin containing spots.

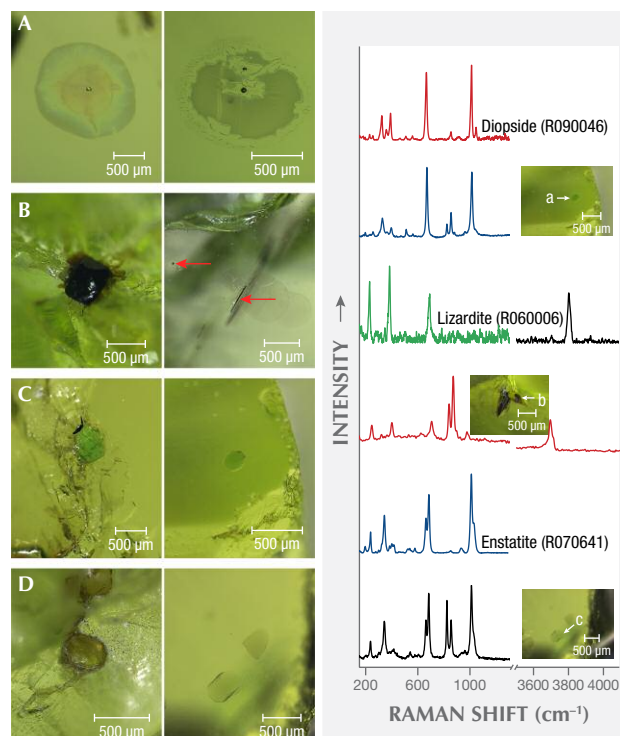
Interesting Inclusions in Peridot from Jilin, China

Zhiqing Zhang, Min Ye, and Andy H. Shen
 Center for Innovative Gem Testing Technology
 Gemmological Institute, China University of Geosciences, Wuhan

Recently we received 50 gem-quality rough peridot from the Yiqisong Nanshan olivine ore district, a new mineral occurrence in Dunhua City in China's Jilin Province. These peridot crystals exhibit a yellowish green hue, rather high transparency, and some visible inclusions. Study of the inclusions showed interesting results (figure 1 left, A–D).

For precise observation and accurate testing, the crystals were windowed and doubly polished. Comprehensive microscopic and Raman spectroscopic analysis indicated the following typical inclusions: “lily pads,” round transparent inclusions, strongly colored minerals with or without healed secondary fractures, green crystals of enstatite and diopside, and a rare dark mineral inclusion of lizardite, identified by Raman spectroscopy and by referencing the RRUFF database (figure 1, right). Further gemological research is being carried out on these samples, and more data will be published in a full article.

Figure 1. Left: “Lily pad” inclusions with patterns of decrepitation halos are typical in peridot (A). Deep-colored minerals are exposed on the host's surface with brownish impregnation, or appear ochre with a columnar, schistose form (B). Blocky and schistose green diopside appears on or near the surface (C). Brownish green enstatite is discernible (D). Right: The spectrum of mineral A matched diopside, B matched lizardite, and C matched enstatite. Double or triple peaks near 823 and 855 cm⁻¹ occur in the peridot, not the inclusions.



IR Absorption Spectrum of Type Ib HPHT-Created Diamonds as an Indicator of Their Growth Conditions

Viktor Vins¹, Alexander Yelisseyev², Dmitry Bagryantsev¹, and Alex Grizenko³

¹Velman, Ltd., Novosibirsk, Russia

²Sobolev Institute of Geology and Mineralogy SB RAS, Novosibirsk, Russia

³Lucent Diamonds, Inc., Los Angeles

Donor nitrogen atoms are the simplest crystal lattice defect, and their one-phonon absorption spectrum is well studied. The spectrum shows two main features: a main band at 1130 cm⁻¹ and a narrow peak at 1344 cm⁻¹. The absorption intensity and exact position of these two peaks give information about diamond growth conditions and crystal lattice perfection. In particular, our results showed that a decrease in growth rate corresponded to a decrease in the ν_{1130}/ν_{1344} absorption intensity ratio. The ratio decreased from 2 to 1.5 in samples grown in the Fe-Ni-C system and from 1.64 to 0.95 in samples grown in the Fe-Co-C system. Since the ν_{1130}/ν_{1344} ratio is sensitive to growth conditions, it could serve as a criterion for diamond quality, showing the content of impurity defects as well as the amount of internal tensile stress.

Studying isotopically modified diamonds is also informative. For example, if the carbon part of the growth system was 50% ¹²C graphite and 50% ¹³C graphite, an isotopic shift at 1344 cm⁻¹ was observed, while the main band at 1130 cm⁻¹ did not shift. The samples containing ¹⁵N isotope, conversely, revealed a 15 cm⁻¹ shift toward long wavelengths of the 1130 cm⁻¹ band, whereas the 1344 cm⁻¹ peak remained at its frequency. It can be concluded that the

1130 cm⁻¹ band is associated with the resonant vibrations of the N-C bond, while the 1344 cm⁻¹ peak is related not to the donor nitrogen atom but to local vibrations of the carbon atom, which is bonded to the unpaired electron of the impurity nitrogen. The position of the Raman peak on the spectra taken at different points of the sample with 47% ¹³C showed that the biggest shift of the diamond peak ($\nu = 1312.8$ cm⁻¹) was seen in parts of the crystal immediately adjacent to the seed region. The Raman peak varied from 1321.1 to 1322.5 cm⁻¹ in other parts of the sample, which corresponds to 25 ÷ 27% of ¹³C. The full width half maximum (FWHM) of the Raman peak was the largest (7.8 cm⁻¹) at $\nu = 1312.8$ cm⁻¹. In all other points it ranged from 6.2 to 7.4 cm⁻¹. In addition to an unusually high ν_{1130}/ν_{1344} intensity ratio, which in "traditional" nickel-containing diamond ranges from 1.5 to 2.0, this indicates that isotopically modified diamonds have a rather imperfect crystal lattice. This could be caused by internal stress resulting from the incorporation of an isotope with a larger atomic size than that of ¹²C.

This work was supported by grant 16-05-00873a from the Russian Foundation for Basic Research and by the state assignment project 0330-2016-0006.

Laue X-Ray Backscatter Spot Patterns: A Novel Way of Identifying Various Gemological Crystals

Hollis Milroy and Sandra Hektor

University of Toronto

Although Laue X-ray backscatter imaging of crystals dates back to the 1920s, the application of this technique to the study of gemology is very much a new concept. This study investigates the use of Laue backscatter spot patterns (also called Laue-grams) to positively identify several gem crystals of varying crystal structure and atomic complexity. Approximately 50 exposures were taken using a tungsten filament running at 2000 W (50 kV × 20 mA), with the resulting Laue backscatter images captured on medical X-ray film. Using a high-resolution scanner, the spot patterns from

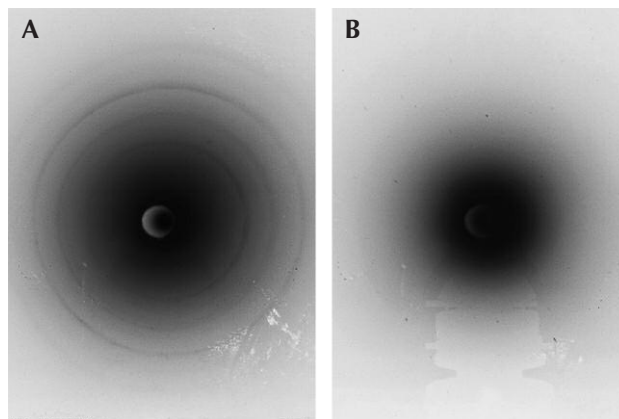


Figure 1. Laue backscatter spot patterns for two single-crystal samples.

A: Yellow tint lab-grown single crystal diamond. B: Single-crystal tungsten in [110] orientation. Photos by Hollis Milroy.

the developed film were compared to computer-generated models, which agreed with the film images to a high degree of accuracy.

Exposure times and crystal orientations relative to the X-ray beam axis were varied. Control exposures were run to ensure background effects (e.g., from the sample holder) did not contribute at all to the spot patterns.

The advantage of the noninvasive and nondestructive Laue backscatter method is that material can be identified from any

orientation of the crystal. This is helpful when gemstones are embedded in jewelry or other materials such as rocks. Furthermore, anomalies from crystal impurities will appear on the film proportionately: The spot pattern of the predominant material will appear most visible and thus always easily determinable. For instance, the small impurities that produce different-hued gemstones will not affect the produced spot pattern from the underlying crystal structure.

Multifunction Spectrometer for Color Grading and Identification of Diamonds and Gemstones

Yan Liu

Liu Research Laboratories, South El Monte, California

A multifunction dual integrating sphere spectrometer has been developed for color grading and identification of diamonds and gemstones. The spectrometer has nine functions: spectral reflectance measurement, spectral transmittance measurement, color measurement, UV fluorescence measurement, photoluminescence (PL) measurement, color grading of gemstones, color grading of colored diamonds, color grading of jadeite, and grading of alexandrite effect. The color grading by artificial intelligence and the fine spectral measurement of PL at room temperature are particularly useful for gemological laboratories and the jewelry industry. The artificial intelligence for color grading includes a neural network and a fuzzy logic algorithm. The PL measurement is calibrated by

a NIST-traceable lamp to measure the relative spectral distribution of photoluminescence, and a mathematic algorithm is developed to obtain a fine PL spectrum at room temperature. In addition, the photoluminescence measurement can amplify a weak spectrum up to 1,000 times for gemological research and identification purposes. The function for color grading of jadeite has adjustments for color area percentage and shape curve for accurate color grading of carved pieces. The grading of alexandrite effect is calculated under five standard CIE illuminants: A, D65, F3, F7, and F11. The spectrometer can be used to perform most tasks of color grading, spectroscopic identification, and research in advanced gemological laboratories.

Nephrite from Luodian, Guizhou Province of China

Quanli Chen¹, Xianyu Liu^{1,2}, Haitao Wang³, Wenjing Zhu¹, Sujie Ai¹, and Zuowei Yin¹

¹Gemmological Institute, China University of Geosciences, Wuhan

²College of Jewelry, Shanghai Jian Qiao University, Shanghai

³School of Jewelry, Guangzhou College of South China University of Technology, Guangzhou

In recent years, a new variety of nephrite has been discovered in Luodian County in Guizhou Province, China (figure 1). It lacks greasy luster but possesses a distinctive “porcelain” luster and a fine texture. The white samples tend to show a more or less gray hue.

Samples with a white to bluish white colors were studied via X-ray fluorescence (XRF), X-ray diffraction (XRD), ICP-MS, and FTIR. The results reveal that Luodian nephrite (figure 2), whose SG ranges from 2.77 to 2.90 and is slightly lower than that of Hetian nephrite, is mainly composed of tremolite, and parts of the samples contain a small amount of quartz. The chemical constituents of Luodian nephrite are SiO₂ (56.75–59.01 wt.%), MgO (23.69–25.03 wt.%), and CaO (11.25–12.00 wt.%, lower than the standard value of tremolite).

Among the trace elements of Luodian nephrite, Ti, V, Cr, Mn, and Co show higher relative mass fraction, with Ti ranking top (relative mass fraction: $2.05\text{--}4.52 \times 10^{-8}$). The content of these elements is exceptionally low in Hetian white nephrite, which may shed some light on the gray hue of Luodian nephrite. Light rare earth elements are relatively concentrated, and Eu shows both positive and (more frequently) negative anomalies. Compared with Hetian white nephrite, the total content of rare earth elements of Luodian nephrite is higher, especially the elements La, Nd, Sm, Tb, and Er, indicating that the ore-forming environment is different between the two localities.

Observing the microstructure characteristics using scanning electron microscopy (SEM) revealed that the tremolite in Luo-



Figure 1. Map showing the location of the Luodian nephrite deposit.



Figure 2. These nephrite pieces are from Luodian County in Guizhou Province, China. Photos by Quanli Chen.

dian nephrite has a mainly fibrous crystalline structure, and the various microstructure features of the aggregate are based on the different aggregation modes of fibrous tremolite. Therefore, the

fibrotic range, geometric size, form combination, interaction of the tremolite, and tightness of polymerization are the basis of quality in Luodian nephrite.

“Raindrop” Turquoise from China

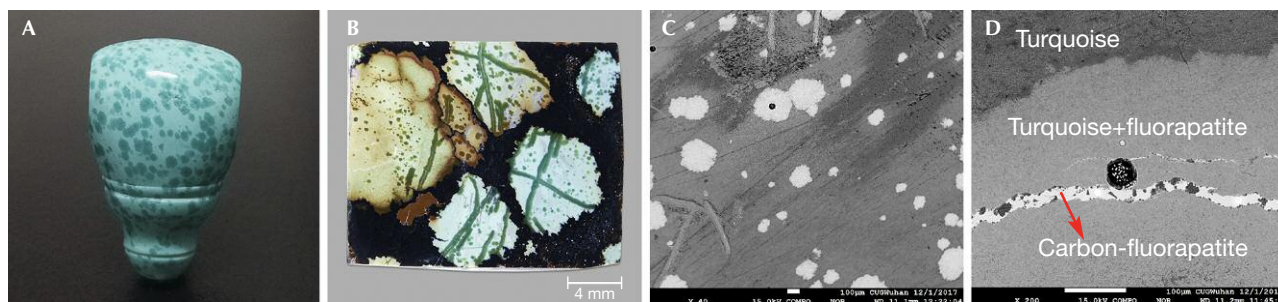
Ling Liu, Mingxing Yang, Yan Li, Yalun Ku, Jia Liu, and Zenmin Luo
Gemmological Institute, China University of Geosciences, Wuhan

Recently, a new type of turquoise with randomly distributed spots (figure 1A) from Hubei Province, China—where there are abundant gem-quality turquoise mines—has become popular with jewelry consumers and collectors. The material is called “raindrop turquoise” because of the unique inclusions with blue, blue-green or (rarely) yellow color. The raindrop-like inclusions and the substrate always display a similar hue, but the color of the raindrop-

like inclusions is much deeper, and their transparency and hardness are higher.

It appears that so-called raindrop turquoise has not been well studied. Several typical specimens from the jewelry market were systematically investigated for their mineral compositions and spectral characteristics using micro-XRD, micro-FTIR, Raman, and electron microprobe analysis. The raindrop inclusions (figure 1B) were

Figure 1. A: The circle-shaped inclusions were unevenly distributed in this piece of raindrop turquoise. Photo by Yalun Ku. B: Inclusions seen in one of the samples from this report. The sample measures 21 × 18 × 6 mm. C: Backscattered electron imaging of the sample shown in figure 1B revealed that the gray area between the raindrop and the substrate is distinct. D: A lighter and narrower (~10 μm) line observed in the vein of the sample is pure carbon-fluorapatite.



mainly composed of turquoise and fluorapatite, while the substrate was mainly turquoise. The Raman spectra of the raindrop inclusions showed the characteristic peaks of turquoise, with strong and sharp peaks at 965–968 cm^{-1} caused by PO_4^{3-} of fluorapatite. In addition, a weak shoulder at 1070 cm^{-1} was observed in some samples because of CO_3^{2-} replacing PO_4^{3-} (Awonusi et al., 2007). The micro-FTIR spectra of the raindrop inclusions showed double weak peaks near 1460 cm^{-1} and 1430 cm^{-1} , resulting from the asymmetric stretching vibration of CO_3^{2-} (Fleet, 2009). The backscattered electron images (figure 1C) showed that the gray between the raindrop and the substrate was distinct, indicating the difference in their mutual mineral

phases. Some raindrop inclusions kept the perfect hexagonal shapes of apatite (again, see figure 1C). In addition, a lighter and narrower line ($\sim 10 \mu\text{m}$) was also observed in the vein of the sample (figure 1D). The chemical compositions of the raindrops and veins were Al_2O_3 , P_2O_5 , CaO , CuO , FeO , and F , while the narrow line mainly consisted of P_2O_5 , CaO , and F .

From the X-ray diffraction (XRD) and Raman results, the raindrop and vein inclusions are mixed with turquoise and fluorapatite, while the lighter and narrower line is pure carbon-fluorapatite. Hence, the deeper color of raindrop-like inclusions can be attributed to the mixture of turquoise and fluorapatite/carbon-fluorapatite.

REFERENCES

Awonusi A., Morris M.D., Tecklenburg M.M. (2007) Carbonate assignment and calibration in the Raman spectrum of apatite. *Calcified Tissue International*, Vol. 81, No. 1, pp. 46–52, <http://dx.doi.org/10.1007/s00223-007-9034-0>

Fleet M.E. (2009) Infrared spectra of carbonate apatites: ν_2 -region bands. *Bio-materials*, Vol. 30, No. 8, pp. 1473–1481, <http://dx.doi.org/10.1016/j.biomaterials.2008.12.007>

Tianhuang Stone—The Most Valuable Seal Stone in China

Tao Chen¹, Yungui Liu², and Quanli Chen¹

¹Gemmological Institute, China University of Geosciences, Wuhan

²State Key Laboratory of Geological Processes and Mineral Resources, China University of Geosciences, Wuhan

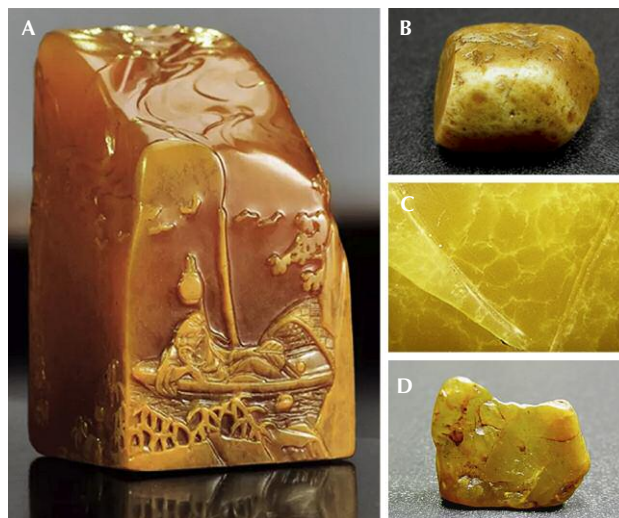
Tianhuang stone, from the village of Shoushan in Fujian Province, is the most precious Chinese seal stone. It has a profound cultural heritage in China and is quite expensive. Therefore, systematic research on the identifying gemological and mineralogical characteristics of Tianhuang stone has important value implications. Tianhuang stone mainly has a yellow color, though it can sometimes be white, red, or black. Most Tianhuang stones have weathered skins, red cracks, and “turnip” inclusion veins.

According to X-ray diffraction and FTIR results, Tianhuang stone can be divided into three types: dickitic, nacrific, and illitic. Dickitic-type Tianhuang stone can be further divided into ordered dickitic and disordered dickitic. Illitic-type Tianhuang stone is usually composed of $2M_1$ illite and a small amount of $1M$ illite.

The weathered skin and matrix have the same mineral composition. LA-ICP-MS results suggest that iron content is higher in the skin than in the matrix. These findings, along with total iron analyses, indicate that the yellow color of Tianhuang stone is caused by Fe^{3+} ions in the crystal structure of dickite, nacrific, or illite. Red cracks are caused by iron minerals that entered along the cracks. The iron minerals display three forms: thick film-state, short needles, and film or fine granular, as observed by scanning electron microscopy (SEM). The “turnip” vein is a kind of fine, white spiderweb inclusion in Tianhuang stone, which has no obvious boundary between matrix and vein. SEM,

energy-dispersive spectrometry (EDS), and laser Raman microspectrometry results show that turnip vein is composed of svanbergite.

Figure 1. A: This 58 g yellow Tianhuang seal stone was sold at a Chinese auction from 2017. B: Weathered skin on the surface of a Tianhuang stone. C: Fine and white “turnip” veins. D: Red cracks extending into a Tianhuang stone from its surface.



Unusual “Vorobyevite” Beryl from Afghanistan

Yang Hu and Ren Lu

Gemmological Institute, China University of Geosciences, Wuhan

Beryl is an important gem species that includes goshenite, aquamarine, emerald, heliodor, morganite, and red beryl varieties. An unusual blue beryl sold as “vorobyevite” or “rosterite” is sometimes seen on the market. This crystal has a special hexagonal tabular morphology, sometimes concave, convex, or fibrous-like on basal pinacoids. The material is mined from the Deo Darrah, Khash, and Kuran Wa Munjan districts in Badakhshan Province, Afghanistan. It most likely formed in granitic pegmatite, as evidenced by the associated dark blue tourmaline and spherical muscovite aggregates (figure 1, left). Characteristics of an Afghan vorobyevite sample and the use of the term are discussed here.

This sample was pale blue with a yellow hue in the center. Parallel intergrowth and a hexagonal growth texture were shown on a two-sided basal face. Dichroism was medium, appearing pale blue along the ordinary (o-) ray and blue along the extraordinary (e-) ray. The fluorescence response was inert to both long-wave and short-wave UV. The sample had a refractive index (RI) of 1.570–1.575 and a specific gravity (SG) of 2.53. Abundant two-phase inclusions with various shapes were observed (figure 1, right). All of these gemological properties were in agreement with aquamarine.

LA-ICP-MS analysis showed that alkali content in the form of Na and Cs (Cs_2O 0.03–0.04 wt.%, and Na_2O 0.07–0.08 wt.%) was relatively low according to our chemical database of all beryl varieties, classified as “low-alkali” beryl in agreement with the dominance of type I water in structural channels revealed by Raman

and IR spectra. In addition, Ge, Sn, Nb, and Ta were relatively rich compared with aquamarine from other origins. Due to few substitutions in the Al octahedral and Be tetrahedral crystal site, this Afghan sample was identified as “normal beryl.” UV-Vis-NIR spectroscopy showed absorptions of Fe ions (FeO 0.56–0.60 wt.%) at 372, 425, 600, and 820 nm, and the blue color was stable under sunlight. Therefore, the blue color was attributed to Fe ions rather than natural or artificial irradiation. A yellowish area in the center of the sample indicated that the blue color was natural.

The term “vorobyevite” was first applied to colorless to yellowish rose beryl containing large amounts of lithium and cesium (Cs_2O 3.04 wt.% and Li_2O 1.43 wt.%) from Lipovka, Russia (Yakubovich et al., 2009). The term “rosterite” designated a cesium beryl of colorless or pink color from Elba, Italy, almost synonymous with “vorobyevite” (Hänni and Krzemnicki, 2003). But neither term is officially accepted by the International Mineralogical Association or normally used for a beryl variety. Based on gemological, spectroscopic, and chemical characteristics, we confirmed this Afghani vorobyevite belonged to the beryl species, specifically the low-alkali aquamarine variety. However, similar tabular beryls from Mogok (Myanmar) and Sichuan (China) with a pale blue to dark blue color (see figure 1, left) were identified as “alkali-rich” aquamarine in our study. Although the tabular morphology in this Afghan sample was quite uncommon, tabular morphology is not a criterion for identifying vorobyevite or rosterite.

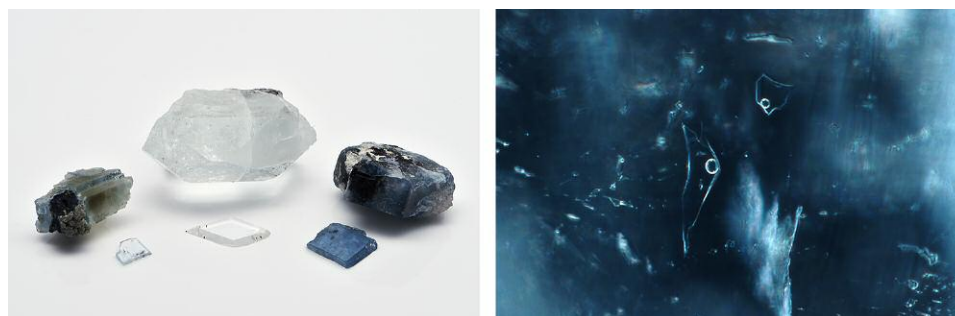


Figure 1. Left: A 16.5 × 13.2 × 7.5 mm vorobyevite with tourmaline and muscovite aggregate from Afghanistan, a 31.3 × 25.2 × 7.3 mm pale blue Chinese aquamarine, and a 22.1 × 15.5 × 7.8 mm dark blue Burmese aquamarine. Right: A two-phase inclusion hosting a round bubble in the vorobyevite. Field of view 0.37 mm. Photos by Yang Hu.

REFERENCES

- Hänni H.A., Krzemnicki M.S. (2003) Caesium-rich morganite from Afghanistan and Madagascar. *Journal of Gemmology*, Vol. 28, No. 7, pp. 417–429.
- Yakubovich O.V., Pekov I.V., Steele I.M., Massa W., Chukanov N.V. (2009) Alkali

metals in beryl and their role in the formation of derivative structural motifs: Comparative crystal chemistry of vorobyevite and pezzottaite. *Crystallography Reports*, Vol. 54, No. 3, pp. 399–412, <http://dx.doi.org/10.1134/S1063774509030067>

Young Blue Sapphires from Muling, China

Yimiao Liu and Ren Lu

Gemmological Institute, China University of Geosciences, Wuhan

The area around Muling, a small town located in northeastern China, produces attractive corundum in a wide variety of color, clarity, and sizes (Liu and Lu, 2016), along with gem-quality pyrope, zircon, and black spinel. Some of its facet-quality sapphires (figure 1) are comparable to those from the finest sapphire localities in the world.

Sapphire from Muling is mostly extracted from alluvial (or secondary) deposits. Information on genesis, general formation environment, and deposit type is still incomplete and being researched to support efficient exploration.

Muling is distributed along the northern section of the Dunhua-Mishan Fault, which is a lithospheric extension between the Xing-Meng orogenic belt and the Pacific subduction zone (Ling et al., 2017). The volcanic eruptions of the Dunhua-Mishan graben began at about 44.9 Ma and ended about 5,140 years before the present (Wang et al., 2001). Gemstones were found in the placer derived from Miocene (5.3–23 Ma) basalt, which is regarded as the gem carrier. The corundum-bearing layers underlie a few meters of soft sandy clay and fertile topsoil.

This study arose from a preliminary examination of 14 faceted and 74 rough corundum from the Muling deposits. During examination of the internal characteristics, we found zircon inclusions in three blue sapphires. As one of the best geochronometers, zircon provided an initial estimate of the formation age through U-Pb dating methods.

Zircon inclusions were identified by laser Raman spectroscopy. Euhedral crystals with no evidence of surface corrosion or oxidation could indicate that the zircon inclusions within the host sapphire were syngenetic and nearly unaffected by radiation (called “high” zircon in gemology). Therefore, the ages obtained on zircon inclusions are in equilibrium with the initial formation time of the host sapphire.

U-Pb dating analyses of zircon inclusions were conducted using LA-ICP-MS at the State Key Laboratory of Geological Processes and Mineral Resources, China University of Geosciences, Wuhan. Due to the small size of the target inclusions (approximately $150\ \mu\text{m} \times 50\ \mu\text{m}$) and unavoidable interference from common lead, only some subsets of information could be preserved for the age calculation. The analyses of zircon inclusions gave $^{206}\text{Pb}/^{238}\text{U}$ ages ranging from 8 to 10 Ma (i.e., Miocene). Being completely enclosed within the host sapphires, the trans-

parent euhedral zircons were protected throughout their history from interaction with permeating fluids. Thus, the obtained ages correspond to the formational ages of these sapphires. Combined with the geologic settings, this time period would have allowed numerous volcanic events to deliver the corundum as xenocrystal from the source to the top. The formation condition of Muling sapphires might be associated with the Miocene volcanic events.

The U-Pb ages of zircon inclusions (along with a full range of trace elements within zircon) can also provide distinctive provenance characteristics, because the formation ages of sapphires from various well-known deposits are different. Although the sapphires from Muling are much older than the oldest human civilization, they are among the youngest sapphire deposits known to date (e.g., Madagascar, Sri Lanka, Myanmar, and North America). Therefore, the U-Pb age of zircon inclusions is an efficient indicator in separating similar-looking sapphires from various deposits.

Once more age information on sapphires is collected, a totally new system of provenance identification will be established. It is also helpful for further understanding the genesis of gemstones and instructing people on the rational utilization of resources.

Figure 1. This 0.53 ct natural, untreated blue sapphire from Muling, China, shows desirable blue color and saturation. Photo by Yimiao Liu.



REFERENCES

- Ling Y.Y., Zhang J.J., Liu K., Ge M.H., Wang M., Wang J.M. (2017) Geochemistry, geochronology, and tectonic setting of Early Cretaceous volcanic rocks in the northern segment of the Tan-Lu Fault region, northeast China. *Journal of Asian Earth Sciences*, Vol. 144, pp. 303–322, <http://dx.doi.org/10.1016/j.jseas.2016.12.025>
- Liu Y, Lu R. (2016) Gem News International: Ruby and sapphire from Muling, China. *G&G*, Vol. 52, No. 1, pp. 98–100.
- Wang X.K., Qiu S.W., Song C.C., Kulakov A., Tashchi S., Myasnikov E. (2001) Cenozoic volcanism and geothermal resources in northeast China. *Chinese Geographical Science*, Vol. 11, No. 2, pp. 150–154, <http://dx.doi.org/10.1007/s11769-001-0035-z>

Gem Localities

Blue Sapphires from Mogok, Myanmar

Ungkhana Atikarnsakul, Wim Verriest, and Wasura Soonthorntantikul
GIA, Bangkok

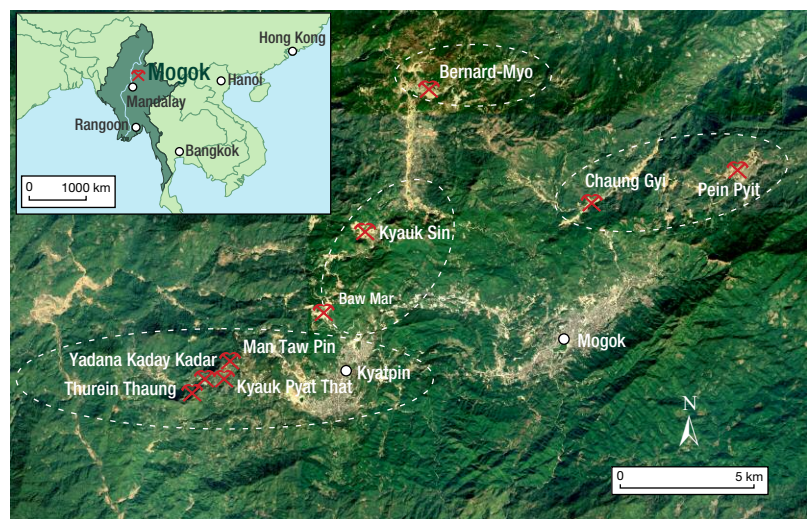
Myanmar (formerly Burma) has been one of the most important producers of high-quality blue sapphires for centuries. The gemstones are mined from various parts of the Mogok Stone Tract and show some variation according to their specific origin within the tract. It is widely known within the gemological community that separating metamorphic sapphires from Myanmar, Sri Lanka, Madagascar, and other geologically similar sources still poses some challenges. In this study, 69 untreated samples from four distinct sapphire mining areas in Mogok were examined (figure 1).

The aim of this research was to characterize the gemological properties, inclusions, spectroscopic features (FTIR, UV-Vis-NIR, and Raman), and chemistry of Burmese blue sapphires in order to assist with country-of-origin determination. The samples exhibited colors ranging from blue to violetish blue. Standard gemological properties recorded were consistent with most natural blue sapphires: refractive index (RI) of $n_o = 1.769\text{--}1.770$ and $n_e = 1.760\text{--}1.762$, birefringence of $0.008\text{--}0.009$, and hydrostatic specific gravity (SG) of $3.81\text{--}4.04$. The samples were inert under short-wave ultraviolet (UV) radiation. The majority were also inert under long-wave UV radiation, although some violetish blue samples displayed a weak red reaction. Under magnification, lamellar twinning, silk, particle bands, negative crystals, variously shaped thin films, brownish platelets of ilmenite, iridescent fluid inclusions, and various minerals (such as crystals of zircon, feldspar, mica, green chromite, and nepheline) were typically observed. The Fourier-transform infrared (FTIR) spectra revealed the presence of minerals such as boehmite, kaolinite, and diaspore, and/or a single very weak peak at 3309 cm^{-1} . Ultraviolet/visible/near-infrared (UV-Vis-NIR) spectroscopy revealed the typical patterns seen in metamorphic blue sapphires, including three absorption peaks at 377, 388, and 450 nm related to Fe^{3+} ions and one absorption band centered at 580 nm in the ordinary (o-) ray and at 700 nm in the extraordinary (e-) ray of $\text{Fe}^{2+}\text{-Ti}^{4+}$ pairs.

One of the most interesting results to come from the study was the slight variation observed in the chemical signatures be-

tween sapphires from the different areas in Mogok and other metamorphic blue sapphire sources, revealed by laser ablation-inductively coupled plasma-mass spectrometry (LA-ICP-MS) analysis. In cases where few or no inclusions were present to assist with origin determination, plotting Fe versus V provided useful supporting data by which to separate Mogok sapphires from Sri Lankan and Madagascan sapphires. The moderate to high Fe content (up to 2300 ppm) of these sapphires from certain areas of Mogok sets them apart from other sources with lower Fe. This study proved that a combination of various analytical techniques and interpretation of the subsequent data, especially that obtained from LA-ICP-MS, FTIR, UV-Vis-NIR, and microscopic observation, should be taken into account when providing opinions on the country of origin for Burmese blue sapphires.

Figure 1. The four mine locations in the vicinity of Mogok from which the samples in this study were sourced. Inset: A map of Myanmar showing Mandalay and Mogok.



REFERENCES

- Kan-Nyunt H.P., Karamelas S., Link K., Thu K., Kiefert L., Hardy P. (2013) Blue sapphires from the Baw Mar mine in Mogok. *G&G*, Vol. 49, No. 4, pp. 223–232, <http://dx.doi.org/10.5741/GEMS.49.4.223>
- Kane R.E., Kammerling R.C. (1992) Status of ruby and sapphire mining in the Mogok Stone Tract. *G&G*, Vol. 28, No. 3, pp. 152–174, <http://dx.doi.org/10.5741/GEMS.28.3.152>

- Soonthorntantikul W., Verriest W., Raynaud-Flattot V., Sangsawong S., Atikarnsakul U., Khowpong C., Weeramonkhonlert V., Pardieu V. (2017) An in-depth gemological study of blue sapphires from the Baw Mar mine (Mogok, Myanmar). *News from Research*, <https://www.gia.edu/doc/Gemological-Study-Blue-Sapphires-Baw-Mar-Mine-Mogok-Myanmar-GIA.pdf>

Geographic Origin Determination of Ruby and Sapphire Using Sr-Pb Isotopes

Mandy Y. Krebs^{1,2}, D. Graham Pearson², Andrew J. Fagan³, and Chiranjeeb Sakar²

¹GIA, New York

²University of Alberta, Edmonton, Canada

³Hummingbird Geological Services, Vancouver, Canada

The geographic origin of gemstones has emerged as one of the major factors affecting their sale on the international market, in large part due to the prestige attributed to certain origins (e.g., rubies from Myanmar or sapphires from Kashmir), but also because of political and ethical reasons (trade bans and fair trade). This provides a strong motivation to establish accurate scientific methods to identify the provenance of high-end colored gemstones such as ruby and sapphire.

Methods used to determine ruby provenance include the observation of inclusions and gemological features, trace element analysis, and oxygen isotope analysis. All these have proven useful in distinguishing corundum from different geological settings, but none of these methods are yet able to reliably distinguish between gems from different geographic regions that share a similar geological setting (Groat and Giuliani, 2014). So far, no unique fingerprint exists and geographic origin remains a challenge, especially for high-clarity stones, emphasizing the need for a more powerful tool.

REFERENCES

- Groat L.A., Giuliani G. (2014) The geology and genesis of corundum deposits. In *Geology of Gem Deposits*, Second Edition. Short Course Series Volume 44. Mineralogical Association of Canada, Quebec, pp. 113–134.
- Krebs M.Y., Pearson D.G., Fagan A.J. (2016) Constraining ruby provenance

Using a novel offline laser ablation technique followed by column chromatography and thermal ionization mass spectrometry (TIMS), we were able to precisely measure radiogenic isotope compositions in ruby for the first time. We demonstrate, using rubies from three different localities and two different deposit types, that radiogenic isotopes offer a potentially powerful means of provenance discrimination even for geologically similar deposits (Krebs et al., 2016).

Here we present Sr and Pb isotope data for gem corundum from several localities of geologically similar deposits: rubies from amphibole-related (Mozambique, Greenland, Madagascar, and Tanzania) and marble-related deposits (Myanmar, Vietnam, Afghanistan, and Tanzania) and metamorphic blue sapphires (Myanmar, Sri Lanka, and Madagascar). This data will be evaluated with regard to its usefulness in determining the geographic origin of both ruby and sapphire, and the method's usefulness for the development of a unique fingerprint for the country-of-origin determination will be discussed.

using Sr-Pb isotopes and trace elements and dating ruby crystallisation using Pb-Pb geochronology: a new approach. *Geological Society of America Meeting Abstracts with Programs*, Vol. 48, No. 7, <https://gsa.confex.com/gsa/2016AM/webprogram/Paper285603.html>

Golden Sheen Sapphire and Syenite/Monzonite-Hosted Sapphire From Kenya

Yusuke Katsurada, Makoto Miura, and Kazuko Saruwatari

GIA, Tokyo

Golden sheen sapphire (GSS) has recently become popular in the gemstone market. This material was recovered from undisclosed deposits in a remote locality in northeastern Kenya near the Somali border. Its unique shimmering effect is created by hematite and ilmenite inclusions, and chromophores of its blue and yellow bodycolors have been studied in some publications. We compared the trace-element concentrations of these GSS with published data for blue sapphires from other localities and found similar compositions in sapphires from Garba Tula, central Kenya (Miura et al., 2018). The Garba Tula sapphire mine is known as a primary deposit of syenite/monzonite dikes within migmatites and gneisses

in the Mozambique belt. The purpose of this study is to clarify the relationship between these localities by comparing GSS with Garba Tula sapphires.

In addition to the 23 GSS samples documented by Miura et al. (2018), we obtained six blue and five yellow cabochons from the same supplier. These 11 samples were reportedly from the same deposit. Being less included, they were more suitable for comparing trace-element concentrations. We also obtained more than 60 rough samples from Garba Tula from another reliable source. These samples were mainly blue with some yellows, and some were heavily included with hematite/ilmenite needles. The included

samples were similar to GSS in their characteristic mineral inclusions such as hematite, ilmenite, magnetite, zircon, mica, and carbonate minerals. From the Garba Tula samples, pieces with fewer inclusions were randomly selected for quantitative analysis with LA-ICP-MS.

The 11 less-included GSS samples and the included GSS had similar trends in their key elements. Less-included samples also showed a Mg-Ti ratio corresponding with coloring theory: a higher ratio in yellows and a lower ratio in blues. The blue sapphires from Garba Tula had a wider range of elements but overlapped with GSS in all key elements for both blue and yellow bodycolors. The similarity of inclusions and trace-element trends indicates that the geological background of GSS is strongly related to that of Garba Tula sapphires. Garba Tula is located in the up-slope area of a drainage basin of the Juba and Shabelle Rivers, which flow into the Indian Ocean. Bimodal seasonal precipitation

and poor vegetation coverage can cause severe weathering and erosion, and the weathered corundum-hosting rocks are sometimes washed and transported downstream. Topographic features suggest that materials with high specific gravity such as corundum might be deposited close to the Somali border, where meandering channels are predominant in the sub-basin of the Lag Dera seasonal river, a branch of the Juba and Shabelle Rivers. This is a useful example of combining chemical analyses and inclusion studies with geomorphological interpretation to approach origin determination of gemstones whose placer deposit locality is unknown.

REFERENCE

Miura M., Katsurada Y., Saruwatari K. (2018) Gem News International: Update on trace-element chemical characteristics of golden sheen sapphire. *G&G*, Vol. 54, No. 2, pp. 238–241.

Magmatic Sapphire from Yogo Gulch, Montana, and from Bingham Canyon, Utah: Some Surprising Commonalities

Jeffrey D. Keith¹, Aaron C. Palke², and James E. Shigley²

¹Brigham Young University, Provo, Utah

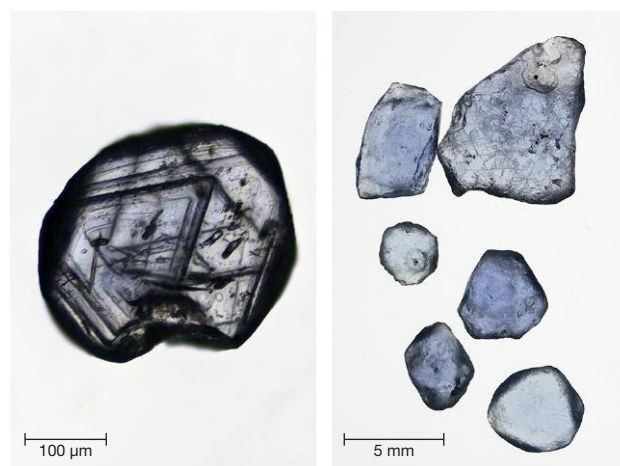
²GIA, Carlsbad, California

Recent LA-ICP-MS analysis performed on sapphire crystals from Bingham Canyon, Utah (figure 1, left), found broad similarities with sapphire from Yogo Gulch, Montana (figure 1, right). Bingham Canyon sapphire occurs in at least nine different volcanic units that are approximately the same age as the Cu-Au-Mo mineralization (which occurred 39 Ma). These volcanic units are small-volume block-and-ash flow eruptions that comprise the flanks of a large inferred stratovolcano. Sapphire does not occur in older or younger magmatic events unrelated to Cu mineralization. Bingham Canyon and Yogo Gulch sapphires have broadly similar chemistry in terms of Mg, Fe, and Ga. V and Cr contents are moderately higher in Bingham Canyon sapphire. However, one important distinction is that the Ti enrichments (as well as Nb and Zr) found in the Bingham Canyon sapphires suggest the presence of significant Ti-rich micro-inclusions, which is not typically seen in Yogo sapphires. Broad similarities are not unexpected considering that they are both related to mafic/potassic Eocene magmatism in the western United States. Sapphire at Bingham Canyon occurred after primitive magma transected Proterozoic mica-rich lithospheric mantle and melted Al-rich rocks such as phlogopite-bearing veins. At Yogo, phlogopite is also a fundamental mineral in the lamprophyric dike that hosts the sapphire. Modeling suggests that primitive mafic magma ponded at the base of the crust and melted Al-rich Proterozoic metapelites.

At Bingham, sapphire crystals (50–500 μm) are two orders of magnitude *smaller* than those at Yogo, but they are uniformly dis-

tributed in most of the intrusive and volcanic units that comprise the stratovolcano. The question of origin remains for both Bingham Canyon and Yogo sapphires: Are they xenocrysts in the traditional sense, or are they intimately related to formation of each magma?

Figure 1. Side-by-side example comparing the morphology of sapphires from Bingham Canyon (left) and Yogo Gulch (right). Photos by Aaron Palke.



Tourmaline-Sapphire-Phlogopite Rocks of the Badakhshan Province of Northeastern Afghanistan: Insights into a Favorable Environment for Blue Sapphire Development

Darrell Henry¹, Barbara L. Dutrow¹, and Ziyin Sun²

¹Department of Geology and Geophysics, Louisiana State University, Baton Rouge

²GIA, Carlsbad, California

The sapphire-bearing metamorphic rocks found in the Badakhshan Province of northeastern Afghanistan provide insights into the chemical and mineralogical environments that favor development of the blue sapphire variety of corundum. These rocks comprise a matrix of randomly oriented pale brown to pale green phlogopite with porphyroblasts of dark blue tourmaline and blue to colorless sapphire. Minor amounts of green spinel, feldspar, and apatite have also been noted as coexisting phases in these rocks. The tourmalines are prismatic. The phlogopite exhibits minor alteration to clinocllore. The sapphires display a range of color intensities from colorless to dark blue, and some show color variation in different sectors. As expected, no quartz occurs in the samples.

Backscattered electron imaging and electron microprobe analysis of a representative sample reveal the intriguing textures and mineral chemistry of the tourmaline and phlogopite. The tourmalines commonly display oscillatory zoning in the interior of the grains, with patchy zoning on the outer portion that mimics the texture of the matrix phlogopite. Analytical data collected along traverses across a tourmaline porphyroblast establish that they are Ca-rich dravite ($X_{Mg} = 0.92-0.97$) with an average core zone formula of $(Na_{0.60}Ca_{0.32-0.07})(Mg_{2.70}Fe_{0.23}Al_{0.07})(Al_{6.00})(Si_{5.93}Al_{0.07}O_{18})(BO_3)_3(OH_{3.00})(OH_{0.63}O_{0.25}F_{0.12})$ and an outer zone formula of $(Na_{0.64}Ca_{0.24-0.12})(Mg_{2.73}Al_{0.15}Fe_{0.12})(Al_{6.00})(Si_{5.97}Al_{0.03}O_{18})(BO_3)_3(OH_{3.00})(OH_{0.69}O_{0.24}F_{0.07})$. A narrow overgrowth of magnesio-foitite occurs at the outer margin of the grain. The tourmaline core zone has a

more intense blue color and is notably more enriched in Fe. The phlogopites are extremely magnesian ($X_{Mg} = 0.94-0.96$) and exhibit a range of compositions $(K_{1.66-1.80}Na_{0.06-0.11=0.10-0.27})(Mg_{8.95-5.24}Al_{0.39-0.73}Fe_{0.23-0.37})(Si_{5.47-5.91}Al_{2.09-2.53}O_{20})(OH_{3.70-3.92}F_{0.07-0.27})$. Tourmaline and phlogopite have unusually low Ti contents of near or below electron microprobe detection limits of ~150 ppmw. The blue coloration of the tourmaline is presumed to be related to interactions of Fe²⁺ and Fe³⁺ in the absence of appreciable Ti, similar to that in blue-colored elbaïtes. LA-ICP-MS data on the tourmaline confirm the unusually low Ti (262 ppmw) and V (27 ppmw) contents of the tourmaline, but other trace elements are relatively enriched, including Sr (240 ppmw), Ga (21 ppmw), Ce (10 ppmw), and La (5 ppmw). The blue coloration in sapphire is considered the result of interactions of Fe²⁺-Fe³⁺ and Fe²⁺-Ti⁴⁺ intervalence charge transfer.

The unusually K-, Mg-, Al-rich and Si-, Ti-poor bulk composition of the sapphire-bearing rock is consistent with a metasomatic modification of a precursor rock composition. It is likely that boron-bearing fluids fluxed the rock system. The oscillatory zoning in tourmaline suggests the former presence of dynamic fluids during initial tourmaline growth. Patchy zoning on the outer portions suggests that the tourmalines overgrew and replaced matrix micas. A metamorphic overprint on rocks with these unusual bulk compositions and mineral assemblages is commensurate with the development of sapphire.

Trends in World Colored Gemstone Production, 2006–2016

Thomas Yager

U.S. Geological Survey, Reston, Virginia

The U.S. Geological Survey (USGS) publishes world production figures for more than 80 mineral commodities annually. Colored stone production, unlike that of diamond, is inherently difficult to estimate because of the fragmentary and commonly informal nature of the industry, the lack of government oversight in many of the source countries, and the wide quality variations for each gem material. For these reasons, world production figures for colored stones were not published by the USGS until 2008, when production of emerald, ruby, sapphire, and tanzanite between 1995 and 2005 were estimated. Based on government data, company reports, and a review of the colored stone mining literature, the agency has estimated global production of amethyst, emerald,

lapis lazuli, ruby, sapphire, spinel, tanzanite, and tourmaline for the years 2006–2016.

From 1995 to 2005, Colombia was the world's leading emerald supplier, accounting for about half of global production by volume. Because of the long-term decline in Colombia's production and the increased production at Zambia's Kagem mine, Zambia subsequently became the world's leading producer. In Brazil, mining continued in Bahia and Minas Gerais states and ended in Goiás. Russia's Malyshev mine accounted for a substantial share of world production before shutting down in 2008. Ethiopia, which previously produced emeralds intermittently, emerged as a potentially large-scale source in late 2016.

Ruby production in Myanmar (formerly Burma) continued the long-term decline that began in the late 1990s. Madagascar's ruby production also declined sharply between 2006 and 2016. In Kenya, production of mostly low-grade ruby gradually increased. Mozambique emerged as a new source of gem-quality ruby, and large-scale mining operations started at Montepuez.

Sapphire mining declined in Cameroon and China. Madagascar's output fell with the depletion of near-surface deposits at Ilakaka and Sakaraha, as well as the 2008 ban on rough gem exports, before increasing because of new discoveries. Mozambique became a source of sapphire with the discovery of new deposits at Montepuez. Production also increased in Kenya.

Rio Grande do Sul State in Brazil appears to produce a substantial majority of the world's amethyst (table 1). Uruguay's production was estimated to have nearly tripled between 2006 and 2016. In Bolivia, Tanzania, and Zambia, production peaked in 2009.

TABLE 1. World amethyst production (in metric tons).

	2006	2008	2011	2014	2016
Bolivia	176	228	480	189	152
Brazil	3,800	4,200	4,710	10,977	4,800
Tanzania	75	107	45	29	30
Uruguay	468	520	1,000	1,400	1,300
Zambia	1,100	880	870	756	965
Other ^a	40	40	120	140	140
Total ^a	5,700	6,000	7,200	13,500	7,400

^aEstimated; data are rounded to no more than three significant digits.

Sources: U.S. Geological Survey Minerals Yearbook, company reports, and unpublished data.

In Kenya and Mozambique, tourmaline production peaked in 2013. The Democratic Republic of the Congo, Namibia, and Rwanda also emerged as sources of tourmaline in recent years.

General Gemology and Jewelry

Advances in Hydrocarbon Gemology: The Jet Group

Sarah Caldwell Steele

Whitby Museum, Whitby, United Kingdom

In mainland Europe, we first witness the utilization of gem-quality hydrocarbons for beads and amulets in the Upper Paleolithic. This was the period during which our hominid ancestors first developed complex language, culture, and art, laying the foundation for modern human civilizations. In the Americas, such artifacts are seen as early as 13,000 years ago. In the British Isles, Whitby jet (figure 1), arguably the highest-quality gem hydrocarbon in terms of stability, luster, workability and other attributes, first appears in the Early Neolithic. Almost certainly utilized for shamanic ritual, the jet group's unique gemological properties make it quite literally a "magic" material. During the Medieval Era, these same attributes brought it to the attention of the alchemists as a potential candidate for the philosopher's stone.

Despite this illustrious history, very little gemological research has been carried out on this culturally important material, and myth and folklore tend to prevail over hard geological facts. Adding to the problem, confusion in the nomenclature of gem hydrocarbons has given rise to a situation in which several structurally and chemically unrelated materials are often termed "jet."

Exhibiting the phenomenon of reflectance impedance, jet has erroneously been described as a lignite—a low-grade coal deficient in hydrogen. In reality, jet forms a complex group of hydrocarbons, observed to be natural polymers with varying stability and durability, that are believed to reflect the level of crosslinking between polymeric chains. They are certainly far from the chemically homogenous and structurally amorphous materials previously described in the gemological literature.

Figure 1. Victorian Whitby jet beads, with rough, cored, soft, brittle, and hard Whitby jet. Photo by Sarah Caldwell Steele.



Indigenous jet-working communities are still found in the Americas, Europe, and Asia. Yet a lack of gemological research has led to a situation where trading standards authorities cannot prevent the commercialization of foreign materials and simulants sold fraudulently as indigenous jet. Time is running out: The world's gemologists must embrace the latest research to mitigate the threat to those communities maintaining one of civilization's oldest gem trades.

REFERENCE

Steele S.C. (2016) Advanced jet testing. *Gems & Jewellery*, Vol. 25, No. 5, pp. 22–25.

Color Origin of Gem Diaspore: Correlation to Corundum

Che Shen

Gemmological Institute, China University of Geosciences, Wuhan

Gem-quality diaspore, commercially known as “Zultanite,” occupies an important position in the gem market due to its unique optical phenomena, rarity, and color-change phenomenon. The material’s value depends on these factors. A clear understanding of color origin offers considerable benefits for gemological testing, cutting, and even valuation of diaspore. This study uses ultraviolet-visible (UV-Vis) spectra and laser ablation–inductively coupled plasma–mass spectrometry (LA-ICP-MS) to examine the color origin of color-change diaspore and to compare it with corundum. Diaspore and corundum have a similar chemical composition and crystal structure. The crystal structure of diaspore is connected by $\text{AlO}_4(\text{OH})_2$ octahedra, whereas the corundum crystal structure is connected by AlO_6 octahedra (Hill, 1979; Lewis et al., 1982). Both types of crystals are composed solely of octahedral units. Due to their closely related crystallographic structure, chemical composition, and spectroscopic (UV-Vis) properties, we may speculate that there is a close color correlation between diaspore and corundum. Consequently, this study adopts an analogy to address the color origin of diaspore by quantitatively analyzing diaspore from two geographic origins—Myanmar (formerly Burma) and Turkey—and comparing them with high-quality natural and synthetic corundum. The research aims to use the color correlation between diaspore and corundum to confirm the former’s color origin.

Table 1 shows the chemical composition (expressed in ppm) of two diaspore samples from Turkey (Dia-006, Dia-008) and two from Myanmar (Dia-Bur-001, Dia-Bur-002). We concluded that the Burmese samples contained more Cr, while the Fe content was higher in the Turkish diaspore. However, the V content of the Burmese samples was higher than that of the Turkish material, especially Dia-Bur-002 (358 ppm).

We compared the spectra of corundum collected from the o-ray with those of diaspore collected from the orientation of polarized light parallel with the a-axis (figure 1). In addition, all the UV-Vis spectra are calculated based on the Lambert-Beer law. The author used this method to acquire spectra in certain chromophore concentrations and path lengths. The results are convenient for comparison. In color-change diaspore, Cr^{3+} , $[\text{Fe}^{2+}\text{-Ti}^{4+}]$, and V^{3+} may all play a role in causing the color-change effect. The chromophore ef-

centrations and path lengths. The results are convenient for comparison. In color-change diaspore, Cr^{3+} , $[\text{Fe}^{2+}\text{-Ti}^{4+}]$, and V^{3+} may all play a role in causing the color-change effect. The chromophore ef-

Figure 1. The UV-Vis spectra of diaspore (Burmese and Turkish) and corundum exhibit closely matched absorption features. The color circles, calculated under standard illuminants D65 and A, demonstrate coloration for diaspore and corundum with uniform chromophore (Cr^{3+} , $[\text{Fe}^{2+}\text{-Ti}^{4+}]$, and V^{3+}) concentrations for a 5 mm path length. The color swatches of Fe^{3+} are only calculated under D55 light. Since the diaspore’s color swatches below the spectra of chromophore $[\text{Fe}^{2+}\text{-Ti}^{4+}]$ do not show a clear color change, we calculated the colors, which are shown in the spectra at a higher concentration of Fe-Ti pairs (250 ppm) for a 5 mm path length.

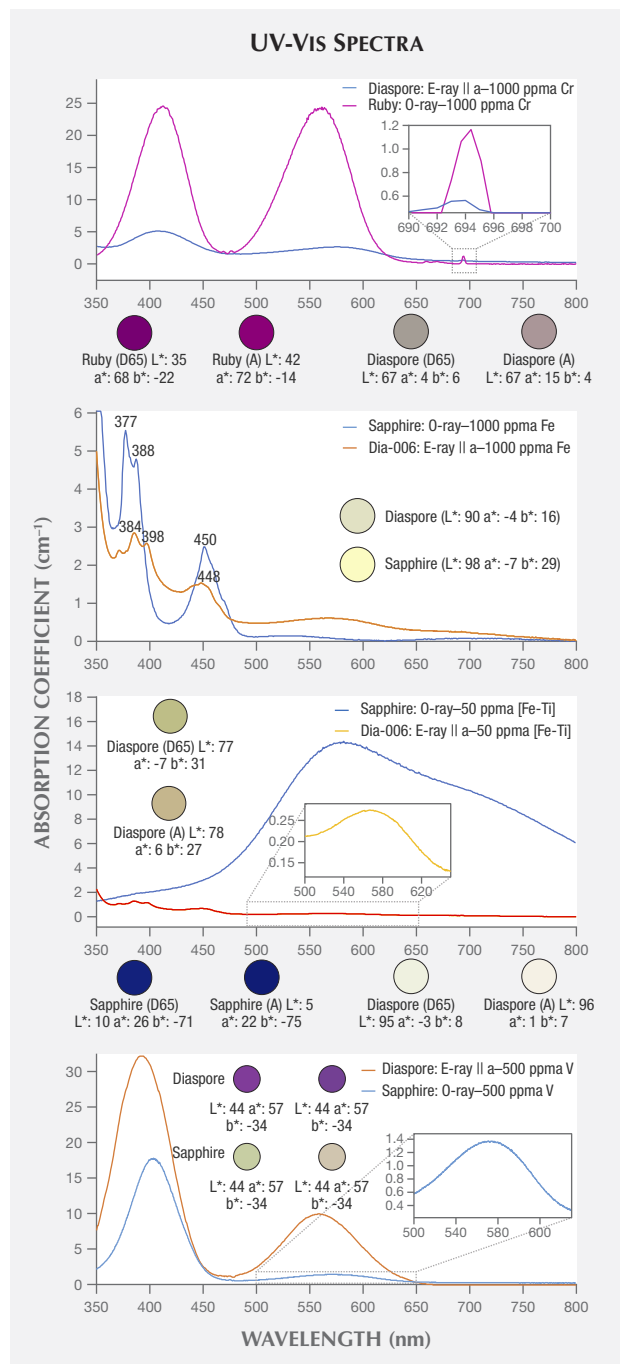


TABLE 1. Chemical composition of diaspore by LA-ICP-MS (in ppma).

Sample	Dia-006	Dia-008	Dia-Bur-001	Dia-Bur-002
				
Si	982	948	1053	1057
Ti	110	185	220	418
V	6	4	44	359
Cr	36	32	2166	2081
Fe	1169	548	4	1

fectiveness of Cr^{3+} , Fe^{3+} , $[\text{Fe}^{2+}\text{-Ti}^{4+}]$, and V^{3+} differs between diaspore and corundum. According to the calculation, the chromophore effectiveness of Cr^{3+} , Fe^{3+} , and $[\text{Fe}^{2+}\text{-Ti}^{4+}]$ in corundum is about 5–

10, 1.6, and 50 times higher, respectively, than in diaspore. However, the chromophore effectiveness of V^{3+} in diaspore is approximately 2–7 times higher than that in corundum.

REFERENCES

Hill R.J. (1979) Crystal structure refinement and electron density distribution in diaspore. *Physics and Chemistry of Minerals*, Vol. 5, No. 2, pp. 179–200, <http://dx.doi.org/10.1007/BF00307552>

Lewis J., Schwarzenbach D., Flack H.D. (1982) Electric field gradient and charge density in corundum, $\alpha\text{-Al}_2\text{O}_3$. *Acta Crystallographica*, Vol. 38, No. 5, pp. 733–739, <http://dx.doi.org/10.1107/S0567739482001478>

Education as a Tool for Development in East African Gem-Mining Regions

Marvin Wambua¹, Norbert Massay², Robert Weldon³, Pedro Padua³, and Dona M. Dirlam³

¹Amor Gems Ltd., Nairobi

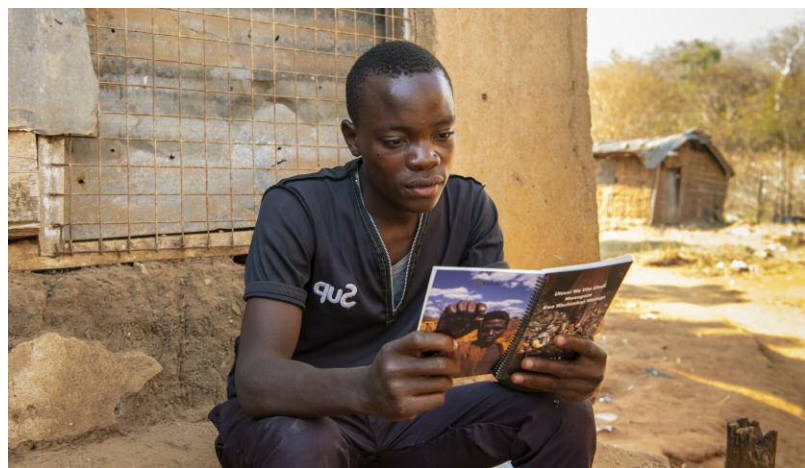
²Pact, Washington, DC

³GIA, Carlsbad, California

In 2014, GIA distinguished research fellow Dr. James Shigley conceived an idea to help artisanal miners in some of the poorest gem-producing regions of East Africa. Dr. Shigley and Dona Dirlam and Robert Weldon of GIA's Richard T. Liddicoat Library and Information Center, with GIA executive support, developed a plan for a guidebook for artisanal miners. The goal was to provide miners with very modest but valuable gemological concepts, empowering them to negotiate better prices for the rough material they sell.

Over the course of a year, the authors photographed numerous collections of rough material, mineral specimens, and cut stones. The authors conferred with members of the gem trade who are familiar with distant gem localities. They also received invaluable advice from Brad Brooks-Rubin, formerly of the U.S. State Department. The result of these efforts was a mainly pictorial booklet to accommodate all levels of literacy. Its few words were translated into Swahili. *Selecting Gem Rough: A Guide for Artisanal Miners* was printed on waterproof paper and made durable to withstand the rigors of mining activity. A resilient translucent plastic tray was de-

Figure 1. A miner from the corundum-rich region of Tunduru, Tanzania, examines the guide created for artisanal miners. Photo by Robert Weldon/GIA.



signed to hold the booklet, and to evaluate and sort rough. Using the tray with transmitted light, miners could understand rough color zoning and determine gem integrity and clarity.

Because of the East African material represented, mining locations in Tanzania were the first to receive the booklet. GIA partnered with Pact, a U.S.-based nongovernmental organization (NGO), to identify Tanzanian regions where the book could be deployed as a pilot project. Pact's plan incorporated government support of the project, and they identified the Tanzania Women Miners Association (TAWOMA), with mining projects east of Tanga, as an excellent group to participate in the pilot program.

In 2017, a GIA team and GIA East Africa consultant and alumnus, Marvin Wambua, met with Pact's Tanzania branch representative, Norbert Massay, to start the pilot project. Some 80 miners received the education and the booklets. Two subsequent trips to different regions were conducted. A Pact report concluded that a 12% social return on investment (SROI) had been achieved. During the course of the study, the miners acknowledged an educational benefit that would last them a lifetime, with key concepts of gemstone value that could be passed on to other miners. Additional mining areas in central and southern Tanzania received training in 2018.

Enameling Chinese Cultural Relics

Shangjia Wen and Ren Lu

Gemmological Institute, China University of Geosciences, Wuhan

Jing-Tai-Lan, popularized in China more than 500 years ago and synonymous with cloisonné enamel, is characterized by opaque enamel materials on bronze, one of several classic enamel techniques dating back to the thirteenth century BCE. Furthermore, Chinese *Jing-Tai-Lan* is readily recognizable by its iconic set of colors—cinnabar red, malachite blue-green, pararealgar orange-yellow, and white—as well as traditional cultural patterns and religious reflections (figure 1). This particular style is deeply rooted in Chinese culture and has remained virtually unchanged over time. Yet the traditional combination of colors and patterns unique to *Jing-Tai-Lan* are not the best fit for a new generation of consumers.

Over centuries, various enamel techniques have been developed and used to create lasting artworks from many cultures of the world. In addition to cloisonné enamel, there are several other classic enamel techniques. *Champlevé*, which dates back to the twelfth century, features engraved or struck recessed areas subsequently filled with vitreous enamel. Some historic examples are religious plaques and emblems. Painted enamel (Limoges enamel) originated in the fifteenth century in southwestern France and is well known for its portraits and scenes on vessels. *Piqué à jour* enamel, which probably originated in the sixth century, has metal wires or cells filled with transparent vitreous enamel. This technique was used in some of the most iconic Art Nouveau pieces such as jewelry depicting delicate butterfly or dragonfly wings, Tiffany lamps, and luxurious vases. Today, these classic techniques and the overlap between them, along with choices of precious base metals and a full spectrum of opaque, semitransparent, and transparent enamel materials, have provided artists and jewelers worldwide with tools for unbounded creativity.

Contemporary Chinese consumers are increasingly searching for expressive styles and colors and diversified cultural reflections that suit their personal preferences and lifestyles. The 500-year-

old historic *Jing-Tai-Lan* technique needs to evolve for the twenty-first century.

Figure 1. A classic *Jing-Tai-Lan* (cloisonné enamel) vase from the Ming Dynasty, sixteenth century. Courtesy of Sotheby's.



The authors are exploring the full potential of classic enameling techniques in revitalizing traditional Chinese cultural icons and historic relics. Our efforts are focused on fusing contemporary jewelry

making with widely identifiable and readily acceptable Chinese elements drawn from cultural heritage and folk art, with the aim of enriching enamel jewelry for contemporary Chinese lifestyles.

The Evolving Supply Chain—How Greater Awareness of the Value of Mineral Resources Spawned a Movement to Restrict Their Outflow From Producing Nations

Stuart Robertson

Gemworld International, Inc., Glenview, Illinois

Traditionally, the colored stone industry has depended on a fragmented distribution channel of small-scale operators to transport gems through the multiple levels of the marketplace. In recent decades, producing nations, especially in Africa, have increasingly questioned the equity of a system in which the least economic benefit of the resource is retained by producers, while the vast majority of benefit is achieved by those closest to the retail consumer. Governmental regulations enacted to counter this perceived inequity have had a number of unintended consequences, such as forcing otherwise honest small-scale laborers to operate outside of the law just so that they can compete in the market.

This presentation examines changes in Tanzania's gem market to illustrate the major challenges the gem industry faces in balancing the growing demand for supply chain transparency with a profitable finished product. As the traditional model for producing gem material faces increasing pressure, it is clear that the supply chain of the future will be significantly different. The emphasis on retaining value at the source is already influencing price and demand for certain popular gems. This move toward increased value capture by producing nations will inevitably reduce the size of the traditional wholesale market.

The Gem Collection at the Natural History Museum, London: A Collection of Collections

Robin Hansen

Natural History Museum, London

Gemstones, gem rough, and worked objects have been collected alongside mineral specimens in the Natural History Museum (NHM), London—previously known as the British Museum (Natural History)—for more than 270 years, creating one of the world's outstanding mineralogical collections. Some 5,000 of the 185,000 specimens are gemstones or worked objects that constitute the Gem Collection. This collection grew by incorporating many smaller ones. The earliest gems are from Sir Hans Sloane, physician to the royal family in the late 18th century, whose vast collections formed the basis of what are known today as the British Library, the British Museum, and the NHM. Most notable were Lady and Sir A.H. Church's gemstone rings (1915), Prof. Archibald Liversidge's Australian gemstones (1927), Dr. A.C.D. Pain's Burmese gemstones from Mogok (1973), and the collections of T.B. Clarke-Thornhill (1934) and C.R. Mathews (1993). Gemstones from Edward Hopkins (between 1906-1933) included a 598 ct morganite from Madagascar. The largest addition

came from the merger of the British Geological Survey collection with that of the NHM in 1985, adding around 1,500 gems. Highlights included a pale blue 2,982 ct topaz from Brazil (the collection's largest cut gemstone), a 57 ct *padparadscha* sapphire from Sri Lanka, a 424 ct kunzite from Brazil, a rare 20 ct Burmese sillimanite, a 146 ct peridot from St. John's Island in the Red Sea, and the impressive diamond-studded gold snuff box of Sir Roderick Murchison, gifted to him by Czar Alexander II.

This historically important collection is a treasure trove of scientific, historical, and cultural knowledge. It serves as a reference for many of the developments and uses of different gem materials over time. Working alongside the mineral collection, the geological context is often preserved, adding significant scientific value. The collection is currently undergoing a re-curation program to enhance the data. Efforts to increase its accessibility and availability for focused research within the gemological and mineralogical communities will help to realize the Gem Collection's full potential.

Gemology and Appraising: Similarities and Differences

Susan Eisen

Susan Eisen Fine Jewelry & Watches, El Paso, Texas

There are many similarities between the science of gemology and the science of appraising. When done accurately, both involve the study of information on a university level and a continued dedication to lifelong learning to stay aware of the constant changes happening. Both represent an amazing amount of enlightened knowledge occurring on a daily basis around the world. Both professions also require dedication to detail, the ability to do exhaustive research to come up with the correct answer, and a deep understanding and application of technology. Another similarity

is the need to use subjective and objective reasoning to determine the results. Since both are sciences, using intellectual truths and adapting them to solve the problem helps in determining the correct results.

Identifying a gemstone is just half the battle in the appraisal of gems. Once the identity is determined, other parameters must be considered to estimate a gem's value. In gemology, identification of the material and its internal characteristics is only part of the conclusion.

Gemstone Durability Chart

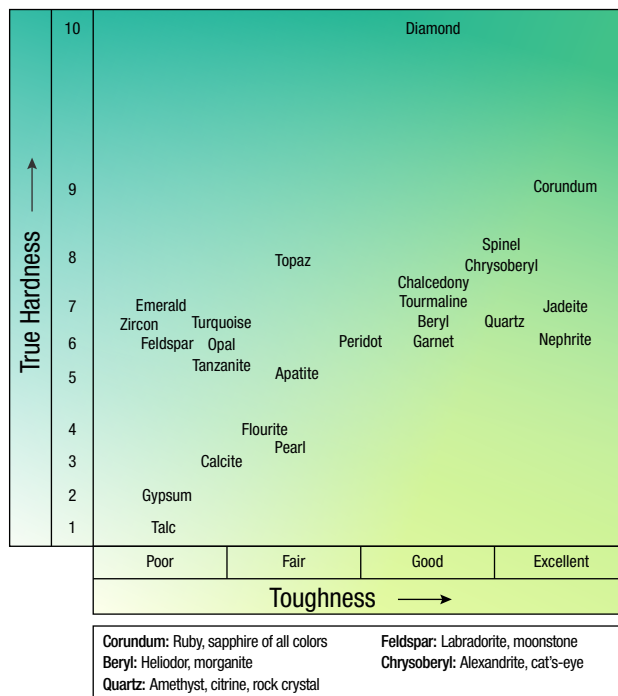
Kennon Young

Vermont Gem Lab, Burlington, Vermont

One of the most commonly misunderstood traits of a gemstone is durability. Many people believe that durability is based strictly on a gemstone's hardness. Hardness is a gemstone's resistance to scratching, but it does not account for a gemstone's resistance to breaking and cleaving. Resistance to breaking and cleaving, as used in this presentation, will be described as "toughness."

The chart to the right reflects common gemstones and their relative durability. Accounting for resistance to scratching, breaking, and cleaving can allow us to better understand how durable gemstones are.

The gemstones listed are mostly group names. Some species of these groups are noted at the bottom of the chart.



Good News and Bad News: Two Tales of Products of Endangered Species Used in Jewelry

Charles Carmona¹ and Jo Ellen Cole²

¹Guild Laboratories, Los Angeles

²Cole Appraisal Services, Los Angeles

Elephants as a species (figure 1, left) have been given a better chance to survive the twenty-first century and beyond thanks to the abolition of the legal ivory trade in China as of January 1, 2018. The world watched in horror as thriving populations of this ma-

jestic animal plummeted by 90% over the last 50 years, mostly due to poaching of their tusks for use in jewelry and decorative art. European export of ivory was banned in 2016, as were sales (with a few exceptions) in the U.S.



Figure 1. Left: With new ivory bans in place, elephants have a greater chance of survival. Photo by Muhammad Mabdi Karim. Right: Precious coral, a gift from the sea, is being harvested beyond sustainability. Photo courtesy of Lushome.com.

Ivory markets still exist in Asia and other parts of the world, but with lower demand from the largest consumers, prices will drop and the slaughter will lessen. Only when legislation and education reach this level in all markets will elephants and other sources of ivory be safe.

That's the good news. Now the bad news.

The various species of precious coral (figure 1, right) are not so fortunate, as they are still not listed as threatened by the Committee on the International Trade in Endangered Species (CITES). Although some regions are restricting the harvesting of precious coral, in other areas there is no such concern. Divers are going deeper every year to take more coral for the demand created by the jewelry and decorative arts industries, which is far beyond

its level of sustainability. Adding to that are the rising temperatures and acidification of the oceans due to climate change. At this rate, extinctions could occur in our lifetimes.

Only a concerted effort on all fronts can save these corals. Listing by CITES and research into coral farming are good starts, but ultimately it will require public education and research into alternatives to taking coral from the sea. Coral is already a gift. Let it be an inspiration to create jewelry and art from materials that are not endangered.

In response to the threats against coral, 2018 has been declared the third International Year of the Reef (www.iyor2018.org). Join The Ocean Agency, the Tiffany Foundation, Google, and many others to save this most precious resource for future generations.

The History and Current Status of Colored Gemstone Grading

Henry Ho and Barbara Wheat

Asian Institute of Gemological Sciences, Bangkok

Before color-grading systems were available on the market, people developed their own systems for judging color. The lead author has been involved in the gemstone business since he was a young child, helping his father sort and grade gemstones in his office. He has 55 years of experience in examining and judging color in gems and will share the history of colored gemstone grading in this poster.

The history will cover the GIA color system, Gemval, the CIE system, the Munsell color wheel, GemDialogue, Gemewizard, the

Tanzanite Foundation grading system and the Miner's System, and the ICSL System. References will be made to expert analysis in the field from notable industry leaders such as Joel Arem and Richard Drucker.

The current status of color grading will be addressed from the lead author's perspective based on his extensive experience with colored gemstones, as a gemological laboratory owner and in the trade, as well as his discussions with color experts from around the world.

The Human (Humane) Trail: Finding Relevance in Jewelry Along the Pathway of Transparency

Brian Cook

Nature's Geometry, Tucson, Arizona/Bahia, Brazil

Economic opportunity from the earth and sea comes into the hands of artisanal and small-scale miners (ASM) through hard labor and good luck. By 2017, approximately 40.5 million people were directly engaged in ASM mining, with five times that number dependent on ASM mining as a route out of poverty (Fritz et al., 2018). The chain of custody of gemstones mined by ASM, extracted from the earth and traveling as far as the red and green carpets at the Cannes Film Festival (the latter of which features celebrities wearing sustainable couture and jewelry) is a long, mostly opaque road. Mine-to-market transparency is the key to increasing consumer trust in the gem and jewelry industry while relating the rich stories associated with the lands, the cultures, and proud people that are the cornerstone of our trade.

As an industry, we have the opportunity to bring more benefit to ASM communities. Opportunities to invest in microfinance, mining and reclamation improvement, processing, and value-added enterprises—especially in parallel economic development with practices such as regenerative agriculture/agroecology—would align our industry with areas identified by the United Nations in 2015 as their Sustainable Development Goals (n.d.). In doing so, we would reshape the portrayal of gem mining as having a negative impact on people and the environment. Mining gemstones would be viewed as a way to bring economic benefit and environmental stewardship to potentially thousands of remote miners and their dependents.

In a remote exotic biome deep in Brazil, a model is forming around a unique gem resource known as Bahia golden rutilated quartz (figure 1). This material is sourced from the Rio dos Remedios group in the Espinhaco supergroup, a 1.7-billion-year-old narrow volcanic sequence with a range of unusual elements including yttrium, lanthanum, neodymium, titanium, iron, barium, and gold. The author and Kendra Cook have been associated with this mining community since 1983. In recent years, the author has

helped to formalize operations and register miners into cooperatives. An initiative to implement sustainable economic, environmental, and cultural activities in this ASM community and connect it to our industry is underway, including the formation of a local NGO specifically to advance this initiative for the region. The aim is to create stories that add relevance to the jewelry industry, while initiating sustainable and measurable benefits for our first tier suppliers and their communities.

Figure 1. Natural golden rutilated quartz from the Rio Remedios group in Novo Horizonte, Bahia, Brazil. Photo by Brian Cook.



REFERENCES

Fritz M., McQuilken J., Collins N., Weldegiorgis F. (2018) *Global Trends in Artisanal and Small-Scale Mining (ASM): A Review of Key Numbers and Issues*. International Institute for Sustainable Development, Winnipeg, Canada, 91 pp. <https://www.iisd.org/sites/default/files/publications/>

[igf-asm-global-trends.pdf](#)
 United Nations (n.d.) Sustainable Development Knowledge Platform: Sustainable Development Goals. <https://sustainabledevelopment.un.org/sdgs>

The Impact of Fluorescence on Current Marketability

Richard B. Drucker

Gemworld International, Inc., Glenview, Illinois

According to GIA research conducted over a ten-year period and reported in *Gems & Gemology* (Moses et al., 1997), about 25–35% of all diamonds submitted to the GIA laboratory exhibited fluorescence. The listed range of fluorescence on a GIA grading report is *none, faint, medium, strong, and very strong*. Blue was the most common fluorescence color, accounting for about 97% of all cases (Shigley, 2014). About 10% of the occurrences of blue fluorescence were rated as medium or stronger. Other possible colors include yellow, green, orange, white, and red, with yellow a distant second. However, the GIA laboratory only lists the color when the fluorescence is medium or stronger, so data on the frequency of other colors is minimal.

Past research has found that in almost every case, any degree of fluorescence is a deterrent to market value. Prior to the late 1970s and early 1980s, some diamonds with fluorescence traded for a premium, but it was perhaps the investment craze and the demand for no fluorescence that started the initial deductions for fluorescence (Drucker, 2014). Over the years, the negative perceptions persisted and discounts became greater. Current research shows that the pricing deduction on average could be anywhere from a few percentage points for faint fluorescence to 30% for very strong. This study analyzed more than 89,000 diamonds to determine the approximate distribution of fluorescence strengths and colors for diamonds in the most popular carat weights and grades. The analysis also determined approximate discounts to the wholesale selling prices associated with these fluorescence categories, analyzing more than 76,000 diamonds.

Results of the study showed that 33.5% of the diamonds in this sampling did exhibit fluorescence, similar to results of the pre-

Average Discount for Fluorescence (GIA Only), Excellent Cut, 1.00 to 1.19 ct

D–F	IF/VVS	VS	SI–I ₃
Faint	–7%	–9%	–6%
Medium	–17%	–14%	–10%
Strong	–19%	–18%	–11%
Very Strong	–20%	–31%	–15%
G–H	IF/VVS	VS	SI–I ₃
Faint	–8%	–5%	–4%
Medium	–10%	–8%	–7%
Strong	–12%	–11%	–8%
Very Strong	–24%	–16%	–7%
I–K	IF/VVS	VS	SI–I ₃
Faint	–2%	–2%	–3%
Medium	–6%	–7%	–4%
Strong	–6%	–8%	–8%
Very Strong	–17%	–12%	–14%

vious GIA research. Where the GIA research had about 10% of those fluorescing medium or stronger, this study indicated 15% at medium or stronger (of those that fluoresced). In the GIA study, 97% of those that exhibited fluorescence fluoresced blue, whereas in this study 99% were blue.

The chart shows the discounts, calculated from this study, that are currently associated with fluorescent diamonds on the market. These percentage discounts have continued to be greater than in years past when similar research was conducted by this author.

REFERENCES

- Drucker R.B. (2014) Effects of fluorescence—New research on pricing. *World of Gems Conference*, Rosemont, Illinois, September 21–22.
- Moses T.M., Reinitz I.M., Johnson M.L., King J.M., Shigley J.E. (1997) A contribution to understanding the effect of blue fluorescence on the appearance

of diamonds. *G&G*, Vol. 33, No. 4, pp. 244–259, <http://dx.doi.org/10.5741/GEMS.33.4.244>

- Shigley J.E. (2014) Fluorescence, what's changed. *World of Gems Conference*, Rosemont, Illinois, September 21–22.

Impacts and Expectations for the Fourth Industrial Revolution in Gemstone Faceting

Lee W. Haynes

LWH, Berkeley, California

As the world enters the Fourth Industrial Revolution, powered by computer and robotic technologies, the nineteenth- and twentieth-century manufacturing practices within the gemstone industry are being transformed. From computer numerical control (CNC)

machining to high-resolution scanning and faceting optimization tools, yield and brilliance have increased substantially, and automation is projected to grow as more material is processed. These issues do not come without challenges and risks, and the economic model

of low-cost labor to high-skill processing is a slow progression. In reviewing current automation processes and future technologies, there is a shift to enhance human capabilities with complementary automation processes. This shift is driven by many factors, from ease of implementation to material-dependent variables. Although

there is progress in automation, there are challenges that constrain full automation. As a result, we will continue to see a need for continuing manual and human-driven processing for the next generation as full automation is adopted slowly based on labor force skill sets and capital return on investment (ROI) for new technology.

The Importance of Precious Metal Marks: Past, Present, and Future

Danusia Niklewicz, William Whetstone, and Lindy Matula
Hallmark Research Institute, San Francisco

Today there is a lack of understanding of the various types of marks that can be found on precious metals. This presentation seeks to enlighten the observer about the changing variety of marks and to better understand their importance.

When looking at the marks on precious metal jewelry, it is important to make the distinction between *hallmarks* and *maker's marks*. They each serve as a guarantee of quality. Maker's marks are applied by the actual maker or sponsor, retailer, and/or importer, and are generally referred to as a responsibility mark. These are guarantees that, by law, require that the fineness marked on the item actually state the metal's true fineness.

Hallmarks (figure 1) are applied by a nationally authorized assay office to an item that has been submitted by the manufacturer or sponsor for scientific testing to verify the precious metal's actual purity or fineness. Depending on the country and their hallmarking methodology, assay office hallmarks identify not only a metal's composition but also the country of origin, the city of assay, the year or time period when the item was struck, and the approximate weight or length of that item. Hallmarks can be compared to an independent laboratory grading report on a gemstone or diamond: Both provide trusted testing and unbiased reporting of the facts about the item. While a diamond may have the report number inscribed on the stone's girdle, a hallmark reports the test results by being struck into the mounting itself.

Not all countries in the world hallmark, but most European, Middle Eastern, North African, and some Asian countries have legislated compulsory hallmarking as a strong measure for consumer protection against the under-karatting of precious metals so often found in non-hallmarking countries.

In the United States, the 1906 Gold and Silver Stamping Act, along with its 1961, 1970 and 1976 amendments, has clearly stated that any item with a fineness stamp (e.g., 18K, 950Pt, Sterling, etc.) *must* also be stamped with a federally registered maker's or responsibility mark, referred to as a trademark. While manufacturers and retailers are required to register their marks as trademarks before applying a fineness mark on any precious metal item, the laws unfortunately are seldom enforced. Thus, many small companies, artisans, and importers do not register their trademark names or marks. Consequently, there are limited resources avail-

able for identifying modern U.S. maker's marks, especially from the second half of the twentieth century.

As global foreign trade streamlines, so does the need for easier trading between hallmarking countries. Previously, when importing items between hallmarking countries, the item's hallmarks had to be re-verified by a second assaying and hallmarking before being allowed for sale. In 1972, the Hallmarking Convention members signed a treaty to uphold consistent standards between member assay offices. Today, their strength comes from the unity of the 21 contracting member nations, all using the same agreed-upon Common Control Marks (CCM) as proof of compliance. These common marks are recognized by each member nation and also accepted by many countries globally. For more information, see www.hallmarkingconvention.org.

Introduced in 1988, Fairtrade and its certification mark have become internationally recognized proof that a product has met the required standards for responsible sourcing. With respect to an item of gold and associated precious metals, a Fairtrade stamp indicates that the metal, from ground to market, has followed ver-

Figure 1. This hallmark says in Arabic that the ring was marked in Damascus, Syria, and the metal is 18K gold. Photo by Danusia Niklewicz, Hallmark Research Institute.



ifiably traced fair and economic practices. As Fairtrade International notes, “Gold certified to Fairtrade Standards provides small-scale miners and their communities in developing countries the opportunity for better living and working conditions. Fairtrade also certifies Ecological (ECO) gold, which is mined under stringent ecological restoration practices, without the use of chemicals.” It is expected that the FAIRTRADE mark will become more prevalent on items of precious metal in the future. For more information, see www.fairtrade.net/products/gold.html.

Offshore hallmarking originated from the concept that hallmarking at the source could streamline the hallmarking regulations of the importing country. By setting up assay offices in countries

that produce and export precious metal jewelry items but do not have the required hallmarking facilities—Indonesia, Thailand, and China, for example—the required hallmarking laws of the destination country can be fulfilled. This expedites the marking needs of the manufacturer/exporter by offering hallmarking services nearby.

Including offshore hallmarking services in Asia, Europe, Central Asia, the Middle East, North Africa, and the Far East, hallmarking now influences nearly 60% of the world’s population. Currently, with no nations in the Americas hallmarking, they are missing out on the best proven method of real consumer protection in the trade of jewelry and other precious metal items.

Jewelry Development Impact Index at the University of Delaware

Patricia Syvrud and Saleem H. Ali

Minerals, Materials and Society Program, University of Delaware, Newark

At present, the international jewelry industry lacks any measure or standard of how the sourcing and manufacture of jewelry and its components impacts developing countries. Because of its global complexity and fragmented nature, the jewelry industry supply chain calls for study and monitoring to enable countries and companies to exert a more positive influence, particularly in emerging economies.

After discussions at the Jewelry Industry Summit in Tucson, Arizona, in January 2017, multiple stakeholders within industry, government, and the academic community came together to propose the creation of a comprehensive, ongoing Jewelry Development Impact (JDI) index. The University of Delaware (UD) invited the JDI to become the signature project of a new interdisciplinary, graduate-level academic project, “Minerals, Materials and Society,” under the leadership of Dr. Saleem H. Ali. A grant was awarded by Tiffany & Co. Foundation to create The Gemstone and Sustainable Development Knowledge Hub (GemHub: <http://sustainablegemstones.org>), which will serve as a research arm within the Minerals, Materials and Society program at UD. GIA distinguished research fellow Dr. James Shigley sits on the GemHub Advisory Board, and senior research scientist Aaron Palke is an affiliated scholar and research partner.

The JDI is conceived as a relative country score that will measure the degree to which the jewelry and gemstone industries impact the economic and social well-being of each country in which they function. Created within the framework of the United Nations indicators of human security, the JDI will also capture examples of responsible sourcing and transparency initiatives that can be replicated, creating a “Roadmap to Responsibility” to assist with the implementation of the UN Sustainable Development Goals, the Organisation for Economic Co-operation and Development’s (OECD’s) Due Diligence Guidelines and environmental, social, and supply chain audits. As an initial step to the conceptualization of the JDI, academic research in the format of comparative case studies was conducted by graduate students at American University’s School of International Service in the fall of 2017 and spring of 2018. Elizabeth Orlando, Foreign Service Officer with the U.S. Department of State Office of Threat Finance Countermeasures, serves as special advisor to this project.

The results of the initial academic research will serve as a basis for the creation of a robust methodology for the JDI. The countries and products presented in this poster are: gold in Peru and diamonds in Botswana (fall 2017) and rubies in Myanmar and lapis lazuli in Afghanistan (spring 2018).

The New Economics of Diamond Mining

Russell Shor

GIA, Carlsbad, California

The discovery of diamonds larger than 50 carats used to be a rare occurrence, but in the past decade many such specimens have been found. The majority of these come from low-yielding “boutique”

mines, which have been developed only recently. In addition, many existing mines have changed their diamond recovery processes to preserve larger crystals.

Two factors have brought about these changes:

- A vast increase in the number of high-net-worth individuals around the world, particularly in the Middle East, Russia, and China. These people and the dealers who work with them have become very active buyers of large diamonds, both privately and in the major auctions conducted by Sotheby's, Christie's, and others. As a result, the per-carat price differential between commercial-size diamonds and those over 10 carats increased nearly fourfold during the previous decade. Such price increases enabled these low-yielding boutique mines to become profitable.
- The development of new technologies to help identify larger crystals before they enter the recovery process. Improved X-ray technology can identify large crystals, fancy colors and stones without fluorescence that once might have been missed. In addition, the speed of X-ray identifi-

cation has improved to the point where such units can be deployed prior to the crushing process, which previously destroyed or damaged many large rough diamonds.

The result is that discoveries of diamonds over 100 carats, a rare occurrence 20 years ago, have become relatively commonplace. Some of the largest diamonds ever discovered, including an 1,109 ct giant (1,111 ct before cleaning) from Botswana's Karowe mine and a 910 ct stone from the Letseng mine in Lesotho, have been found in the last ten years.

The case study will be Letseng, which reopened in 2006. Its ore grade is about 1.5% that of the benchmark of one carat of diamonds per ton of ore. But the per-carat average price of Letseng's production ranges between \$1,800 and \$2,100, compared to the industry average of \$118 per carat. Rio Tinto and De Beers mined it unprofitably during the 1970s before closing the operation in 1982. Rising prices for large diamonds in the 2000s have allowed the new owners to open and operate it profitably.

A Rare Nearly Pure End-Member Grossular Garnet with Color-Change Effect

Supparat Promwongnan and Apitchaya Buathong
Gem and Jewelry Institute of Thailand, Bangkok

Most color-change garnets (figure 1) in the gem market are intermediate in composition or solid-solution between pyrope and spessartine end members, with a trace of vanadium or vanadium-plus-chromium responsible for their color-change phenomenon. Some chromium-rich pyrope and grossular-andradite solid-solution with color-change effect have also been reported. In this study, two new color-change grossular garnets were examined at the Gem and Jewelry Institute of Thailand Gem Testing Laboratory (GIT-GTL). Their UV-Vis spectra (figure 2) and chemical compositions revealed a rare, almost pure end-member grossular with chromium plus iron as the significant color-causing elements.

Figure 1. The distinct color-change effect of two grossular garnets. The 13.18 ct stone (left sample) appears yellowish green with a daylight-equivalent source and brownish red using an incandescent light source. The 6.73 ct stone (right sample) is strong green with daylight-equivalent illumination and purplish brownish red using incandescent light. Photos by Supparat Promwongnan.

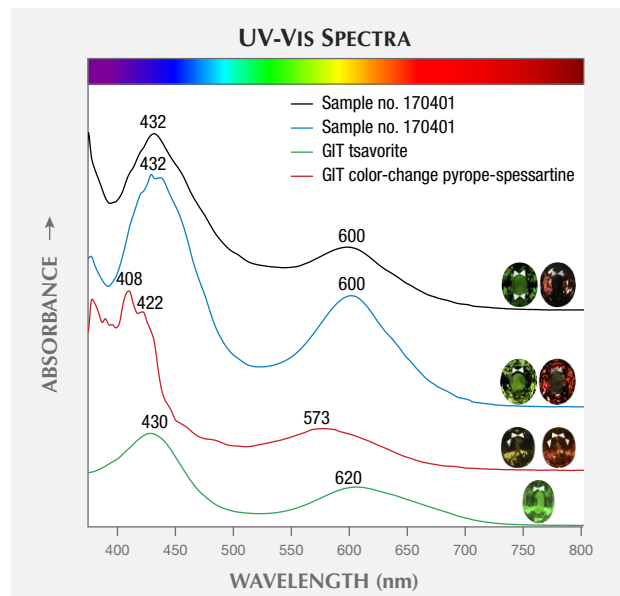
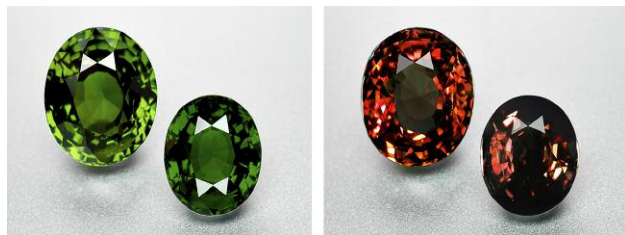


Figure 2. Visible absorption spectra of the color-change grossular garnets with typical absorption bands around 432 nm (due to Cr³⁺ plus Fe³⁺) and 600 nm (Cr³⁺). GIT's tsavorite spectrum shows absorption bands at ~430 and 620 nm toward the red region (due to V³⁺), while GIT's color-change pyrope-spessartine spectrum shows bands at ~573 and 415 nm (due to V³⁺ and/or Cr³⁺) with small bumps at 408 and 422 nm in the violet region (due to Mn²⁺). Spectra are offset for clarity.

Rolling Around in the Light—A Spherical Exploration of Gem Optics

Sylvia Gumpesberger
University of Toronto

Optical mineralogy theory has been thoroughly covered in many excellent gemology texts and journal articles, yet newcomers long to bridge the gap between theory and meaningful firsthand witness to the concepts that are so vital to the testing and characterization of faceted gems. The author investigated a variety of polished, transparent, single-crystal mineral spheres (including isotropic, uniaxial, and biaxial) using white light and polarizing filters to illuminate directional optics such as pleochroism, optic figures (interference figures), and their interrelationships through simple, accessible methods.

The spherically polished form of these transparent specimens (figure 1) eliminated the need for an external interference sphere/conoscope, avoiding much of the visual impediment of facet edges and their often confusing color reflections while allowing accurate approximation of angles for easily and successfully navigating and locating light effects.

Using transmitted light and a calcite or London-style dichroscope, it was evident that the greatest color separation of the ordinary (o-) and extraordinary (e-) rays in dichroic *uniaxial* minerals is at 90 degrees to the optic axis and that this axis, indicated by the optic figure seen through crossed polars and appearing at two opposite ends of the sphere, exhibited no pleochroism through the dichroscope. Further to this, it was clear from using the dichroscope that the e-ray departed in color from the o-ray in increments as the angle of the rays departed from the optic axis to the maximum color divergence or maximum differential absorption at 90 degrees to the optic axis.

Among other observations was the extinction effect. This was seen clearly down the c-axis in transparent tourmaline spheres, evident to the unaided eye in certain orientations when spheres were rolled slowly over diffused, transmitted light. The extinction direction was then confirmed by observing uniaxial optic figures in the same extinguished locations at opposite ends of the sphere when viewed under crossed polars. Note: In uniaxial minerals like corundum, the unpolarized optic axis direction and c-axis are the same direction, though conceptually different.

Biaxial gem spheres exhibited four typical biaxial interference figures that were easily located, and the 2V angle could be approximated. A dichroscope confirmed that the optic axis directions of biaxial gems also exhibited minimal pleochroism. Strong directional color could be seen in trichroic biaxial minerals such as the spodumene variety of kunzite and synthetic chrysoberyl, even unaided. A dichroscope separated the differentially absorbed wavelengths at angles other than the optic axes.

Rolling double refractive spheres slightly off the optic axis direction when viewed under crossed polars provided an insightful view into the variety of shadow pattern variations of conoscopic interference patterns sometimes seen through a petrographic microscope, when viewing polished thin sections containing crystal grains positioned with the optic axis slightly off-perpendicular to the thin section plane.

An instructional set of polished transparent gem spheres in a gemology classroom or lab can be very effective in engaging students in playful exploration, facilitating helpful observations that students can photograph for their notes, and builds skills and confidence prior to tackling high academic theory or testing small faceted gems. Further exploration could include the observation of directional spectra.

Of note to lapidaries, the preferable direction of color in synthetic ruby, though somewhat subjective, was observed down the optic axis of the sphere. Any angle of double refraction in this specimen exhibited some degree of differential absorption, a necessary consideration when choosing the relative angle of the table facet. Pleochroic spheres reveal the importance of considering directionality in cut design.

Figure 1. Synthetic ruby sphere viewed without filters. Photo by Sylvia Gumpesberger.



Science Has a Place on the Selling Floor

Maureen Moses

Adventure Gemstones, San Diego, California

Gemology, geoscience, and mineralogy—the sciences that help us understand gemstones—are the primary ways to comprehend gemstone rarity relative to the composition of the planet. Additionally, history and anthropology provide context to the value of gemstones, offering perspective on humans' relationships with one of the most ancient luxury goods. Complete dismissal of the sciences can disproportionately weight the value of gemstones on their durability and beauty. This may result in an inadequate scope of selling points necessary for closing sales, especially for clients new to the high-end gem and jewelry industry. While there are clients who may find this information to be superfluous, preparation of talking points through gemology coursework and continuing education can help build an arsenal of information useful to sales professionals. A problem still exists where recent scientific literature is not disseminated in a meaningful way to the lay public, and the relevance of these discoveries remains masked by the authors'

technical language that is necessary to gain credibility within their own academic circles.

To bring science to the selling floor, Adventure Gemstones provides an additional tool geared to address this professional shortcoming. By utilizing modern science communication practices, the essence of these discoveries can be lifted and digested in a way that can be absorbed at the lay level, while furthering society's understanding of the geosciences. Talking points, which can now be disseminated through blog posts and social media, will give sales professionals a way to speak to the adventure of gem formation, discovery, and recovery. They can also provide positive anchors for potential buyers to continue to weigh during their buying decisions. Adventure Gemstones seeks to add training modules for sales staff, with in-person trainings at stores and professional events, to give further clarification of modern research, and to democratize the science as a viable resource for the selling floor.

Supplementary Techniques with Potential to Assist in Freshwater Pearl Identification

Artitaya Homkrajae¹, Chunhui Zhou², Ziyin Sun¹, and Troy Blodgett³

¹GIA, Carlsbad, California

²GIA, New York

³GIA, Flagstaff, Arizona

Real-time microradiography (RTX) and X-ray computed microtomography (μ -CT) are the main techniques used by gemological laboratories to analyze a pearl's internal structure in determining whether it is natural or cultured (non-bead cultured or bead cultured). Most freshwater non-bead-cultured (NBC) pearls contain characteristic twisted voids or elongated linear features toward their centers that easily separate them from their natural counterparts. However, some pearls possess borderline or overlapping growth features and exhibit external appearances that do not readily assist in their identification.

This presentation covers two supplementary techniques that offer some assistance in the identification of challenging freshwater pearls, specifically between American natural and Chinese NBC. Owing to its rich resource of approximately 300 *Unio* mussel species, North America has been an important source of natural freshwater pearls for centuries. For a number of reasons, however, mussel fishing is currently limited in the United States. Thus, most freshwater pearls in today's market are NBC pearls produced in China.

The first technique is trace-element analysis using LA-ICP-MS. We analyzed 74 natural pearls reportedly from various wild

Unio mussel species collected from North American lakes or rivers and 76 Chinese NBC pearls purchased from various sources. Since the pearls formed within different water environments, differences in chemical compositions and concentrations are to be expected. Linear discriminant analysis (LDA) was applied to the results obtained to provide additional helpful data. To enhance the study, we also included 75 American freshwater cultured pearls (both bead cultured and NBC) that were grown in very specific and well-defined conditions in Kentucky Lake, Tennessee. Therefore, their chemical compositions were likely to be more homogenous than those of the other sample base.

The second technique is deoxyribonucleic acid (DNA) bar coding. The work was first performed on five common pearl-producing species of American mussel collected directly from Kentucky Lake: pink heelsplitter, ebony, washboard, southern mapleleaf, and three-ridge mussels. Additional DNA bar coding experiments were conducted on various freshwater pearl samples, and the DNA sequences of eight samples from different origins (*Hyriopsis* species, *Megalomias nervosa*, and *Potamilus* species) have been successfully identified. If it can be proved that the DNA of a specific pearl matches a native

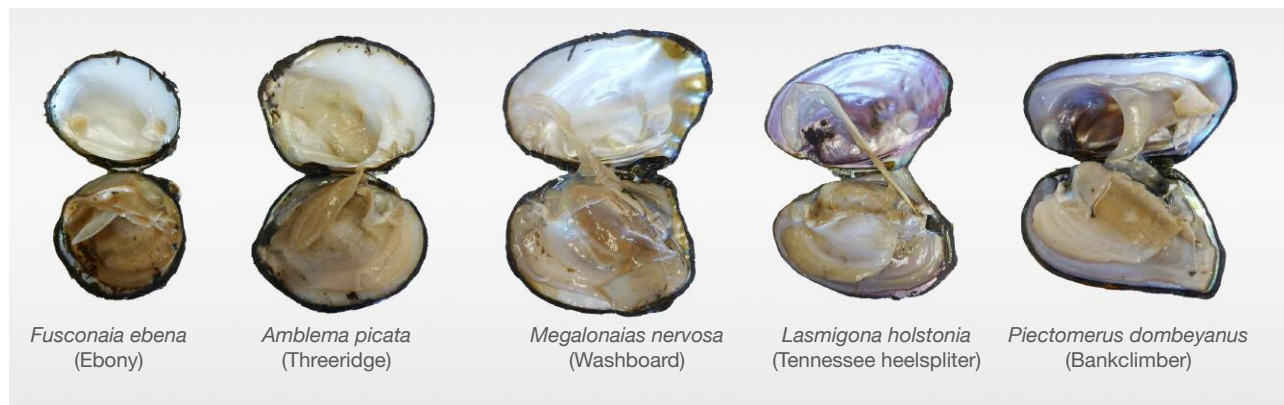


Figure 1. Five pearl-producing freshwater mussel species collected directly from Kentucky Lake, Tennessee, for the DNA barcoding reference library. Photo by Janet Topan and Diego Sanchez.

U.S. mussel species, this would in theory suggest it is natural, since no commercial culturing exists in the United States today. Even though the washboard mussel was once predominantly used to culture American pearls, most American NBC pearls contain unique internal structures that, combined with their characteristic external appearance, allow them to be separated from natural pearls.

LA-ICP-MS and DNA techniques have the potential to help

in determining the identity of freshwater pearls. Further studies on samples from various geographic locations and an even larger data set are needed for trace-element analysis. The DNA barcoding technique is conclusive in identifying mussel species, provided enough DNA can be extracted. However, the analysis requires a suitable sample size, and this may preclude its use on historical and valuable items.

University of Arizona Gem and Mineral Museum and Endowed Chair in Gemology

Zakaria Jibrin, Eric W. Fritz (presenter), and Robert T. Downs
Department of Geosciences, University of Arizona, Tucson

The University of Arizona Gem and Mineral Museum in Tucson supports and advances the study of gems and minerals through the quality and scope of its mineral collection and exhibits. The museum fosters an appreciation for the wonders of Earth and our solar system,

while serving the needs of students, faculty, and the general public. To further this mission, the university is building a state-of-the-art gem and mineral museum in Pima County's historic courthouse (figure 1) featuring a mineral evolution hall, the Arizona Mining &



Figure 1. The historic Pima County courthouse will be the new home of the University of Arizona's Gem and Mineral Museum. Courtesy of Pima County, Arizona.

Minerals Gallery, and a gem hall that includes a vault for special exhibits. The space will encompass approximately 11,700 square feet.

The university's 40,000 specimens will be housed in the new facility. The museum is offering partnerships with organizations and entities related to gems and minerals. This Community Outreach Education Group will have space for offices, public meetings, classrooms, and skill-building workshops.

One of the more exciting aspects of the new museum will be its laboratory with a unique public viewing area where visitors can observe scientists working on gem and mineral research. The lab will feature the latest technology for characterizing minerals and authenticating gemstones: Raman and infrared (IR) for vibrational spectroscopy, X-ray diffraction (XRD) to characterize the crystallographic and structural properties, and mass spectrometry for chemical and isotope analysis of gemstones and minerals.

An undergraduate program and a graduate program for master's and PhD students emphasizing gemological research and skills, along with an endowed professorship, are made possible through a collaboration with The RealReal luxury consignment company. The Gemology Professor will be required to sustain a world-class research program, obtain grants, and publish in peer-reviewed journals. He or she will interact with the existing mineralogy program and share lab facilities such as the X-ray diffractometer, the Raman and IR spectrometers, the electron microprobe, the LA-ICP-MS instrument, and other advanced equipment. The professor will be able to choose his or her own research interests, but it is expected that they will integrate with the university's RRUFF project and provide expanded outreach to the gem trade by adding to the gem database (rruff.info) that is freely available online.

New Technologies and Techniques

Beyond the Four Cs Basics Towards Core Diamond Values

Alexander Mosyaikin¹ and Janak Mistry²

¹OctoNus Software, Moscow

²Lexus SoftMac, Surat, India

Diamond grading systems continuously evolve towards more precise descriptions for relevant discussion and comparison. The basis consists of the Four Cs: carat weight, cut, clarity, and color.

Nowadays, consumers often look for clues beyond the Four Cs. The important and unique polished diamond features for end users comprise the next level of diamond description. In figure 1 (left), the

central four tiles represent the Four Cs graded by the labs: pavilion color, clarity grade, polishing and microsymmetry, and carat weight. The outer tiles are the advanced diamond descriptions based on the unique core diamond features such as brilliance, fire, and table color.

These additional descriptions might provide critically important information for making decisions in cases of

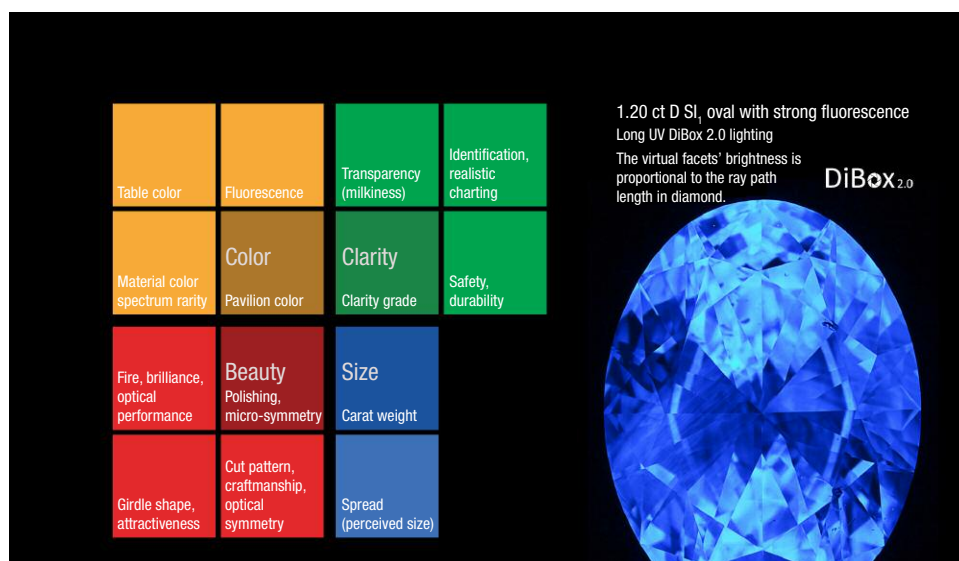


Figure 1. Left: A diamond consumer characteristics chart in which the outer squares represent characteristics beyond the Four Cs shown in the inner squares. Right: A diamond fluorescence image.

1. Diamonds with identical Four Cs grading reports but differences in beauty and value
2. The design of jewelry pieces for balance in fire, brilliance, scintillation, and other factors
3. Uncertainty about a grading report's authenticity
4. Comparing the optical performance of round and fancy cuts

The DiBox 2.0 makes users fluent in a new tier of diamond language. It generates diamond photos (figure 1, right) and videos for professional testing and specific consumer environments (e.g., office, sunlight, nightclub). Controllable long-wave ultraviolet (UV) diodes, along with full-spectrum-visible light-emitting diodes (LEDs) create different lighting conditions (indoor, outdoor, lab, UV-free), revealing the impacts of UV

fluorescence on diamond transparency and color. The selection of lighting conditions includes Fire, Office, ASET/Ideal Scope, Hearts & Arrows, Fluorescence in Long-Wave UV, White Dome Lighting, Darkfield, and Brightfield. The DiBox 2.0 takes 3D videos, allowing virtual appreciation of diamonds remotely in a way that is much closer to reality. DiBox 2.0 images, along with the precise Helium Polish scanner 3D model, can be used to simplify clarity plotting.

The DiBox 2.0 also captures data for automatic assessment algorithms. Brilliance and Optical Symmetry beauty metrics are already available through the Cutwise web platform. These metrics allow the user to compare optical performance of diamonds with different sizes and cuts (round and all fancies) using core consumer values, which form the higher tier of the diamond description system.

Creating Gems Using the Zirconia Sintering Process

Etienne Perret

Ceramique by Etienne Perret, Camden, Maine

Whereas most of us are familiar with the hydrothermal and flux-melt solution methods for growing crystal forms of zirconia, these are not the only way to create gem forms from this material. Using the sintering process, zirconia powder can be baked at high temperatures to create three-dimensional objects.

Sintered zirconia (figure 1), also known as zirconia ceramic, is used in many medical and industrial applications. Zirconia ceramics are now successfully used in the watch and jewelry industry. Its relatively low cost and high durability make it an ideal alternative to precious metals. A wide range of colors in addition to white and black can be achieved by adding trace elements to the zirconia powder before it is sintered. All these factors make zirconia ceramic an extremely interesting material to consider in the manufacture of jewelry.

Figure 1. This necklace contains 29 oval beads of sintered black zirconia measuring 12 × 17 mm apiece, with a diamond pavé clasp set in white gold. Photo by David Stewart Brown.



Fluorescence Spectroscopy for Gemstone Screening and Identification

Tsung-Han Tsai

GIA, New York

Gemologists are always looking for fast, accurate, and cost-efficient methods and tools to identify gem materials. Fluorescence spectroscopy is a highly efficient way to detect a gemstone's defects or impurities, while the characteristic fluorescence response can be used to identify the gemstone. Therefore, this rapid technology

has the potential to be used to separate natural diamonds from laboratory-grown diamonds and diamond simulants, detect multi-treated pink diamonds, and identify colored gemstones. This technique can be applied to test both loose samples and mounted jewelry pieces. An experimental prototype has been built to test

the concept of using fluorescence spectroscopy under room temperature for gemstone screening. The device uses a UV LED as the light source. Optical short-pass and long-pass filters are installed between the light source and the spectrometer to isolate the fluorescence from the excitation. Optical lenses are used to focus the UV source into the reflection fiber probe and then couple the fluorescence into the spectrometer. The prototype uses a reflection fiber probe to enhance the flexibility of sample positioning, allowing the user to easily target individual mounted or unmounted gemstones.

To test the performance of the prototype and the screening software, we measured more than 10,000 samples including natural diamonds, diamond simulants, laboratory-grown diamonds, treated pink diamonds, and colored gemstones such as ruby, sapphire, emerald, spinel, and zoisite to confirm the detection rate of this device. Figure 1 shows the fluorescence spectra of natural diamond, multi-treated pink diamond, and various colored stones. The prototype detected 97% of natural diamond, and referred 100% of diamond simulants and both HPHT and CVD laboratory-grown diamonds for further testing. In pink diamond identification, 99% of natural pink diamonds were detected, while multi-treated pink diamonds and pink laboratory-grown dia-

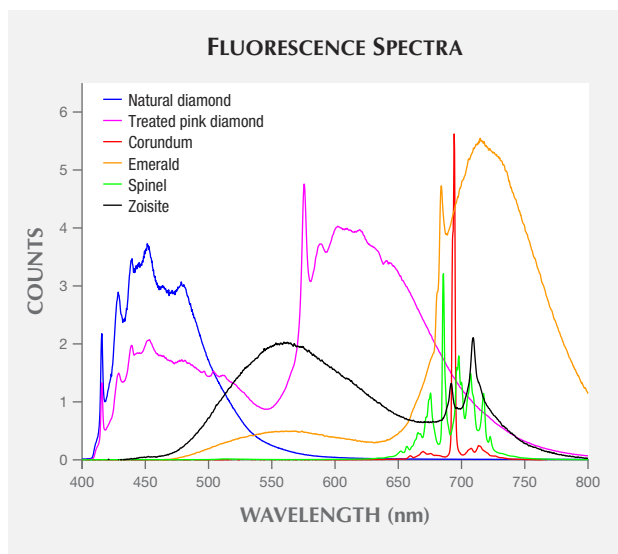


Figure 1. Characteristic fluorescence spectra of natural diamond, multi-treated pink diamond, and the most common colored stones: corundum, emerald, spinel, and zoisite.

monds were 100% referred. Finally, the device detected 93% of corundum, 97% of emerald, 93% of spinel, and 81% of zoisite.

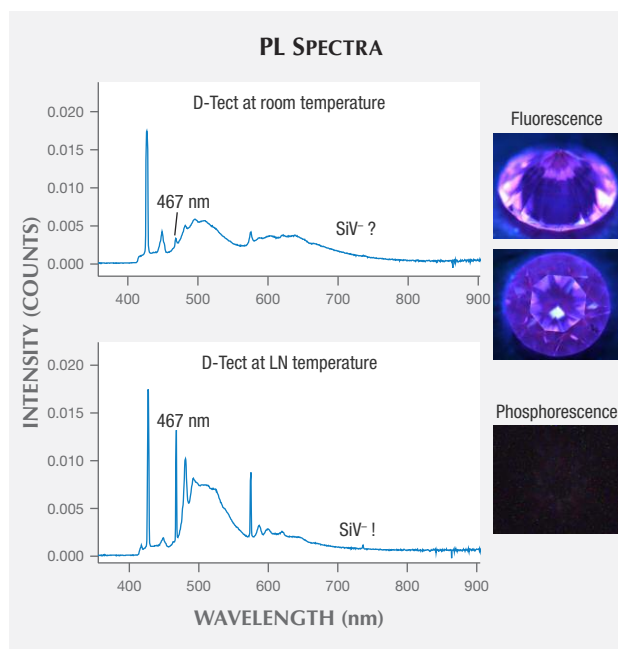
From Screening to D-tection

Marleen Bouman, Ellen Biermans, and Ans Anthonis
HRD Antwerp

Screening diamonds by type is a safe way to sort potentially lab-grown colorless diamonds from natural diamonds. Nevertheless, in many cases the referral rate is too high. Therefore, HRD Antwerp has introduced the use of D-tect, a new screening device that forms a perfect complement to the M-screen⁺. D-tect is a nonautomated device based on UV luminescence imaging and photoluminescence spectroscopy (PL) at room temperature and liquid nitrogen (LN) temperature. In combination with M-screen⁺, this instrument offers the ultimate assurance of distinguishing all laboratory-grown diamonds from natural ones.

In this study, we investigated a parcel of 150 melee-sized CVD-grown diamonds, focusing on features that are challenging for up-to-date screening devices. D-tect checks the SiV⁻ doublet and the 467 nm defect, defects typically seen in CVD laboratory-

Figure 1. Example of a CVD synthetic diamond with purple fluorescence and no phosphorescence. D-tect's PL spectra at room temperature do not reveal the SiV⁻ doublet, but the 467 nm defect is already visible. PL measurements at LN temperatures reveal the SiV⁻ doublet's presence together with the presence of the 467 nm defect.



grown diamonds. At LN temperatures, it is possible to see even the weakest SiV⁻ doublet. This feature, in combination with the presence of the 467 nm defect, identified all of the CVD speci-

mens, even those with uncharacteristic fluorescence colors. An example of a CVD-grown diamond with purple fluorescence and no phosphorescence is given in figure 1.

Image Analysis Techniques Applied to Clarity Issues

Troy Blodgett¹ and Andrew Regan²

¹GIA, Flagstaff, Arizona

²GIA, New York

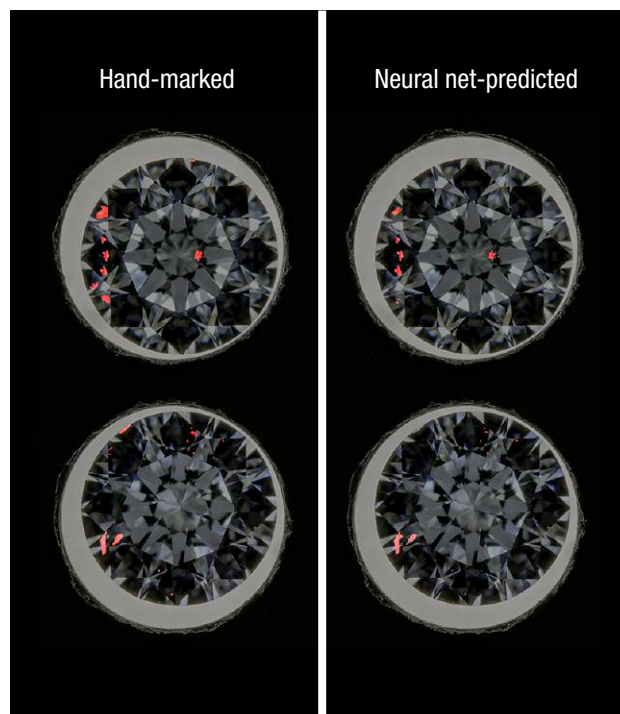
GIA's research in clarity image analysis began around the year 2000 with capturing high-resolution still images to explore whether 2D images could be used as an alternative to clarity plotting. GIA also examined the potential of using image analysis and inclusion-capture algorithms for predicting a clarity grade. Based on this early research, we developed the Imaging System for Automated Clarity (ISAC), which required an operator to select a region of interest encompassing an inclusion and choose the predicted result that best represented the inclusion so that the device could predict a clarity grade. Note that this application pertained mainly to diamonds with single inclusions, although there was a supplemental entry field to adjust the predicted clarity grade if reflections or additional inclusions were reported.

From the ISAC research ending in 2007, a number of patents were filed that same year. The ISAC designs were subsequently re-engineered for a production environment, leading to the implementation of a device for producing images on the eReport in 2012. Further experiments were run on high-resolution manually "stacked" composite images using textural analysis, which showed considerable promise. GIA has undertaken extensive testing of various production-friendly imaging instruments (e.g., Keyence Microscope, Lexus-OctoNus Dibox, and Sarine Loupe) to see which ones could produce images suitable for automated clarity analysis. Artificial neural nets, a type of machine learning, were trained to recognize the shape and texture of inclusions. Examples of such plots are shown in figure 1.

In addition to plotting features, neural nets have also learned to apply clarity factors such as relative size, number, relief, and position of inclusions to calculate a clarity grade. For predicting a grade, the artificial neural nets were trained on a portion of the crown-view images and the remaining images tested the clarity grade prediction. About 70% of the predicted grades matched the clarity grades provided by graders (evaluating the images) when IF–VVS ranges were lumped together and I₁, I₂, and I₃ were clustered. Distinguishing IF and VVS grades likely requires more information from both the pavilion and girdle views. There were not enough I₂ and I₃ images available to treat those grade ranges as separate categories. GIA considers 3D information important

for clarity evaluation. Images of the crown tilted to varying degrees were used to estimate inclusion depth. Results from the 2D clarity plot, inclusion depth information, and a 3D wireframe model can be combined to render a preliminary 3D clarity plot. Future research will be conducted to add more 3D information from the pavilion view to improve the accuracy of the 3D clarity plot and shed more light on the most challenging IF–VVS clarity range.

Figure 1. These muted images show a comparison of hand-marked inclusion plots (left) and neural net-predicted results (right) counting inclusion reflections. In general, the predicted results matched the hand-marked plots, but a few discrepancies occurred in both examples.



Matrix-Matched Standards for Trace-Element Analysis in Ruby and Sapphire

Jennifer L. Stone-Sundberg¹, Timothy Thomas², Zachary Cole³, Yunbin Guan⁴, Ziyin Sun⁵, Troy Ardon⁵, and John L. Emmett⁶

¹GIA, Portland, Oregon

²Applied Materials, Hillsboro, Oregon

³Scientific Materials Corporation, Bozeman, Montana

⁴California Institute of Technology, Pasadena

⁵GIA, Carlsbad, California

⁶Crystal Chemistry, Brush Prairie, Washington

As reported recently (Stone-Sundberg et al., 2017), GIA has created sets of highly accurate matrix-matched corundum standards for laser ablation–inductively coupled plasma–mass spectrometry (LA-ICP-MS) analysis as an alternative to NIST glasses. These standards cover applicable ranges of the key trace elements found in natural ruby and sapphire: Be, Mg, Ti, V, Cr, Fe, and Ga. The concern with using non-matrix-matched standards to quantify trace elements in corundum is twofold: (1) Calibrating with a matrix differing in composition and structure will result in dissimilar interferences and ablation characteristics, which will negatively impact the quantification process. (2) The differences in ratios of matrix elements and trace elements of interest between the non-matrix-matched standard and the samples will result in calibration errors. Possibly the most concerning issue for applying NIST glass standards to quantifying many trace elements in corundum is the fact that they simply are not certified for most of the elements of interest.

To ensure the highest accuracy possible, we created and characterized individual ion implant standards for each trace element of interest in corundum, calibrated a secondary ion mass spectrometer (SIMS) with these implants, and then calibrated each individual corundum standard piece using SIMS. We turned to Czochralski growth to produce large and highly uniform multi-doped crystals for these standards (figure 1). The standards sets include two multi-doped pieces of synthetic sapphire to capture relevant levels of Mg, Ti, V, Cr, Fe, and Ga; a highly uniform piece of Yogo sapphire to capture a greater level of Fe than we could generate synthetically; and an ultra-high-purity synthetic sapphire “blank” with a combined total of less than 0.5 ppma of the key trace elements mentioned above. To incorporate Be, pieces from one of the multi-doped crystals were beryllium diffused for 100 hours at 1800°C in pure oxygen. Each piece for the standards set was screened to ensure high homogeneity.

REFERENCE

Stone-Sundberg J., Thomas T., Sun Z., Guan Y., Cole Z., Equall R., Emmett J.L. (2017) Accurate reporting of key trace elements in ruby and sapphire

GIA has been using these standards for more than a year in its colored stones laboratories and is working to make these standards available outside of GIA. We have also been focusing on optimizing the LA-ICP-MS operating protocols throughout our labs to identify the best conditions for gemological applications. The adoption of these standards by other labs will help in creating industry-wide uniformity when it comes to reporting key trace-element data for ruby and sapphire.

Figure 1. Crystal boules grown by Scientific Materials for multi-doped corundum standards: sample 02-1032 (top) and sample 07-0687 (bottom). Both crystals were doped with Mg, Ti, V, Cr, and Ga in different amounts; only 02-1032 was successfully doped with Fe. Crystal 02-1032 is 40 mm in diameter by 150 mm in length at diameter, and crystal 07-0687 is 30 mm in diameter by 150 mm in length at diameter. Photos courtesy of Scientific Materials.



using matrix-matched standards. *G&G*, Vol. 53, No. 4, pp. 438–451, <http://dx.doi.org/10.5741/GEMS.53.4.438>

Novel Method of Diamond Color Grading by Raman Spectroscopy

Joe C.C. Yuan¹, Ju-Tsung Liu², and Gavin D.S. Pan³

¹ Taidiam Technology (Zhengzhou) Co., Ltd., China

² Taiwan Food and Drug Administration

³ United ID Raman Lab, Taipei

A nondestructive and rapid diamond color-grading method is proposed based upon the 2030 cm^{-1} characteristic Raman peak. The intensity of this N-C bonding peak for natural untreated “cape” diamonds (type Ia, IIa) is strongly associated with the observed color. When the intensity of the 2030 cm^{-1} peak is normalized against that of the second-order diamond bond peak at 2666 cm^{-1} , this can be used as a basis for the color grading of cape diamonds, both loose and mounted. The characteristic Raman peak of diamond at 1332 cm^{-1} corresponds to the vibration mode of the C-C bond. However, the C-N bond peak at 2030 cm^{-1} (Nyquist et al., 1997; Dana et al., 2004) can reveal information related to the diamond's color. The 1800–2800 cm^{-1} spectral range clearly shows additional second-order Raman peaks at 2180, 2256, 2336, 2462, 2490, and 2666 cm^{-1} . The coexistence of the 2030 cm^{-1} peak and second-order peaks in the overlaid spectrum was seen in all 50 type Ia diamonds examined in this study.

To test this approach, we examined a set of eight certified GIA color master diamonds with grades of E, F, G, H, I, J, K, and L. We collected Raman data in the spectral range between 1600 and 2800 cm^{-1} and normalized the 2666 cm^{-1} peak in each data set to 1,000 counts so that we could observe the variation in the 2030 cm^{-1} peak relative to it. The normalized intensity of the

2030 cm^{-1} peak clearly increased with increasing yellow tint. A linear relationship was observed when plotting normalized 2030 cm^{-1} peak intensity versus color grade.

The 2030 cm^{-1} Raman peak in nitrogen-containing type Ia and IIa cape diamonds is considered to be related to C-N bonding and is consistent with reports of other C-N bond vibration modes at 2030 cm^{-1} , such as in $\text{Pb}(\text{SCN})_2$ (Nyquist et al., 1997; Dana et al., 2004). To date, the assignment of the 2030 cm^{-1} peak as N-related mode does need further research work, which is beyond the scope of this research.

This 2030 cm^{-1} peak may be overlooked or undetectable by conventional Raman spectrometers due to its low intensity relative to the C-C bonding mode. The instrumentation used in our study has an exceptionally high sensitivity, with $S/N > 10,000$, supplemented by Auto Baseline Software System, which allows us to detect and analyze this bond mode.

This method for color grading cape diamonds is rapid and nondestructive, with no requirement for sample preparation. It may serve as a novel and semi-quantitative method complementing the conventional colorimetric method. It cannot be applied to HPHT-treated diamonds because the fragile C-N bond peak at 2030 cm^{-1} may be totally or partially destroyed by the treatment.

REFERENCES

Mayo D.W., Miller F.A., Hannah R.W. (2004) Characteristic frequencies of molecules with triple bonds and cumulated double bonds. In *Course Notes on the Interpretation of Infrared and Raman Spectra*. John Wiley & Sons, Hoboken, New Jersey, pp. 85–99.

Nyquist R.A., Putzig C.L., Leugers M.A. (1997) *Handbook of Infrared and Raman Spectra of Inorganic Compounds and Organic Salts*. Academic Press, San Diego, California, pp. 1–14.

Quantitative Determination of Cr^{3+} and V^{3+} Contents in Rubies by Spectral Fitting of UV-Vis-NIR Spectra

Tom Stephan^{1,2}, Tobias Häger², Ulrich Henn¹, and Wolfgang Hofmeister²

¹ German Gemmological Association, Idar-Oberstein

² Center for Gemstone Research, Johannes Gutenberg-University, Mainz, Germany

For this study, the ultraviolet/visible/near-infrared (UV-Vis-NIR) absorption spectra of various natural and synthetic rubies and sapphires were mathematically decomposed into Gaussian and Lorenz curves. For this purpose, we used MagicPlot Pro curve fitting software.

With the help of synthetic corundum samples that were colored respectively by Cr^{3+} or V^{3+} , we developed two models that allow a comparable and reproducible description of the UV-Vis-NIR spectra (see figure 1). The applicability of the models, the transferability

to the absorption spectra of natural rubies and sapphires, and the correlation with chemical analyses were successfully tested.

The investigations showed that by the use of such models and knowledge of the samples' thickness, it is possible to determine concentrations of coloring trace elements (in this case chromium and vanadium) quantitatively from the absorption spectra. Additionally, the simultaneous application of Cr^{3+} and V^{3+} models is also possible, despite the superposition of the absorption bands of both chromophores. Therefore, the detection of vanadium in ru-

bies is made possible even at low concentrations. This allows first information on the samples' origin.

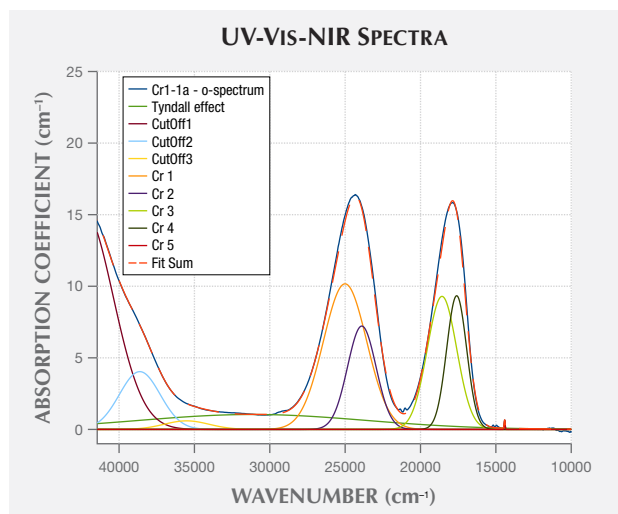
Additional information can be obtained from the absorption spectra, such as:

1. Exact position and shape of the cutoff (absorption edge toward the UV region)
2. The strength of the Tyndall effect, to estimate the concentration and size of the light-scattering inclusions
3. Detection of underlying color causes

The investigations are part of the first author's ongoing PhD thesis. The work's aim is a model for each cause of color in corundum, which would allow a simultaneous quantification of the concentration of the involved chromophores—as well as for mixed colors. We have also tested the applicability for faceted samples. The first results show that fitting is possible, with appropriate sample orientation.

Additionally, comparable models for other gemstones incorporating Cr³⁺ and V³⁺ (e.g., emerald, tourmaline, and garnet) will be developed and tested.

Figure 1. The o-spectrum of a Verneuil synthetic ruby has been fitted using MagicPlot Pro curve fitting software. Curves Cr 1–Cr 5 are then used to define the Cr³⁺ model.



A Simplified Species Classification for Gem-Quality Tourmaline by LA-ICP-MS

Ziyin Sun¹, Aaron C. Palke¹, Christopher M. Breeding¹, and Barbara L. Dutrow²

¹GIA, Carlsbad, California

²Department of Geology and Geophysics, Louisiana State University, Baton Rouge

In the trade, gems from the tourmaline species are often identified by sight based on the typical colors of the various species rather than accurate chemical analyses. However, the same color can be exhibited by several different species. In other words, tourmaline color is not species specific. Electron microprobe analysis is the most widely accepted method to determine tourmaline species. Unfortunately, it is also expensive and time-consuming. Most gemological laboratories are not equipped for it and cannot justify the overhead costs associated with outsourcing this analysis. Therefore, the electron microprobe is not a practical everyday tool for a gemological laboratory. Here, we present a comprehensive method for using LA-ICP-MS analyses to accurately determine tourmaline species. The new method allows for inexpensive, clean, fast, and largely nondestructive analysis of tourmaline chemistry. With this method, we are able to produce LA-ICP-MS data for major and minor element concentrations in tourmaline that closely match values determined by electron microprobe (within ±10% error). The ability to accurately measure the range of chemical compositions found in gem tourmaline using LA-ICP-MS allows GIA to help the colored stone industry better understand the varieties of tourmaline being bought and sold.

Figure 1. Much of the brown and yellow tourmaline on the market is sold as dravite or uvite but could just as easily be elbaite. These six tourmalines in various colors, ranging from 1.51 to 11.33 ct, are from Lundazi, Zambia. Photo by Robert Weldon/GIA, courtesy of Bjorn Anckar.



Swept-Source Optical Coherence Tomography for Imaging the Internal Structure of Pearls

Nick DelRe¹, Nate Kemp², Joey Jabbour², and Andres Zuluaga²

¹Gemological Science International, New York

²Axsun Technologies, Billerica, Massachusetts

The popularity of pearls (figure 1, left) over the centuries led to their cultivation to meet marketplace demand. This has resulted in numerous pearls and pearl imitations that at times prove to be an identification challenge, even when using X-ray tomography. Some examples include the differentiation of certain kinds of natural vs. cultured pearls. The difficulty is compounded because pearls must be tested nondestructively, a cornerstone of gemology.

Traditionally, the internal structure of pearls has been examined by radiography. This imaging method uses X-rays (figure 1, center), which are at the higher-energy end of the electromagnetic spectrum. This technique generates two- and three-dimensional images. To get a clearer picture of the internal structure, 3D images are generated by computed tomography (CT), where multiple 2D images from different angles undergo computer processing. The time to generate an image with good resolution can vary from seconds to several minutes. While passing through the pearl, a certain amount of X-ray radiation is absorbed (dependent on the pearl's density and structural composition) as well as scattered. Although the radiation is not harmful, there may be a slight degree of ionization occurring when the X-rays are absorbed by the pearl. In addition, the operator must take safety measures while working with ionizing radiation.

Here we present an alternate form of imaging that uses the lower-energy end of the electromagnetic spectrum, namely the near-infrared region. Optical coherence tomography (OCT; figure 1, right) is a noninvasive, micron-resolution cross-sectional scanning of visually translucent to opaque structures. It allows live 3D imaging of sample morphology without sample preparation or exposure to ionizing radiation. OCT fills the imaging gap between ultrasound and MRI (deeper coverage and lower spatial resolution) on one end, and confocal microscopy (shallower coverage, higher spatial resolution) on the other. It can be likened to sonar or medical ultrasound, but using light waves instead of sound waves. OCT has proved very successful in ophthalmology and cardiology applications.

In this technique, a beam of light (typically in the near-infrared spectrum) is used to scan the sample. Coherence refers to the fact that an interferometric, low-coherence technique is used for depth discrimination. Tomography means cross-sectional imaging. To further explain the basic optical setup, the light is split between

TABLE 1. Specifications of the two Axsun SS-OCT pearl scanning systems.

	1060 nm	1310 nm
Lateral resolution	16 microns	35 microns
Axial resolution	4 microns in air	7 microns in air
Scan depth	4.2 mm in air	6 mm in air
FOV diameter	12 mm	27 mm
Axial line rate	100 KHz	100 KHz
DAQ sampling rate	500 Msamples/second	500 Msamples/second

Note: Msamples = acquisition memory depth, which equals the number of samples that are stored with each acquisition.

two arms, one for the sample and one for the reference mirror. The reflected beam from the sample and the reflected beam from the reference mirror interfere with each other. That interference represents the intensity of the reflection from a specific depth in the sample. In classic time-domain OCT, scanning the position of the reference mirror in the interferometer allows the interference signals from different depths to be acquired and processed, thus forming an axial line representing the intensity of reflections from each depth in the sample. In swept-source OCT, a laser source produces a rapid sweep of wavelengths (colors). For each wavelength, an interference pattern is formed. This interference pattern can be processed with exquisite sensitivity, leading to exceptional rejection of signals from depths outside the detection window.

In the case of the 3D data presented here, a pair of galvanometer scanners were used to scan the light in two directions perpendicular to each other and both perpendicular to the depth direction (see the table for the scanning systems' specifications). Although there have been attempts in the past 20 years to apply OCT technology for pearl examination, none have garnered sufficient interest. Part of this has to do with the cost-effectiveness of this technology for commercial use. In addition, the resulting imaging was still not suitable for pearls, since the penetration depth and sensitivity from available systems was insufficient. Our studies have demonstrated the exceptional performance of a compact and cost-effective advanced swept-source OCT system in delivering high-quality noninvasive 3D images of pearls in real time.

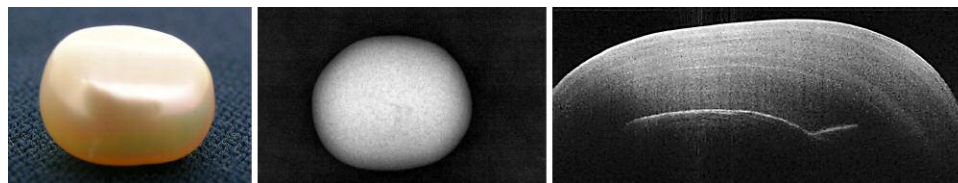


Figure 1. A freshwater tissue-nucleated cultured pearl, shown in visible light (left), in an X-radiograph (center), and an optical coherence tomography image (right).



The 2018 Symposium's finale, the Futurescape Forum, brought together six industry leaders in a panel discussion moderated by Dr. David Ager, managing director of executive development at the Harvard Business School. The panelists were Bruce Cleaver, CEO of the De Beers Group; Gina Drosos, CEO of Signet Jewelers; Jason Goldberger, CEO of Blue Nile; Andy Johnson, CEO of Diamond Cellar Holdings; Rahul Kadakia, international head of jewelry at Christie's; and Kent Wong, managing director of Chow Tai Fook.

The forum began with an industry forecast via video from Scott Galloway of the NYU Stern School of Business. The discussion centered around several key points:

- Technologically driven changes in retailing and trading, and continued consolidation across the value chain. These market shifts include challenges from giants such as Amazon and an increase in manufacturers selling direct to consumers, bypassing traditional retail channels.
- Evolving consumer tastes and desires, including concerns over gem sources and sustainable production
- The need to appeal to a rapidly changing workforce
- Disruption caused by laboratory-grown diamonds, both in the marketplace and in laboratory testing and identification

Technical Challenges

There was broad agreement that retailers must adapt to technology, not just in sales channels, but in ways it can help individualize each customer.

Drosos explained that omni-channel retailing is a necessity because customers routinely cross channels in their shopping experience, starting online and ending in the store. Online channels

can enhance the in-store experience by making it possible for customers to make appointments online—90% of such appointments result in a sale, she noted.

Wong said that 15% of Chow Tai Fook's sales by volume are done online, but mainly in small gold items and in charms such as Hello Kitty and Disney characters. At the high end, Kadakia said that 90% of Christie's auction business is still done by traditional bidding, but the remainder is online, mainly from younger clients buying pieces under \$10,000. "This is how we target younger customers," he said.

Bruce Cleaver of the De Beers Group listens as Signet Jewelers' Gina Drosos explains the importance of omni-channel retailing. Photo by Denise Conrad/GIA.





An audience member poses a question for the panel at the Futurescape Forum. Photo by Denise Conrad/GIA.

A Changing Workforce

The changing workforce was a key discussion point in the session. Businesses must adapt to a millennial workforce comprised of people who switch careers because they value diverse experiences and often do not want to stay with a company over the long term.

Goldberger told the audience that organizations should not become too insular and that people with diverse backgrounds bring new thinking. He added, “The reality of today is that tech people move every two or three years, so we have a choice: Do we lose them entirely or benefit from their talent while they are here?” Cleaver noted that there are excellent opportunities to diversify the traditionally conservative diamond industry, while Wong said his company brings in gifted designers by offering them a platform to create and sell their designer pieces. “Talented people need that freedom,” he pointed out. Johnson added that not everyone wants to switch careers, and businesses must adapt to workers who cannot be on hand full-time.

Natural and Laboratory-Grown Diamonds

Laboratory-grown diamonds occupied a great deal of discussion in the Futurescape Forum. Panelists agreed that while they have a place in the market, natural diamonds will still be the choice to celebrate life’s landmark occasions. Kadakia was confident that natural diamonds will remain the consumer choice because they will always have value, while synthetics will not hold value over time.

Goldberger noted that while today’s engagement ring buyers invariably prefer natural diamonds, we cannot take this for granted in the future. He cited the example of consumers who in the 1990s loved to browse bookstores but then deserted them for online channels. Cleaver said that synthetic diamonds’ place in the market was firmly in the “fun and fashion” side.

Gemstone Sourcing and Production

Cleaver also related the economic and political success of Botswana, once one of the world’s poorest nations. Diamond revenues, coupled with good governance, helped transform Botswana into one of Africa’s most prosperous countries.

As Cleaver noted, “It’s a story not always told—the good that diamonds can do in employing people and development.” Drosos said customers are interested in knowing the origins of their diamonds and that Signet is working to familiarize all employees with its corporate social policies regarding sourcing.

Russell Shor
GIA, Carlsbad, California

Kent Wong discusses Chow Tai Fook’s approach to attracting talented designers while David Ager (left) and Rabul Kadakia (right) look on. Photo by Denise Conrad/GIA.





Index of Presenters

This index lists presenters from GIA's 2018 Symposium. It includes research speaker presentations, poster sessions, and the Futurescape Forum.

Ali, Saleem	281	Henry, Darrell	324	Sevdermish, Menahem	286
Alonso-Perez, Raquel	280	Ho, Henry	331	Shen, Che	326
Anthonis, Ans	265	Ho, Joyce Wing Yan	300	Shirey, Steven	272
Atikarnsakul, Ungkhana	321	Hodgins, Gregory	260	Shor, Russell	335
Blodgett, Troy	343	Homkrajae, Artitaya	338	Singbamroong, Sutas	310
Boehm, Edward	282	Hu, Yang	319	Sivovolenko, Sergey	287
Bouman, Marleen	342	Johnson, Andy	348	Smit, Karen	307
Breeding, Christopher M.	275	Kadokia, Rahul	348	Smith, Evan	274
Butler, James	303	Katsurada, Yusuke	322	Soonthorntantikul, Wasura	298
Carmona, Charles	330	Keith, Jeffrey	323	Stachel, Thomas	271
Celestian, Aaron	309	Kessrapong, Promlikit	294	Steele, Sarah	325
Chen, Quanli	316	Kitawaki, Hiroshi	267	Steinbach, Martin	258
Chen, Tao	318	Krebs, Mandy	322	Stephan, Tom	345
Choudhary, Gagan	308	Larson, William	283	Stone-Sundberg, Jennifer	344
Cleaver, Bruce	348	Li, Yan	313	Sturman, Nicholas	301
Cohen, Haim	276	Link, Klemens	281	Sun, Ziyin	346
Cook, Brian	332	Liu, Ling	317	Syvrud, Patricia	335
Cui, Danlu	313	Liu, Yan	316	Tsai, Tsung-Han	341
Day, James	297	Liu, Yimiao	320	Twitchen, Daniel	285
Deljanin, Branko	305	Lu, Taijin	268	Vertriest, Wim	283
DelRe, Nick	347	Luo, Zemin	259	Villegas, Cristina	284
D'Haenens-Johansson, Ulrika	273	Lyckberg, Peter	278	Vins, Viktor	315
Diggie, Phil	265	Marshall, Dan	297	Wambua, Marvin	327
Drosos, Gina	348	Milisenda, Claudio	258	Wang, Wuyi	262
Drucker, Richard	333	Milroy, Hollis	315	Wen, Shangjia	328
Dutrow, Barbara	256	Moe, Kyaw Soe	307	Wong, Kent	348
Eaton-Magaña, Sally	269	Moses, Maureen	338	Xu, Yafen	311
Eisen, Susan	330	Mosyaikin, Alexander	340	Yager, Thomas	324
Fisher, David	263	Niklewicz, Danusia	334	Yazawa, Emiko	294
Fritsch, Emmanuel	257	Odake, Shoko	304	Young, Kennon	330
Fritz, Eric	339	Palke, Aaron	262	Yu, Jinding	302
Galloway, Scott	348	Payne, Jason	286	Yuan, Joe	335
Goldberger, Jason	348	Pearson, D. Graham	270	Zaitsev, Alexander	304
Groat, Lee	277	Perret, Etienne	341	Zhang, Zhiqing	314
Gu, Tingting	306	Promwongnan, Supparat	336	Zhao, Jiahui	266
Gumpesberger, Sylvia	337	Robertson, Stuart	329	Zhou, Chunhui	261
Hansen, Robin	329	Saeseaw, Sudarat	300	Zhou, Qishen	295
Haynes, Lee	333	Serov, Roman	276		

GIA VOLUNTEERS

Kaz Abe
Mariam Aboushadi
Shaina Aceves
Mohit Agrawal
Nicole Ahline
Jennifer-Lynn Archuleta
Troy Ardon
Rick Baca
Laurie Bailyn
Nellie Barnett
Marianne Barrett
Maria Bartolome
Kristi Bathany
Kelly Bennett
Asha Bhasker
Karanbir Bhatia
Nirupa Bhatt
Sharon Bohannon
Maria Brachetti
Elizabeth Brehmer
Sonia Chaves
Carl Chilstrom
Grace Cho
Linda Chudomelka
Judy Colbert
Lo Combs
Denise Conrad
Ruby Contreras
Anna Cournoyer
Kathleen Dailey
Ulrika F.S. D'Haenens-Johansson
Marcia Dillenback
Tina Di Nitto
Shayne Ebrahimi
Martha Erickson
Michael Evans
Cathy Ezzo
Debi Flores
Leslie Gargas
Lisa Garris
Jared Giangulio
Kellie Giordano
Jim Gonzalez
John Hall
Martin Harmon
Peter Harts
Brenda Harwick
Erik Hinds
Erin Hogarth
Peter Hsu
Tao Hsu

Joseph Jean
Lee Johnson
Cathy Jonathan
Doug Kennedy
Jennifer Kim
John King
Renada Koebel
John Koivula
Sam Kong
Michael Koyle
Jessica Kramer
Mandy Krebs
Sharat Kuncha
Tom Kwolik
Emily Lane
Noah Lathrop
Britni LeCroy
Carson Lee
Stella Lee
April Logan
Gaston Lopez
Luz Lopez
Pitchaya Lopiti
Yvonne Loreto
Yun Luo
Michael Magee
Anu Manchanda
Kevin Manley
Jason Marks
Michelle Matlock
Paul Mattlin
Hollie McBride
Shane McClure
Belinda Mekdara
Cheryl Mestas
Lisandra Mioni-Green
Zaudy Miranda
Seung-Hae Moon
Cecilia Morales
Sriram Natarajan
Tali Nay
Lisa Neely
David Nelson
Sarah Ostrye
Jack Owensby
Daniela Pacheco
Pedro Padua
Urvi Parekh
Dianna Parsons
Mary Pietanza
Chris Polley

Julia Popovich
Erica Printz
Augustus Pritchett
Tony Puccio
Ashleigh Ramsey
Waverly Reed
Nathan Renfro
Tim Richardson
Chris Rogers
Chris Ross
Paula Rucinski
Medhi Saadian
Maryam Salimi
Albert Salvato
McKenzie Santimer
Kelsie Santoro
Vicky Scales
Kevin Schumacher
Michele Schwien
Manoj Singhania
Karen Smit
Angela Sousa
Mitch Spencer
Michael Springs
Deepa Srinivasa
Michaela Stephan
Joy Stetler
David Stone
Nicholas Sturman
Nina Switzer-Spano
Jamey Taupule
Tiffany Thiele
Rose Tozer
Kate Trunnell
Rebecca Tsang
Peggy Tsiamis
Shelly Verwymeren
Ryan Waddell
Tim Walkusky
Vivian Wang
Wendy Wang
Glenn Wargo
Kate Waterman
Heather Weishaar
Eric Welch
Rene Wiley
Danielle Yamamoto
Phil Yantzer
Phil York
Forozan Zandi
Veronica Zepeda

